Bioactive Materials 32 (2024) 356–384

Contents lists available at ScienceDirect

Bioactive Materials

journal homepage: www.keaipublishing.com/en/journals/bioactive-materials

Review article

Embedded 3D bioprinting – An emerging strategy to fabricate biomimetic & large vascularized tissue constructs

Harshavardhan Budharaju, Dhakshinamoorthy Sundaramurthi *, Swaminathan Sethuraman *

Tissue Engineering & Additive Manufacturing (TEAM) Lab, Center for Nanotechnology & Advanced Biomaterials, ABCDE Innovation Center, School of Chemical & Biotechnology, SASTRA Deemed University, Thanjavur, India

ARTICLE INFO

Keywords:
Bioprinting
Bioinks
Embedded bioprinting
Complex bioprinting
Supportive bioprinting
Organ models bioprinting

ABSTRACT

Three–dimensional bioprinting is an advanced tissue fabrication technique that allows printing complex structures with precise positioning of multiple cell types layer–by–layer. Compared to other bioprinting methods, extrusion bioprinting has several advantages to print large–sized tissue constructs and complex organ models due to large build volume. Extrusion bioprinting using sacrificial, support and embedded strategies have been successfully employed to facilitate printing of complex and hollow structures. Embedded bioprinting is a gel–in–gel approach developed to overcome the gravitational and overhanging limits of bioprinting to print large–sized constructs with a micron–scale resolution. In embedded bioprinting, deposition of bioinks into the microgel or granular support bath will be facilitated by the sol–gel transition of the support bath through needle movement inside the granular medium. This review outlines various embedded bioprinting strategies and the polymers used in the embedded systems with advantages, limitations, and efficacy in the fabrication of complex vascularized tissues or organ models with micron–scale resolution. Further, the essential requirements of support bath systems like viscoelasticity, stability, transparency and easy extraction to print human scale organs are discussed. Additionally, the organs or complex geometries like vascular constructs, heart, bone, octopus and jellyfish models printed using support bath assisted printing methods with their anatomical features are elaborated. Finally, the challenges in clinical translation and the future scope of these embedded bioprinting models to replace the native organs are envisaged.

1. Introduction

Natural tissues are made up of cells and cellular components (extracellular matrix) that are highly structured to accomplish specified functions within the body. Scaffolds aimed for tissue engineering purposes should recapitulate the native tissue and thus the fabrication of transplantable tissues & organs remains a challenge in tissue engineering and regenerative medicine [1]. Researchers have been fabricating functional tissue structures to promote natural tissue regeneration after injury or illness for a long time using cells, biomaterials, growth factors, and other supporting components [2]. Researchers have utilized conventional tissue engineering approaches such as freeze drying, solvent casting, particulate leaching, electrospinning, hydrogels, etc., to develop functional tissues by fabricating interconnected porous scaffolds with ideal mechanical and biological properties to repair or restore the damaged tissues [3–5]. However, recapitulating the native microenvironment, developing heterocellular tissues, and accommodating high cell densities similar to native tissues is challenging using conventional tissue engineering strategies. Moreover, fabricating complex tissues/organs with intricate geometry, functional microvasculature, and precise shape requirements to match patient needs necessitates advancements in tissue engineering strategies [6–8].

Developments in medical imaging technologies like computed tomography (CT) and magnetic resonance imaging (MRI) have made it possible to create patient–specific tissue geometries and vasculature to integrate with the host vasculature [9,10]. These imaging techniques can be used to design defect–specific 3D models and assist in creating tissues to fit the defective area by printing customized tissue constructs using bioprinting techniques [11]. 3D bioprinting is an emerging additive manufacturing technique where the bioink is dispensed in a

Peer review under responsibility of KeAi Communications Co., Ltd.

* Corresponding authors. Tissue Engineering & Additive Manufacturing (TEAM) Lab, Center for Nanotechnology & Advanced Biomaterials, ABCDE Innovation Center, School of Chemical & Biotechnology, SASTRA Deemed University, Thanjavur - 613 401, Tamil Nadu, India.

E-mail addresses: dhakshinamoorthy@scbt.sastra.edu (D. Sundaramurthi), swami@sastra.edu (S. Sethuraman).

https://doi.org/10.1016/j.bioactmat.2023.10.012

Received 16 June 2023; Received in revised form 16 September 2023; Accepted 10 October 2023

layer–by–layer manner to generate the three–dimensional objects in a pre–defined pattern [12]. Bioink is a mixture of hydrogels, cells, and biological molecules (growth factors) that help to protect cells during printing while maintaining cellular functions such as extension, survival, proliferation, and migration [13]. In medical research, 3D bioprinting has the potential to address a wide variety of applications, including drug delivery, tissue regeneration, and functional organ transplantation. Based on the bioink dispensing mechanism, bioprinting is classified mainly into inkjet bioprinting, laser–assisted bioprinting, and extrusion bioprinting [14].

Inkjet bioprinting is a cost-effective, non-contact printing approach that works on a thermal or piezoelectric dispensing mechanism & requires less viscous bioink to overcome nozzle clogging. Although inkjet printers can produce 3D models, challenges with dispensing high-viscosity materials and inconsistent droplet sizes limit their use in tissue engineering and regenerative medicine [15]. Laser-assisted bioprinting is a non-contact printing approach that utilizes laser (UV or NIR), often requiring metal or metal oxide-coated donor glass slides to transfer the bioink from donor to receiver via photothermal energy absorption. Laser bioprinting has several advantages, such as high print resolution, high printing speed, high cell viability, heterocellular patterning, multi-material printing, etc. However, low shape fidelity, frequent donor slide replacement, and long turnaround time are the major drawbacks of laser bioprinting [16,17]. Extrusion bioprinting dispenses the bioink by applying pressure through the air, mechanical piston, screw, and acoustic waves [18–20]. Bioinks used for extrusion bioprinting possess high viscosity & shear-thinning behavior to maintain high cell viability, shape fidelity, and layer stackability. Extrusion–based bioprinting is a widely explored and cost–effective method among the earlier mentioned bioprinting techniques [21]. However, the fabrication of micro-vascularized and anatomically similar complex structures is challenging due to poor resolution [22]. Also, a conventional extrusion-based bioprinting system requires support to fabricate large–sized and complex structures due to size–based limitations and gravitational forces. A comparison between inkjet, laser, and extrusion bioprinting methods with their features, advantages, and disadvantages are briefly tabulated in Table 1.

As an alternative to conventional extrusion bioprinting techniques, thermoresponsive sacrificial inks, thermoplastic-based supportive inks, and embedded bioprinting were developed to prevent shape deformation during organ fabrication [32–34]. However, the usage of support structures mostly depends on the bioink's gelation mechanism, viscosity, and printability [35–38]. In 3D bioprinting, sacrificial bioinks such as Pluronic F127, gelatin, and agarose are often used when the cross-linking time of bioinks is long or hollow constructs are required for vascularization [39–41]. Support structures may provide structural stability when printing cell-laden inks to retain shape fidelity when using bioinks with a low viscosity. PCL, PEVA, and PLA are typically used to fabricate non-removable support structures, and their strength determines the shape and stability of bioprinted tissues [31,37,42,43].

Embedded bioprinting is an emerging bioprinting technique that uses mechanically weak or low viscous bioinks like collagen, alginate, and gelatin to produce complex tissue architectures such as vascular, kidney, brain, and heart models similar to its native anatomical structures [44]. Several embedded bioprinting strategies were developed in recent years using granular or microgel support baths to create functional tissue constructs with biodegradable, non–immunogenic, and easily removable materials or sacrificial inks to enhance cell–cell communications & complex structures fabrication with overhang angles higher than 45° [45]. The development of innovative biofabrication techniques like embedded bioprinting might transform the area of tissue engineering and regenerative medicine by enabling the construction of functional tissue/organ structures [46,47]. However, literature available on this topic is limited to a few techniques on embedded bioprinting and lacks critical information on various biomaterials used for embedded bioprinting and their suitability to be used as support baths.

Table 1
Comparison between different bioprinting techniques.

Features/ Bioprinting Method	Inkjet Bioprinting	Laser Bioprinting	Extrusion Bioprinting
Dispensing mechanism	Thermal/ piezoelectric	Photothermal energy	Pneumatic/ mechanical
Resolution	10–200 μm	20–100 μm	100 μm–2000 μm
Bioink viscosity range	Low (<10 mPa s)	Low to medium (1–300 mPa s)	Medium to high (30–1 × 10^6 mPa s)
Materials used as bioinks	Alginate, gelatin, collagen, polyethylene glycol (PEG), gelatin methacrylate (GelMA), etc.	Hyaluronic acid (HA), collagen, gelatin, alginate, Matrigel®, fibrinogen, etc.	Alginate, gelatin, collagen, Matrigel®, HA, gellan gum, guar gum, xanthan gum, silk fibroin, decellularized extracellular matrix (dECM), GelMA, fibrinogen, polycaprolactone (PCL), polyethylene glycol (PEG), poly (ethylene/vinyl acetate) (PEVA), polylactic acid (PLA), etc.
Fabrication speed	Fast	Medium	Slow
Cell density	Low (1 × 10^6 to 7 × 10^6 cells/mL)	High (2 × 10^6 to 40 × 10^6 cells/ mL)	High (1 × 10^6 to 1 × 10^8 cells/mL)
Cell viability	~85–90 %	>90 %	~50–95 %
Complex shape printability	Low	Low	High
Organ printing capability	Difficult	Very difficult	Easy
Scalability	Yes	Limited	Yes
Tissues fabricated	Skin, vascular, cardiac, liver, bladder, etc.	Cardiac, bone, vascular, skin, etc.	Vascular, cardiac, skin, liver, lung, meniscus, bone, cartilage, etc.
Advantages	Precise deposition, high cell viability & cost-effective	High resolution & high cell density	Multi-material printing, cost-effective, and high scalability
Disadvantages	Difficult to print high viscosity bioinks and clogging	Costly & unable to dispense highly viscous materials	Nozzle clogging, low resolution, and cell death due to shear stress
References	[19,23–27]	[19,24–28]	[19,24–27,29–31]

Further, the challenges involved in clinical translation of tissues/organs fabricated using embedded bioprinting are not available in literature. This review discusses various embedded bioprinting techniques, the ideal requirements of support bath inks and different materials for preparing support baths (suspension). With special emphasis, different applications and tissue/organ models fabricated using embedded bioprinting systems are discussed with their advantages and drawbacks. Finally, the current limitations, challenges in clinical translation, and future perspectives of embedding bioprinting technology are also discussed.

2. Embedded bioprinting

Embedded bioprinting is a new additive manufacturing technique originally derived from embedded 3D printing, which was used to fabricate strain sensors, software robots, and complex organ models [48]. Extrusion of viscoelastic inks through the nozzles inserted (embedded) into an elastomeric reservoir is the process by which embedded printing is accomplished. Since embedded printing is carried out in an elastomeric reservoir, printed constructs are unaffected by

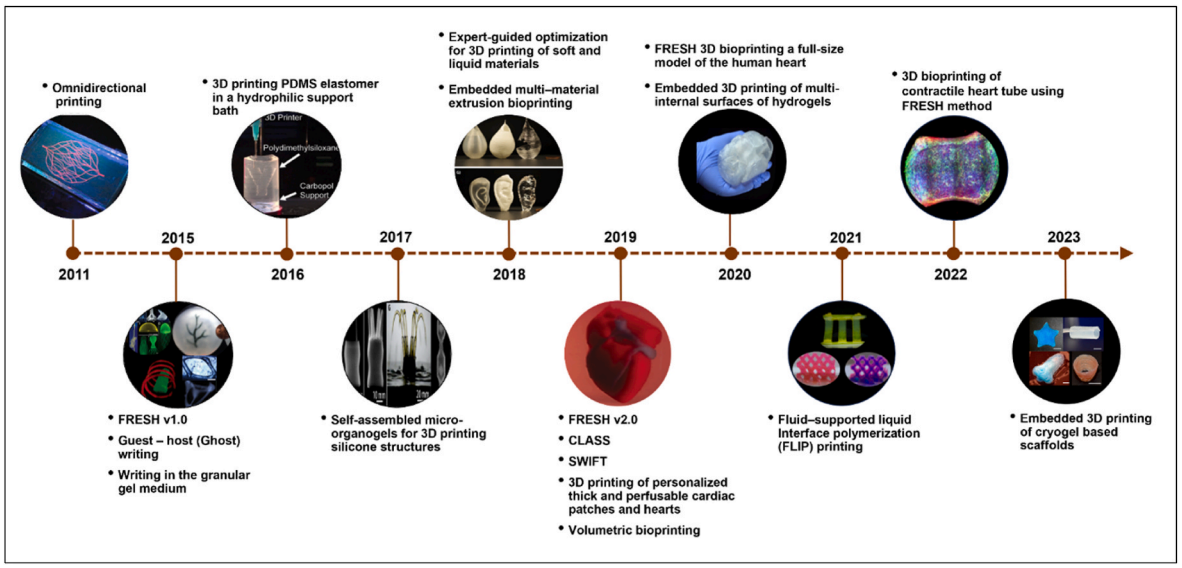

Fig. 1. Progress of embedded bioprinting from 2011 to 2023 (Reproduced with permission from Refs. [49,50,56–59,62–70]).

gravity, and hence no further support is required for printing [48]. To further extend this method, researchers replaced conventional resins/inks/support materials with cell–laden bioinks/biocompatible support matrices with unique rheological properties to print complex structures in the support medium. This strategy is an attractive alternative to conventional 3D printing and other bioprinting methods [49,50]. Embedded bioprinting is a gel-in-a-gel approach where the bioink is dispensed into hydrogel/microgel (micron sized three-dimensional network) based support bath to fabricate large and complex three–dimensional constructs by minimizing the gravitational forces [51–53]. Shear forces generated due to the motion of the print head or nozzle during printing cause the material to liquefy locally by interrupting the non–covalent and reversible bonds between the microgels in support bath systems. Upon removal of the shear forces, the medium re–establishes the bonds, and the support material wrap the bioink as soon as the tip is passed over the medium [54].

Soft hydrogels and bioinks that undergo slow gelation with low viscosity, such as fibrinogen, gelatin, dECM, collagen, etc., could be used to print tissue models or tubular constructs using embedded bioprinting by preventing gravitational forces induced collapse and helps in maintaining the print resolution up to 20 μm. Recently, organs such as the heart, kidney, and complex vascularized patient–specific cardiac patches were fabricated using an embedded printing approach [55]. Embedded bioprinting is divided into two types depending on the form or type of support matrix/ink used in the bioprinting process. In the first approach, the support matrix serves as a reservoir for depositing functional bioinks and allows the fabrication of fully functional, complex, and heterocellular tissue constructs by preventing the collapse or distortion of printed structures during the initial printing stages and holding them in place until they undergo complete crosslinking. Also, using this approach, printed constructs with insufficient mechanical strength or requiring a longer time to fuse (for spheroids) can be cultured in the support bath, where cells in the printed constructs secrete their own extracellular matrix, ultimately offering required mechanical strength comparable to native tissues. In the second approach, the sacrificial ink is deposited directly into the functional bioink, which serves as a reservoir. Sacrificial inks deposited in support baths are typically cell-free and are removed from the printed structures post-printing by altering the temperature, pH & adding chelating agents. This facilitates the creation of channels in the printed constructs that improve nutrient penetration and gas exchange. Usually, the first approach allows the fabrication of high resolution, easily removable complex structures, whereas the second approach enhances the vascularization of tissue constructs fabricated with functional cell–laden bioinks [55]. There are several types of embedded bioprinting approaches, such as omnidirectional printing, Guest–host (Ghost) writing, granular gel medium, freeform reversible embedding of suspended hydrogels (FRESH), embedded multi–material extrusion bioprinting, constructs laid in agarose slurry suspension (CLASS), sacrificial writing into functional tissue (SWIFT), volumetric bioprinting, and several other freeform bioprinting strategies were developed to print the complex constructs (Fig. 1) [34,50,56–61].

2.1. *Omnidirectional printing*

Omnidirectional printing is a variant of direct ink writing where fugitive inks are deposited into specified patterns in thermal or photocurable resins to yield interconnected microvascular networks upon liquefication. In omnidirectional printing, 23 % (w/w) of Pluronic F127 fugitive ink was dispensed in a pre–designed pattern within the photocurable Pluronic F127 – diacrylate 25 % (w/w) to generate a microvascular network upon exposure to UV light (365 nm; 5 min). Fugitive ink was removed from the support gel through liquefication at 4 °C, which led to the formation of vascular networks in desired structures (Fig. 2A). Rheological analysis of fugitive ink showed shear–thinning behavior, and less shear elastic modulus (10^4 Pa) than the support bath, which allowed smooth ink extrusion through the nozzle. Different diameter microchannels (18 μm–170 μm) were developed by varying the pressure and speed proportional to the diameter of the needle. Further, the diffusion of nutrients in hydrogel constructs was analyzed by injecting rhodamine–based fluorescent dye into 125 μm microchannels. Diffusion studies showed the distribution of dye through the matrix with respect to time and indicates the potential of this method to create tissue constructs with native diffusion properties suitable for tissue engineering and regenerative medicine applications [59]. Removing thermoresponsive polymers such as Pluronic from microchannels in omni-directionally printed cell-laden tissue constructs poses a substantial challenge, as it requires lowering the temperature that may reduce the viability of the cells.

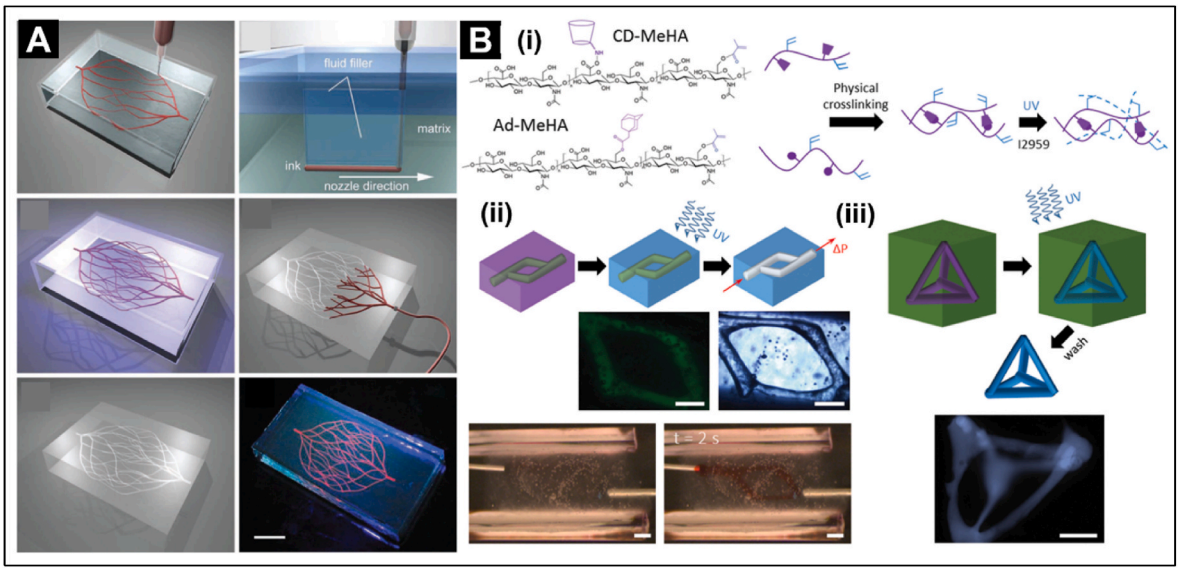

Fig. 2. [A] Omnidirectional printing process where the fugitive ink was deposited into the functional ink to create the vascularized networks (scale bar - 10 mm) (Reproduced with permission from Ref. [59]); [B] Guest – host writing – (i) Hyaluronic acid modified with methacrylate to create guest–host molecules for physical and photocrosslinking; (ii) Printing of microchannels inside support gel and removal of sacrificial ink after secondary crosslinking with UV and (iii) Printing of self–supportive structures inside the support gel (scale bars - 500 μm) (Reproduced with permission from Ref. [58]).

2.2. GHost writing (guest–host)

GHost writing method is based on the supramolecular assembly of host–support materials. Like other support bath fabrication methods, the GHost method also depends on non–covalent and reversible force–based bond disruption mechanisms of supramolecular assembly to print materials in any shape in 3D space [71]. Functional bioink was prepared with 5 % (w/v) hydrogel containing 1:1 ratio of Ad–HA and CD–HA. In both Ad–HA and CD–HA, 25 % of HA repeat units were modified. Further, Ad–HA and CD–HA with 40 % modifications in HA repeat units were mixed at 1:1 to form 4 % hydrogel for support gel. Multicellular constructs were printed using mesenchymal stem cells (MSC) in functional bioink and fibroblasts (3T3s) in the support ink with more than 90 % viability. Though the printing process showed good cellular viability, printability and shape fidelity, lack of mechanical stability of printed constructs limited the performance of these printed structures in perfusion studies. To further improve the mechanical strength, photoactive bioinks were prepared using hyaluronic acid modified with methacrylate groups (20 %) and further attached with Ad or CD to print constructs. This additional photocrosslinking step resulted in supramolecular bonding and covalent crosslinking. In this process, supramolecular bonding helps to stabilize the constructs during printing and UV–based (320–390 nm) photocrosslinking mechanisms help to create mechanical stable constructs post–printing. Finally, the printed constructs were extracted from the support bath by washing with β–CD that competes with CD–HA and Ad–HA leading to dissociation of non–methacrylated support bath hydrogels (Fig. 2B) [58].

2.3. Granular gel medium (printing then gelation approach)

Support bath materials such as Carbopol form microgels that become granular gel support medium to print complex structures at physiological conditions [72]. Polymers with reversible thermal behavior like gelatin, photocrosslinkable materials and ionically crosslinkable alginate hydrogels, have been used as bioinks to fabricate complex structures [73]. It is based on a two–step gelation mechanism where the initial gelation after printing is caused by adjusting the bed temperature, and the second gelation occurs upon addition of divalent cations. Printing bioink into the Carbopol supportive bath helps to extrude and hold the materials in a pre–designed shape before initiating photo/-thermal/ionic gelation (Fig. 3A) [56]. Temperature dependent gelation occurred by incubating the printed constructs in a supportive bath at 25 °C due to the presence of gelatin in the printed constructs. During post–processing, the 37 °C pre–warmed calcium chloride was introduced to crosslink alginate and remove gelatin [74].

Usually, the strength of the supportive medium depends on the concentration of polymers and the pH of the solution. Jin et al., showed that Carbopol can form internal crosslinks by polyalkenyl-polyethers through microgels and prevents complete dissolution in water. Due to higher shear forces at the needle tip during the printing than the local yield stress of supportive baths, Carbopol becomes fluid during printing and eventually forms gel post–printing to keep the printed structure intact without shape deformation (Fig. 3B). This research group had printed blood vessels similar to Y–shaped complex constructs with 3 % alginate and 10 % gelatin bioink in a 0.8 % Carbopol supportive medium. Printed Y–shaped constructs were removed from the Carbopol supportive bath without affecting the shape with 0.9 % sodium chloride, and gelatin was removed by increasing the temperature to physiological conditions. NIH 3T3 cell–laden printed constructs showed more than 80 % viability post–printing, and after three days of culture, the cell viability increased to 86.1 % [74]. This method has several advantages compared to gelation during the printing approach, such as clog–free material extrusion, robust support, complex structure fabrication and easy gelation. Bhattacharjee et al., fabricated a supportive medium with Carbopol to print more complex structures such as a 4 cm long model of DNA with 0.1 % polystyrene microspheres (diameter 100 μm), solid closed shells, capsules, octopus, and jelly fish models with photocrosslinkable PVA. Branched tubular networks with a diameter of 100–200 μm were fabricated with 27 % photocrosslinkable PVA and 0.1 % microspheres containing 40 connected vessels and 12 junctions similar to the native conditions. This study also showed the importance of support medium to fabricate complex structures without shape deformations due to surface tension or gravity [56]. However, removing the printed constructs from a Carbopol support bath requires alterations in pH and salt concentration to liquefy the support bath. These alterations may often influence cellular activities in the printed constructs.

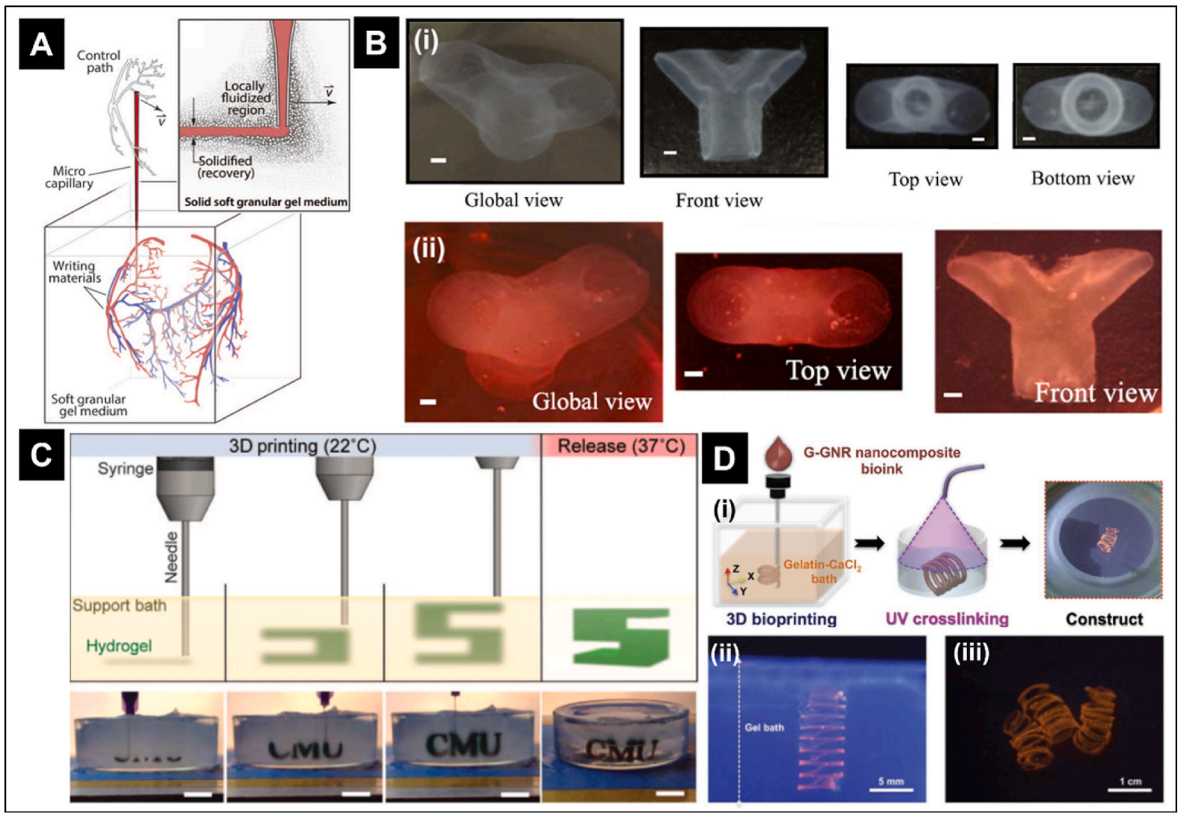

Fig. 3. Schematics of granular gel and FRESH embedded bioprinting strategies. [A] Granular gel medium (Reproduced with permission from Ref. [56]). [B] Printing of Y-shaped construct – (i) Different views of Y-shaped construct printed in 0.8 % carbopol support bath using alginate bioink. (ii) Printed Y-shaped cellular construct (scale bar - 1 mm) (Reproduced with permission from Ref. [74]); [C] Steps involved in FRESH printing (scale bar - 1 cm) (Reproduced with permission from Ref. [50]); [D] Embedded bioprinting using the G-GNR nanocomposite bioink in 2 % gelatin support bath. (i) Schematics of printing process. (ii & iii) Spiral construct after printing & removed from the support bath (Scale bar – 5 mm & 1 mm) (Reproduced with permission from Ref. [75]).

2.4. Freeform reversible embedding of suspended hydrogels (FRESH)

Prof. Adam W. Feinberg and his research group originally developed the Freeform Reversible Embedding of Suspended Hydrogels (FRESH) method at Carnegie Mellon University (CMU). FRESH was patented by Fluidform and commercialized through several companies like Cellink, Allevi and Advanced Biomatrix under the trade name of Life support®. In FRESH method, support bath comprising gelatin microparticles with diameter of 55.3 ± 2 μm is used. Bingham plastic behavior was observed, when the gelatin microparticles are maintained at room temperature during the printing process [76]. The FRESH method has several advantages like material deposition in 3D space, dual materials printing, and complex biological structure fabrication [77,78]. In FRESH based printing, low viscous bioinks (alginate, collagen, fibrinogen, decellularized extracellular matrix, methacrylated gelatin (GelMA), gellan gum, etc.) are printed inside the hydrogel suspension, which has fluid–like behavior at higher shear stress during printing and gel behavior at low shear stress post–printing helps to improve the print fidelity [79–81]. In this method, $CaCl_2$ was added to gelatin support bath and temperature was maintained at 22 °C to retain the sol-gel transition of support bath for printing bioinks like alginate, fibrinogen, collagen, etc. After printing, the printed constructs are removed from the support bath without shape deformation by increasing the temperature to 37 °C (Fig. 3C). C2C12 myoblasts laden printed constructs showed 99.7 % viability after printing, and active cell proliferation was observed within seven days in the constructs printed with Matrigel®, collagen and fibrinogen bioinks [50]. Recently, Lee et al., developed FRESH v2.0, in which the resolution of constructs was improved by the addition of 0.25 % (w/v) Pluronics and 0.1 % (w/v) gum arabic along with the 2 % (w/v) gelatin support bath. Also, FRESH v2.0 contain small diameter gelatin microparticles (25 μm), which helps to obtain a print resolution of 20 μm. Using FRESH v2.0 approach Lee et al., fabricated ventricle models with proper micro vascularization using pH–driven gelation (pH 7.4) of collagen bioink [70]. Further, JM Bliley et al., used FRESH v 2.0 to print contractile heart tubes using human stem cell–derived cardiomyocytes and cardiac fibroblasts to maintain synchronous beating for up to 1 month [65].

Nydus One Syringe Extruder (NOSE) is another approach of FRESH used by Bessler et al., where open–source 3D printer Prusa i3 was converted to dispense hydrogels for bioprinting. By using this approach, cell laden constructs (HEK 293 and embryonic stem cells) were printed with 2 % alginate functional bioink, and gelatin slurry was used as a support bath. The printed construct was found to have greater than 80 % cell viability [82]. Edwin et al., used a FRESH support bath system to print iPSC–laden gradient constructs with an affordable, customizable, open–source bioprinter called ModiPrint. About 100 μm diameter filaments were printed using 2 % RGD linked alginate with a print speed of 12 mm/s, 0.1 mm needle inner diameter, 2000 mm/s^2 acceleration and 0.01 junction deviation. After 24 h, cells in printed constructs showed 69 % viability, which increased to 86 % on day 7. Furthermore, this also can generate concentration gradients embedded in hydrogels with flexible geometry [83].

Spatially complicated structures were printed by Zhu et al., through FRESH printing in a 2 % gelatin supportive bath along with 11 mM $CaCl_2$. Spiral constructs were printed with G–GNR (GelMA coated gold nanorods) and 2 % alginate bioink in a gelatin support bath at 4 °C, where it behaves like Bingham plastic. This behavior helps to maintain the printed spiral shapes within the support bath during printing and crosslink with UV (800 mW, 30 s). After UV exposure, the bioprinted constructs were removed by heating the support bath to 37 °C (Fig. 3D)

[75]. Hinton et al., used a modified FRESH method to print poly (dimethylsiloxane) (PDMS) hydrophobic elastomeric polymer inside a hydrophilic Carbopol support bath. 3D printing of complex structures with PDMS is always challenging due to the long curing time and low elastic modulus of PDMS that requires printing in a support bath to obtain the designed shape. The printed constructs were removed from the Carbopol support medium by washing for 15 min with a monovalent cationic buffer solution such as PBS to liquefy (shrinking Carbopol microgels) the support medium. The potential of this approach was demonstrated by printing helical tubes and perfusable tubes by dye perfusion method. However, this method has some limitations, such as lateral fusion of extruded PDMS filaments, and it required pressurized conditions to hold the constructs in defined shapes [67]. Despite the notable effectiveness of the FRESH bioprinting technique as an embedded printing approach, achieving human-scale organ requires further research on utilizing the support bath itself as culture vessel until the printed constructs completely mature into fully functional tissues and organs.

2.5. Embedded multi–material extrusion bioprinting

This approach involves printing multiple bioinks with customized bioprinting systems with multiple bioink stations in a single cartridge or multiple cartridges. Multi-material bioprinting enables precise deposition of various bioinks, containing biomaterials, cells, and other biomolecules to fabricate complex multi-cellular tissue constructs resembling native biological systems [84]. Various support bath materials, including Pluronics, gelatin, and agarose were used for preparing support baths for embedded multi-material bioprinting [34,85]. Rocca et al., used Pluronics F–127 as a supportive medium to print complex structures with low viscous materials. Rocca et al., developed a customized bioprinter with a unique custom needle design (single nozzle 159 μm; multi-nozzle 210 μm), which allows printing several materials at higher resolution without clogging. The stiffer core needle was covered with multiple needles to prevent needle bending during printing in the support bath. Further, the outer portion of the needle helps remove the Pluronic support medium during the printing process. After removing the needle from the supportive bath, Pluronic returns to its original state due to its thixotropic nature without forming air bubbles. This typical needle design begins with assembling three needles into a core needle surrounded by three layers of support structures with a larger diameter and the Teflon tube for bioink transfer from the reservoir. In this method, 2 % alginate was used as functional bioink and the thermoresponsive support bath comprised of 23 % Pluronic F–127 and 0.05 % $CaCl_2$ for easy crosslinking. By optimizing printing parameters like printing pressure, speed and interline distance, the best–printed constructs in the support bath were observed at 20 PSI, 10 mm/s and interline spacing of 300 μm. Different coloured constructs and organ models such as heart, kidney, and other complex structures like a star, Mobius strip, and Klein bottle were printed through this method [34].

Using a Microfluidic Multi-material Manufacturing (M^3) approach, Hassan et al., developed a compelling approach for bioprinting intricate tissues and organs in gelatin/agarose support baths tailored to meet *in vivo* implantation. In this study, the authors modified the extruder of a

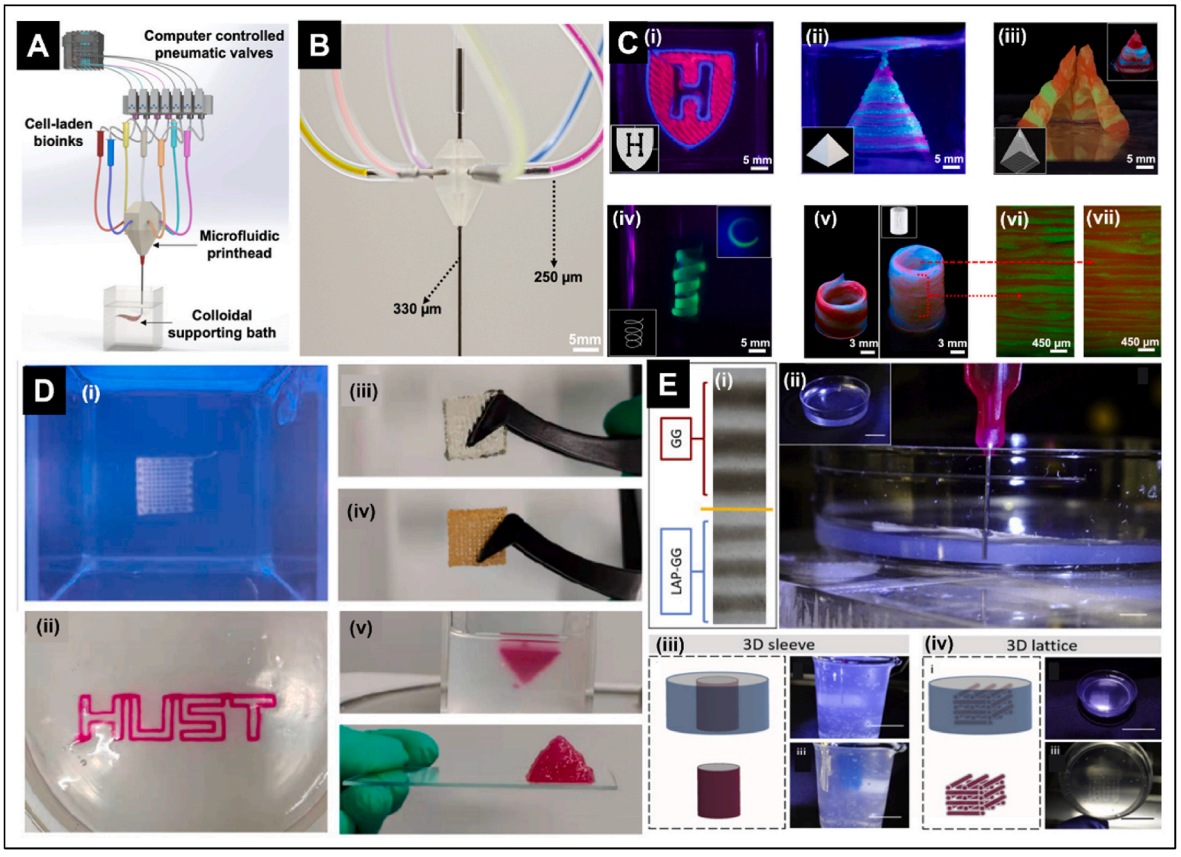

Fig. 4. Constructs developed using multi-material and CLASS embedded bioprinting techniques. [A] Schematic of the M^3 bioprinting system; [B] Illustration depicting the single nozzle seven-ink printhead; [C] Various complex models were printed using the M^3 bioprinting system. (i) Harvard logo. (ii & iii) Solid and hollow pyramids. (iv) Spiral (v) Hollow cylindrical tube (vi & vii) Fluorescence microscopy images of the outer and the inner walls (Transverse section) (Reproduced with permission from Ref. [86]); [D] Scaffolds printed in agarose support bath. (i) Square shape. (ii) HUST letters. (iii) Embedded bioprinted structures. (iv) Constructs printed in air. (v) Inverted triangle printed inside support bath (Reproduced with permission from Ref. [87]); [E] Stability of constructs printed in agarose support bath. (i) Swelling of GG & LAP-GG strands printed in agarose support bath. (ii) Extrusion of strands inside support bath. (iii) Digital model & actual printed 3D sleeve. (iv) Digital file & actual printed 3D lattice structure in agarose support bath (Reproduced with permission from Ref. [88]).

commercial 3D printer with a 3D SLA printed printhead attached to a 23G metal connector to dispense the bioinks (Fig. 4A and B). The main advantage of this system is its ability to extrude up to seven distinct materials simultaneously while maintaining precise structural resolution. The precision was achieved by using Wago valves, which control the opening and closing of channels to facilitate the controlled extrusion of specific bioinks from the reservoirs. Agarose colloidal gel (ACG) and gelatin colloidal gel (GCG) serve as support baths for printing composite bioinks composed of alginate and gelatin methacryloyl (GelMA). Due to the early sol-gel transition, biocompatibility, cell supportiveness, and easy removability, GCG was used for printing different complex shapes such as the Harvard logo, spiral, hollow and solid pyramids, cylindrical tubes, etc. (Fig. 4C). The M^3 system demonstrated successful 3D printing of cellularized liver and muscle-like models, exhibiting high cell viability and expression of native markers (Albumin – Liver; Myosin heavy chain – Muscle). Finally, GCG gels structurally mimicked extracellular matrix, exhibited favorable cell invasion (fibroblasts, immune cells, and endothelial cells) when implanted in rats, along with the ability to retain structural integrity post-implantation [86]. In future, more emphasis on developing multi-material systems for extruding materials with varying viscoelastic properties will aid in addressing the challenges associated with tissue and organ fabrication.

2.6. Constructs laid in agarose slurry suspension (CLASS) method

Constructs Laid in Agarose Slurry Suspension (CLASS) method uses agarose as a support bath to print and maintain low viscous bioinks in cell culture conditions. 1 % agarose support bath was used to print 2 % alginate bioink to optimize printing parameters such as minimal required volume, blending time, speed, and pressure. Compared to the gelatin support bath used in the FRESH approach, the agarose support bath showed better printing reliability regardless of blending time. Bioink deposition and crosslinking capabilities in agarose support bath used in the CLASS system were evaluated using 5 % GelMA bioinks. The printed constructs with 5 % GelMA were crosslinked by exposure to UV light for 60 s. Translucent properties of agarose hydrogels did not influence the photocrosslinking of printed constructs. Cell proliferation and cell spreading were observed for 11 days in the printed cell–laden constructs (5 % Gel–MA, 10 % Matrigel®, and 3 % fibronectin (1 mg/mL)). Compared to other printing methods, the main advantage of this system is culturing the printed constructs inside the supportive hydrogels until the cells start to secrete their own ECM [57].

As a support bath, agarose has also been used by many researchers to bioprint different tissue constructs like skin, bone, and other tissues [87,88]. An agarose support bath was used in a recent study to deposit various materials, including pectin, GelMA, etc., using a technique called suspended layer additive manufacturing (SLAM). Various concentrations of GelMA bioink were extruded in agarose support baths and their printability, water absorption rate, swelling ratio, and deformation rate were evaluated. Based on the rheological properties and printability study on various support baths (0.25 %–1 % agarose), 0.5 % agarose maintained shape fidelity with sufficient mechanical strength and yield stress. The developed agarose bath provided support for printing various structures, including square shapes and triangles, and were easily removed from the bath without deformations (Fig. 4D). Moreover, constructs that were printed and cured in support bath showed a lower mechanical strength than constructs that were exposed directly for curing, demonstrating that support baths influence bioink crosslinking percentages [87]. Cidonio et al., also used a 0.5 % agarose-based support bath to prevent the shape deformation of bone tissue constructs printed using only gellan gum (GG) & Laponite® – GG bioink. GG fibers, when printed within the support bath, exhibited elevated swelling in comparison to Laponite®-GG. Consequently, while GG was used for printing large cylindrical and lattice structures in agarose support bath resulted in poor shape fidelity due to high swelling behavior (Fig. 4E). Conversely, constructs composed of Laponite®-GG facilitated the precise deposition of bioink at high resolutions and sustained their shape fidelity even after extraction from the support bath, with minimal swelling [88]. Although agarose has shown promising results as support bath, there are challenges in using agarose as bath such as difficulties in leaching from printed constructs and potential interference with the physical, chemical & biological properties of the constructs.

2.7. Sacrificial writing into functional tissue (SWIFT)

Fabrication of complex tissues or organ models require mimicking native cell density, cellular organization with biomimetic vasculature and ECM architectures [89]. For example, cell numbers used in bioprinting of cardiac tissues or skeletal muscle tissues are usually two to three folds less than the native tissues due to several limitations in acquiring and printing billions of cells without affecting their viability [71,90]. Hence, self–assembly of cells like induced pluripotent stem cells (iPSC) and embryonic stem cells (ESC) into spheroids to create mini–organoids is an alternative approach for fabricating complex tissues/organs, which require billions of cells [91]. In sacrificial writing into functional tissue (SWIFT) approach, organ building blocks (OBB) are produced using iPSC–derived spheroids and extracellular matrix proteins to generate artificial tissue matrices with high cell density similar to natural tissues (Fig. 5A). ECM solution was produced with 4×10^5 organ building blocks, collagen and Matrigel® at 0–4 °C, where it behaves as a fluid that helps deposit the gelatin sacrificial ink for vascularization. When the tissue construct was incubated at 37 °C, the ECM solution underwent gelation, and the sacrificial gelatin became solution by leaving interconnected tubular constructs in the embedded gel (Fig. 5B). Vascularized tissues with different lumen diameters (0.4 mm–1 mm) were printed with varied print speeds (0.5 mm/s to 4 mm/s). Immediately after printing, the constructs with and without channels were screened for cell viability. Constructs without channels showed reduced viability (no channels – 0.2 (normalized)) and necrotic tissue formation at the core regions and viable cells at periphery. In contrast, constructs with channels showed greater than 90 % cell viability in normoxic (21 % O_2, 5 % CO_2) and hyperoxic (95 % O_2, 5 % CO_2) conditions. Further, constructs perfused for 12 h with a 250 μL/min flow rate showed slight tissue contraction and remodeling compared to constructs without channels. Endothelialized lumens were obtained by perfusing human umbilical vein endothelial cells (HUVEC) with 10^7 cells/mL for 20 h. Perfusable cardiac tissues were printed using stromal cells and human iPSC–derived cardiac OBBs with a cell density of 60×10^6 per mL and 180×10^6 per mL. The construct started beating asynchronously with irregular calcium waves on day 1 and showed spontaneous and synchronous beating with regular calcium waves on day 7 throughout the tissue [60]. Further, these constructs showed enhanced beating upon addition of 2 mM calcium to the medium. In addition, spontaneous contractions were observed when the printed tissues were subjected to paced stimulation with platinum electrodes separated with a distance of 750 μm. Perfusion of non–selective β–adrenoreceptor agonist (isoproterenol) showed an increased beating rate, while the addition of 1–heptanol gap junctional antagonist showed reduced contractile amplitude. Patient–specific left anterior descending (LAD) coronary artery networks were printed in the cardiac OBB matrix specified the ability of SWIFT printing towards the translation of vascularized tissues and organ printing (Fig. 5C). However, common problems such as organoid maturation, micro vascularization and contractile imbalance (SWIFT cardiac tissues – 1 % strain; adult cardiac tissues – 20 % strain) were observed in the printed constructs [60].

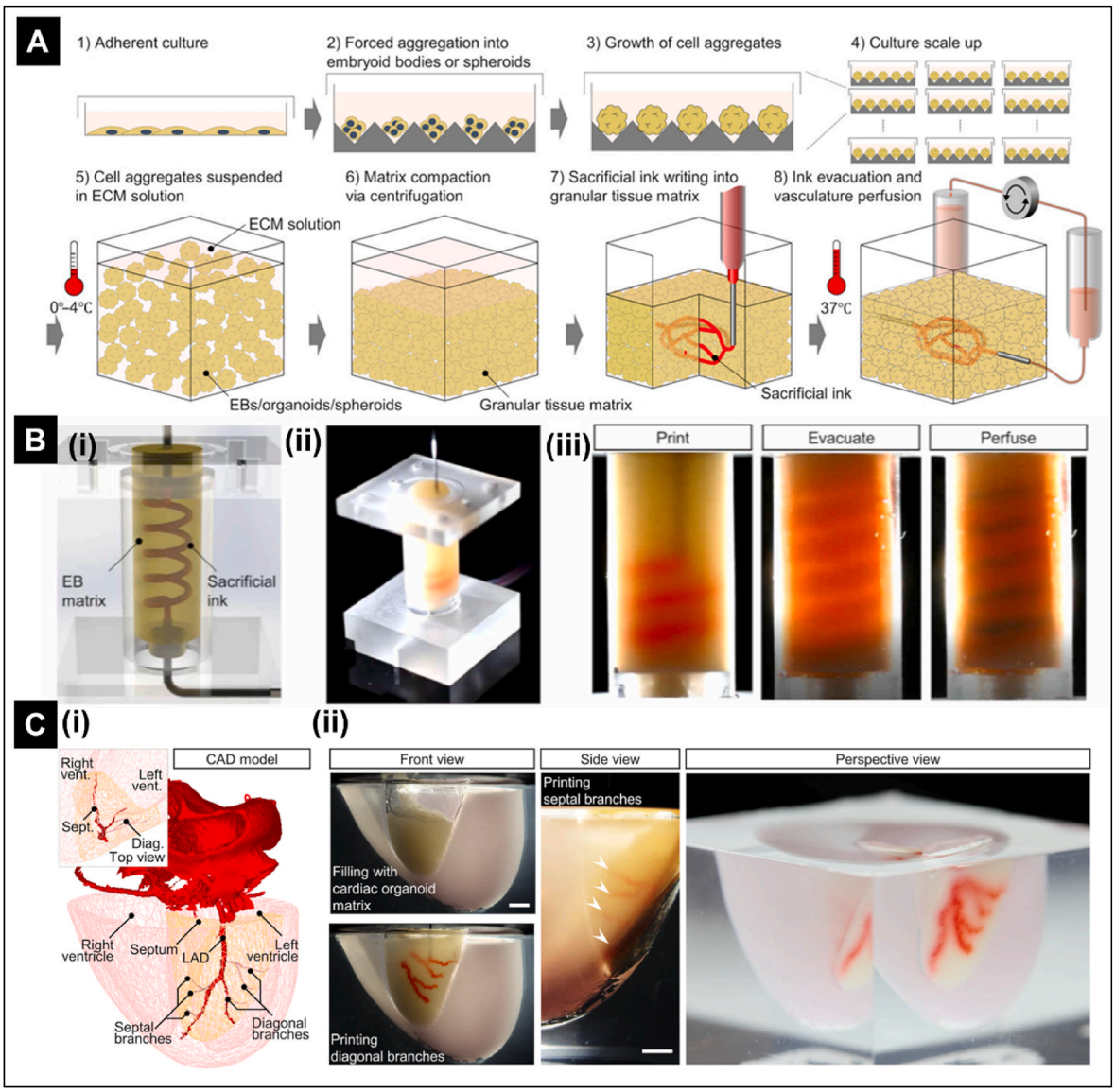

Fig. 5. SWIFT based embedded bioprinting. [A] Steps involved in SWIFT approach. [B] Fabrication of vascularized structures. (i) CAD representation of sacrificial ink and support matrix. (ii) Deposition of sacrificial ink inside support matrix. (iii) Steps involved in developing vascular constructs like printing, evacuation, and perfusion; [C] Fabrication of cardiac tissues using SWIFT. (i) 3D CAD model of human heart with left anterior descending (LAD) artery and a diagonal branch. (ii) Printing of LAD artery along with diagonal and septal branches in Polydimethylsiloxane mold using SWIFT approach (Scale bar – 5 mm) (Reproduced with permission from Ref. [60]).

2.8. *Volumetric bioprinting*

Volumetric printing method was designed to overcome the challenges observed in extrusion–based embedded bioprinting systems where the three–dimensional objects were created by depositing materials in a layer–by–layer manner [92]. In volumetric bioprinting, the entire object creation was carried out at once within seconds by focusing lights on photopolymerizable resins rather than sequential deposition of materials (Fig. 6A and B). Here, the photocurable polymer matrix only solidifies at specific areas where it is exposed to light of specific wavelengths for the required time to initiate gelation [92]. Typically, the bioresins used for volumetric bioprinting should contain an optimal concentration of photoinitiators to penetrate the light into the matrix and allow for maximum polymerization. The main advantage of volumetric bioprinting is the printing time, as it requires much less time for fabricating complex structures of different scales, and it majorly depends on the height of the constructs. Also, compared to extrusion bioprinting and DLP, this bioprinting technique reproduces the surfaces of the printed structures smoothly, as observed in digital models (Fig. 6D). Using volumetric bioprinting approach, Bernal et al., developed 10 % GelMA hydrogel based bioresins (gelRESIN) with LAP photoinitiator (0.037 %) for printing large living tissue constructs by exposing them to the visible light laser (Fig. 6C) and fabricated ball and cage cardiac valve prosthesis, meniscus and trabecular bone models to show the efficacy of the printing method in the fabrication of complex tissue/organ models (Fig. 6E). *In vitro* experiments showed high cell viability (>85 %), proliferation, differentiation, and support for heterocellular constructs. Further, newly synthesized glycosaminoglycans and collagen I in the printed constructs confirmed the cell–supportive nature of the volumetric bioprinting process [93]. In future, alterations to the currently followed post-processing techniques are necessary to minimize the wastage of unpolymerized bioinks and cells that leach out from the printed constructs, as well as to enhance the cell viability.

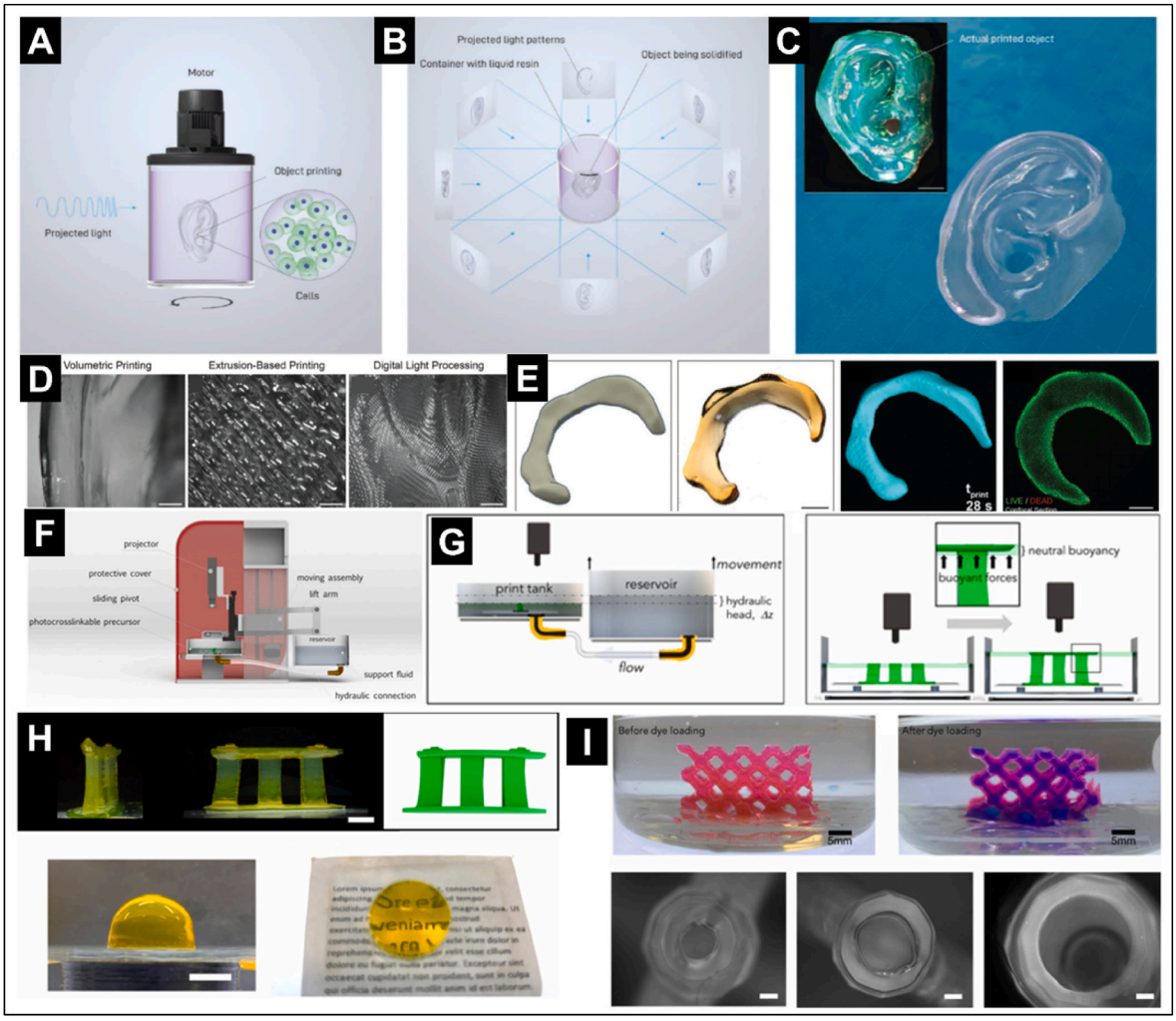

Fig. 6. Steps involved in volumetric bioprinting & Fluid–supported Liquid Interface Polymerization (FLIP). [A & B] Overview of volumetric bioprinting process & printing of human auricle model; [C] Stereomicrograph of the printed hydrogels using volumetric bioprinting (scale bar - 2 mm); [D] Surface images of auricles printed using different printing techniques such as volumetric printing, extrusion printing and digital light processing (scale bars - 500 μm) and [E] Meniscus 3D design and 3D printed model *in vitro* cultured for 28 days (scale bars - 2 mm) (Reproduced with permission from Ref. [93]); [F] Components of FLIP 3D printer; [G] Schematic representation of procedures involved in the FLIP 3D printing process; [H] Printing of Marina Bay Sands Hotel model & dome structures using FLIP printing (Scale bar = 10 mm (top) and 5 mm (bottom)); [I] Hollow structures before and after loading dye & cross–sections of different sized lumens (Scale bars 5 mm (top), and 500 μm (bottom) (Reproduced with permission from Ref. [64]).

2.9. Fluid–supported liquid Interface polymerization (FLIP) printing

Fluid–supported Liquid Interface Polymerization (FLIP) printing is a digital light processing (DLP) based approach developed primarily to overcome the problems encountered in conventional printing strategies by reducing the printing time and also to develop complex structures using soft hydrogels [64]. FLIP uses Fluorinert FC–40 (perfluorinated oil) as a support bath and a thin photocrosslinkable hydrogel precursor as a printable ink for fabricating geometrically complex configurations (Fig. 6F and G). This fluid support bath should satisfy mainly three functions to obtain better print resolution such as lifting the precursor solution from the print bed to allow continuous printing, supporting the printing of overhanging structures without collapsing, and removing of precursor solution from the nearby places of printed structures while the printing process is ongoing. Several precursor solutions like PEG–DA, PEDOT:PSS/PEG575–DA, GelMA and Pluronic F127 were used to fabricate different models such as Marina Bay Sands (MBS) hotel model, geodesic dome, aortic valves, a lymph vessel with an internal valve, cartilaginous structures and hollow channels (Fig. 6H). Similarly, hydrogels with various mechanical properties (10 kPa–3 MPa) were also printed to show the efficiency of the FLIP printing model–based support baths for printing of bioinks with low mechanical strength. Bioprinting of GelMA bioinks inside the FC–40 hydrogels showed excellent biocompatibility of these fluid–based support bath systems in the fabrication of tissue/organ models. However, a reduction in the cell viability at the core of the construct was observed in the thick constructs due to the difficulties in gases exchanges & nutrient deficiency. Finally, free–standing vascularized tissue formation abilities using FLIP printing was evaluated by printing PEG hydrogels with different lumen diameters (1–3 mm) and wall thickness of 500 μm (Fig. 6I) [64]. The FLIP printing process is constrained by its exclusive compatibility with photopolymerizable polymers, thus restricting its applicability to a narrow range of materials, causing variability in printed structures and properties.

2.10. Aspiration Assisted freeform bioprinting (AAfB)

Spheroids are compact three-dimensional cell clusters usually formed into spherical shapes through cell-cell interactions, also playing a crucial role in tissue engineering, drug screening, and disease models owing to their resemblance to native tissues [94,95]. Various bioprinting techniques have been explored for spheroids bioprinting,

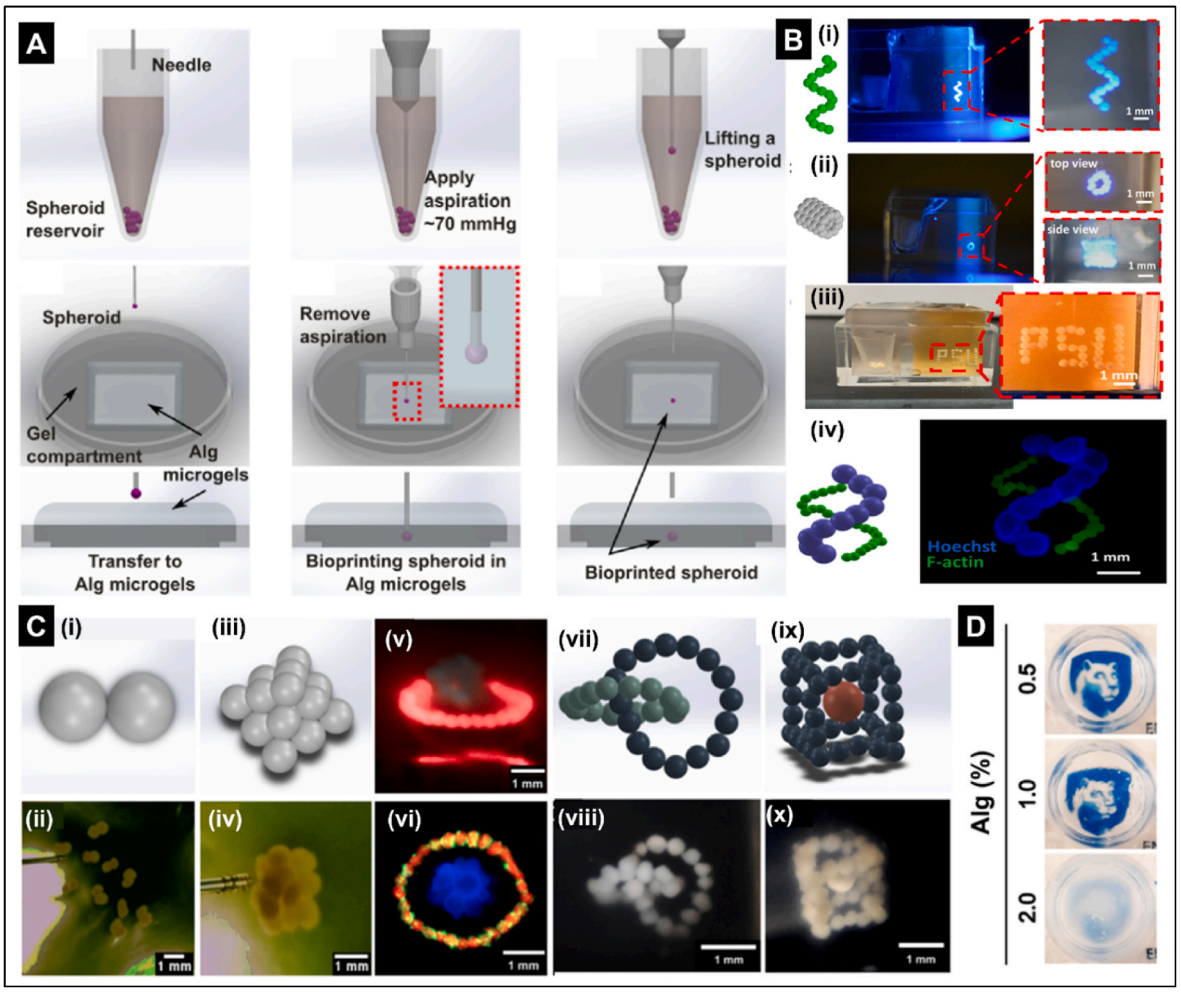

Fig. 7. Schematics & constructs printed using Aspiration Assisted freeform Bioprinting (AAfB). [A] Steps involved in AAfB using spheroids (Reproduced with permission from Ref. [98]); [B] Complex shapes printed using MSC spheroids in 1.2 % Carbopol support bath. (i) Helix-shape. (ii) Five-layer tubular construct. (iii) Initials of Penn State University (PSU). (iv) Double helix-shape construct (Scale bar – 1 mm) (Reproduced with permission from Ref. [97]); [C] Various shapes printed in 0.5 % alginate blended for 30 min support bath. Illustrations (top) and bioprinted structures (bottom) of (i & ii) Dumbbell. (iii & iv) Pyramid. (v & vi) Saturn. (vii & vii) Linked rings and (ix & x) Spheroid-in-a-box constructs (Scale bar – 1 mm); [D] Transparency of alginate microgels blended for 30 min (Reproduced with permission from Ref. [98]).

including extrusion-based methods with spheroids in gel, the Kenzan method using needle skewering, and drop-on-demand with encapsulated spheroids. However, challenges remain in achieving precise 3D bioprinting of spheroids due to limitations in positioning, structural damage, reduced viability, and layer-by-layer building [96,97]. Recently, Ozbolat et al., developed an advanced bioprinting technique known as Aspiration Assisted freeform Bioprinting (AAfB), which aims to fabricate tissue constructs like cartilage, bone, etc. [98]. AAfB printing steps involves stages such as spheroid collection, transfer to a reservoir, aspiration using pressure to position them onto gel substrates or support baths, and repetition for precise tissue formation (Fig. 7A) [98]. Among different concentrations of Carbopol (0.8 %, 1.2 %, 1.6 % w/v) support baths, 1.2 % exhibited enhanced positional accuracy (22 %) and the required yield stress (25.7 Pa) to protect spheroids from damage. Further, 1.2 % Carbopol and 0.5 % alginate were used to evaluate spheroid stability and cell viability. Carbopol showed adverse impact on cell viability (~74 %) in contrast to the effective preservation of viability (~93 %) and spheroid shape with 0.5 % alginate microparticles. Further, the effectiveness of the AAfB technique was demonstrated by successfully bioprinting various structures in a 1.2 % Carbopol support bath, including a DNA-strand, PSU (Penn State University), circle, cartilage, and bone-like tissue substitutes (Fig. 7B). Despite the promising outcomes in terms of differentiating hMSCs spheroids into chondrogenic and osteogenic lineages, the utilization of Carbopol as a support bath remains challenging due to the frequent disassembly of deposited spheroids upon extraction, while the use of alginate microparticle-based support lacks transparency, which is crucial for visualizing the deposited spheroids during the printing procedure [97].

To address the opacity issue of alginate-based support baths in AAfB, the size of alginate microparticles was reduced further through extended blending time, and optimal concentrations & viscoelastic properties for spheroid transferring, and fusion were assessed. Initially, different concentrations of alginate (0.5 %, 1 %, 2 %) were prepared and cross-linked using 4 % calcium chloride and further blended for 10, 20, and 30 min. Further, extended blending time reduced the opaqueness and particle sizes of 0.5 % and 1.0 % alginate microgels to 31 μm and 45 μm from initial sizes of 55 μm and 121 μm respectively. However, compared to 0.5 % & 1 %, 2.0 % alginate exhibited larger particles and was more resistant to size reduction. Moreover, the viscoelastic properties of 0.5 % and 1 % alginate microparticles were more suitable for spheroids printing than 2 %, which had higher yield stress and viscosity that induced deformations in the spheroids. Further, 0.5 % alginate microparticle support bath, blended for 30 min, was subsequently utilized to demonstrate the capability of MSC spheroids in facilitating the 3D printing of intricate shapes, including dumbbell, pyramid, Saturn, linked

rings, etc. (Fig. 7C). Furthermore, printing accuracy, circularity, spheroid fusion, and intersphere angle were observed better in 0.5 % alginate microparticles blended for 30 min compared to other blending times and 1 % alginate microparticles blended for different times (Fig. 7D). Finally, bone tissue constructs were fabricated either by printing only MSC spheroids or heterocellular spheroids by mixing human peripheral blood-derived monocytes THP-1 in different ratios with MSC (2:1 hM SCs:THP1 and 3:2 hM SCs:THP1). The heterocellular spheroids that were 3D printed in a 0.5 % alginate support bath with 30 min of blending exhibited more calcium deposition and expression of bone-specific markers in contrast to the hMSC-only group, offering a more effective model for the study of bone tissue formation [98]. Although these models exhibited substantial potential for developing bone or cartilage tissues for regenerative and drug screening applications, the extended processing time required for spheroids preparation, transfer, and placement (spanning from hours to days) poses challenge in viability for the embedded cells [97,98].

2.11. Other freeform bioprinting strategies

Researchers have also developed several other freeform bioprinting strategies for printing complex tissues and full–length organ models [99]. Daniela et al., developed a viscous, hydrophobic, hydrocarbon–based support bath system using perfluorotributylamine ($C_{12}F_{27}N$) to print centimeter sized complex tubular constructs. Agarose functional bioink (1.5 %) was used to print human mesenchymal stem cells (hMSC) and MG63 cells in support fluid with a custom robotic arm dispensing system. This process showed good spherical droplets during printing due to the density of fluorocarbons, hydrophobicity, and temperature differences between agarose and fluorocarbon. The printed constructs were stable for up to six months in the fluorocarbon support bath system without degradation. Moreover, cell–laden constructs showed more than 95 % cell viability with an increase in modulus from 3 kPa (on day 1) to 10 kPa (MG63) and 15 kPa (hMSC) on day 14, as a result of matrix remodeling. However, the efficiency of extraction procedure and effect of residual support bath needs to be evaluated [100]. Noor et al., formulated a transparent supportive medium to fabricate complex structures (crisscross construct, hollow ball, and hand) based on thermal gelation of omentum bioink and ionic stabilization of the supportive medium (Fig. 8A and B). This study focused on the formulation of a support bath with sodium alginate (0.32 %), xanthan gum (0.25 %), and crosslinker calcium carbonate. The support bath showed slow and steady release of calcium ions from calcium carbonate due to a decrease in pH upon addition of D – (+)– gluconic acid δ–lacton. D– (+)–gluconic acid δ–lacton is a well–known acidifying agent that lowers the pH of the solution through hydrolysis into gluconic acid upon contact with water. Due to thermoresponsive properties, the printed structures formed gel after incubation at 37 °C for 45 min. Alginate lyase (1 U/mL) was added post–printing along with the culture medium to remove encapsulated or attached alginate in the printed constructs [49,101].

Ashley et al., used gellan gum fluid gel as a support bath to print cell–laden constructs using an extrusion–based bioprinter. Four different formulations (0.5 % w/v gellan, 0.5 % w/v gellan with 0.1 % w/v $CaCl_2.2H_2O$ at room temperature and 37 °C, 1.0 % w/v gellan) were

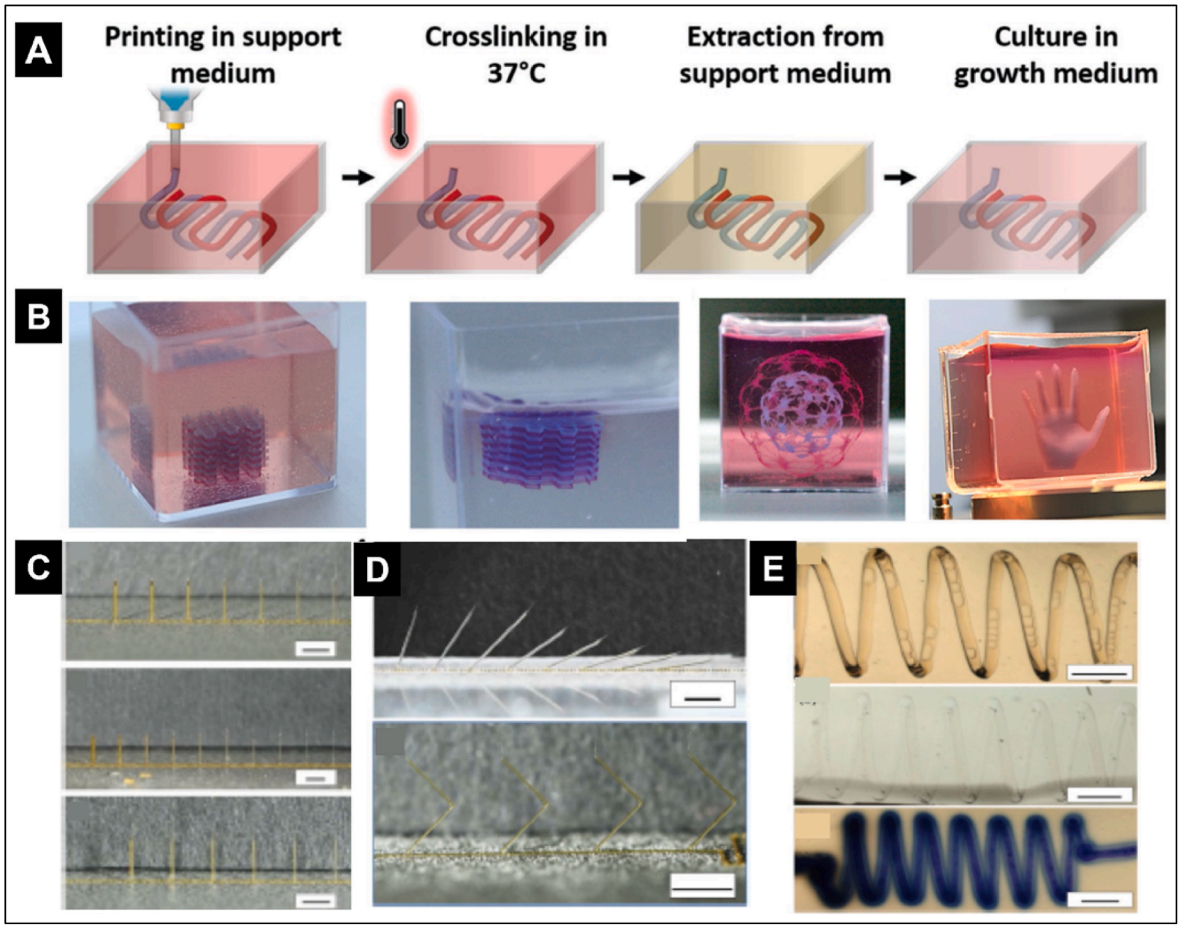

Fig. 8. [A] Sequential steps involved printing personalized hydrogel in a supporting medium; [B] Different constructs printed onside support bath like crisscross construct, hollow ball and hand models (Reproduced with permission from Ref. [49]); [C] Freeform printing of single filaments of PcycloPrOx (Scale bar - 2 mm); [D] Freeform printing of PcycloPrOx with decreasing angles and changing angles during printing (Scale bar - 2 mm) and [E] Embedment of a PcycloPrOx spiral scaffold in agarose (Scale bar - 2 mm) (Reproduced with permission from Ref. [102]).

Table 2
Different types of embedded bioprinting methods with their advantage.

Type of Embedded System	Support Matrix	Bioinks	Cells	Resol-ution	Complex Structures Fabricated	Cell Viability	Advantages	Ref
Omni directional printing	Pluronic F127 diacrylate	Pluronic F127	N/A	18 μm	Microvascular networks	N/A	Fabricated microvascular structures have potential applications in tissue engineering & organ modeling	[59]
GHost Writing	Adamantane (Ad) and β–cyclodextrin (β–CD) modified & methacrylated hyaluronic acid (4 %)	Adamantane (Ad) and β–cyclodextrin (β–CD) modified & methacrylated hyaluronic acid (5 %)	Mesenchymal stem cells (MSC) and fibroblasts (3T3s)	260 μm	Spiral and branching channels	>90 %	Supramolecular assembly of bioinks through guest–host reactions help in fabricating free–standing structures or constructs with open channels	[58]
Granular gel medium	Carbopol	Alginate, gelatin, PVA	NIH 3T3, human aortic *endo*-thelial cells	100 μm	Octopus model, Russian dolls model, jellyfish, hierarchically branched tubular networks	>80 %	Various complex structures were fabricated using ionic, photocrosslinkable and thermoresponsive bioinks by adjusting the concentration and pH of the Carbopol support bath.	[74]
FRESH	Gelatin	Fibrinogen, collagen, alginate, Matrigel®, hyaluronic acid	C2C12 myoblasts, embry-onic stem cells, human stem cell–derived cardiomyocytes & cardiac fibroblasts	20–40 μm	Vascular networks, heart, octopus, brain	80–99.7 %	Fabrication of large size biomimetic organs with vascularization support, easy process, commercially available	[50, 62, 65]
Embedded multi–material extrusion bioprinting	Pluronic F127	Alginate	N/A	50–100 μm	Cube, heart cartoon, MIT letters, Mobius strip, Klein bottle and kidney like structure	N/A	The multi–material printing approach is a low–cost method for faster, heterogenous tissue and organ fabrication	[34]
CLASS	Agarose	GelMA, Matrigel® and fibronectin	HEK 293	N/A	Honeycomb construct, two helixes	N/A	CLASS system supports soft tissue constructs in agarose slurry in cell culture conditions to promote better cell–cell interactions and ECM production	[57]
Sacrificial writing into functional tissue	Gelatin (sacrificial)	dECM & Spheroids	Human umbilical vein *endo*-thelial cells (HUVEC), iPSC–derived cardiac organ building blocks	400 μm	Hollow channels	Significantly increased cell viability in channelled tissues compared to no channel	Fabrication of highly dense and perfusable tissues for patient–specific tissue and organ fabrication	[60]
Volumetric bioprinting	GelMA	GelMA	Arti-cular chondroprogenitor cells, mesenchymal stromal cells (MSCs)	33 μm	Ear and meniscus	>85 %	Fabrication of large–sized constructs within a short time (seconds to minutes) with high cell viability and matrix remodeling	[93]
FLIP printing	Fluorinert FC–40 (perfluorinated oil)	PEG –DA, GelMA	Mouse fibroblasts	100 μm	Marina Bay Sands (MBS) hotel model, geodesic dome, aortic valves, a lymph vessel with an internal valve, cartilage-nous structures and hollow channels	>97 %	Printing of hydrogels with different mechanical stiffness without affecting the cell viability	[64]
Hydrophobic support bath	Perfluoro-tributyl-amine support bath	Agarose	Human mesenchymal stem cells (hMSC) & MG63	575 μm	3D construct mimicking a vascular bifurcation and printed cylinders	>95 %	The printed structures were maintained for 6 months in a support bath. Histological and immunohistochemical analyses showed cell proliferation & matrix production	[100]
Gellan support bath	Gellan gum	Alginate & gelatin	NIH 3T3	N/A	Spiral cone and branching tube	N/A	Gellan support baths support the printing of functional bioinks that can crosslink with physical, enzymatic, and photocrosslinking mechanisms	[103]
Noor et al. Support medium	Alginate & xanthan gum	Decellularized omentum bioink	Induced pluripotent stem cells (iPSCs)–derived cardio-myo-cytes (CMs) and *endo*-thelial cells, rat neonatal cardiomyocytes, human umbilical vein endothelial cells (HUVECs) and lumen–supporting fibroblasts	10 μm	Channels and whole heart with the vasculature	>90 %	Support bath composed of alginate and xanthan gum supports printing of precise structures with good biocompatibility, transparency, and stability	[101]

evaluated for using as support bath in which 0.5 % w/v gellan + 0.1 % w/v $CaCl_2.2H_2O$ showed better results compare to other formulations. The prepared bulk gel (0.5 % w/v gellan + 0.1 % w/v $CaCl_2.2H_2O$) were passed through stainless steel mesh to form 20–40 μm sized microgel particles. Addition of calcium ions to the microgel particles made the support bath with better shear–thinning properties and helped to extract printed constructs from the support bath easily [103]. This study demonstrated the use of gellan gum as a support bath and different functional bioinks that can crosslink with physical, enzymatic, and photocrosslinking mechanisms. Bioink with 5 % gelatin and 2 % alginate ink was used due to the thermo–responsive physical crosslinking system, and gel formation was observed by lowering the temperature (<37 °C). Constructs were printed and covalently crosslinked using the enzyme transglutaminase, where the enzyme was mixed with the support bath. Further, the biocompatibility and crosslinking abilities of the gellan gum support bath was evaluated by comparing it with the laponite support bath and poly (ethylene glycol) diacrylate (PEG–DA) bioinks. Compared to the laponite support bath, the developed gellan gum support bath formed intact printed constructs after crosslinking. However, while using photocrosslinkable PEG–DA bioinks, the support bath system could not maintain the printed structures due to long printing times for larger constructs, which causes diffusion of the printed materials into the gellan gel. Various shapes were printed using gelatin/alginate hydrogels such as spiral cones, branching tubes, dog bone, and lattice cubes. The print quality of the hydrogels was analyzed by measuring the swelling ratio and extraction of the printed constructs from the support medium. Swelling of the printed lines with fuzzy edges were observed in the gellan gum support bath, while sharp edges and fines lines were seen in the laponite support bath. However, compared to laponite, gellan gum support bath systems showed less material deposition and easier extraction of printed constructs from the support bath. Cell–laden constructs printed using NIH 3T3 fibroblast cells showed good cell viability, proliferation, cell spreading and cell–cell communication during a culture period of 72 h [103].

Recently, Mair et al., developed a new free–form printing strategy using poly (2–cyclopropyl–oxazoline) (PcycloPrOx) to generate hollow channel networks in cell–laden hydrogels. PcycloPrOx printed structures were embedded within the hydrogel to create hollow channels after maintaining them below a lower critical solution temperature (LCST). This system is compatible with various bioinks and crosslinking mechanisms (agarose – thermoresponsive; gelatin methacryloyl (GelMA) – photocrosslinking; gelatin microbial transglutaminase – enzymatic; alginate – ionic crosslinking mechanisms). This strategy was successfully used to fabricate hollow channels less than 100 μm in diameter to develop vascularized tissues with micron level resolution (Fig. 8C–E) [102]. Table 2 shows the comparison between different embedded bioprinting strategies with their advantages.

3. Designing & ideal properties of support bath systems

In general, functional bioinks and supporting baths must have complementary relationships and distinct rheological features, such as shear–thinning properties, quick sol–gel transition etc., to print and maintain printed constructs with morphological and structural integrity. A rheology modifier is a substance that is added to inks and support baths to change their rheological characteristics to make them more suitable for embedded bioprinting. Critical characteristic features of polymers to be used in support baths, such as viscoelastic properties, transparency, crosslinking ability, post–processing and extraction are discussed in detail below.

3.1. Support bath & viscoelastic properties

3.1.1. Sol–gel point

Determination of the sol–gel transition point is crucial to obtain suitable constructs by 3D printing of hydrogels [73]. Gelation points can be determined by performing temperature sweep measurements in rheometers where the crossover of elastic (G′) and viscous modulus (G″) are observed. However, only thermoresponsive polymers exhibit changes in modulus with changes in temperature. In such cases, the support bath should maintain at sol–gel transition temperatures to maintain the shape of printed constructs while using low viscous bioinks [70]. For example, support baths in FRESH printing are made up of gelatin, which needs to be maintained at 22 °C to maintain the shape of printed structures. Further, the functional bioinks should be curable at higher temperatures or contain different gelation mechanisms [62,76].

3.1.2. Yield stress & shear–thinning

Yield stress is the minimum pressure required to initiate the flow of hydrogels. Support baths should behave as solid (non–flowable material) before attaining the yield stress and turn to flowable liquid–like behavior after applying stress. Usually, support bath strength depends on the type, concentration of polymer used for support bath preparation, pressure and speed required to print the functional bioinks into the support bath [55]. High–concentrated support bath systems require higher yield stress compared to low concentrated support baths [73]. Shear–thinning occurs in support baths when the nozzle of the printing head exerts a higher force than the normal steady–state and helps to extrude bioinks into the support bath [104]. Jeon et al., also showed the solid–like properties of alginate microgel based supportive medium at low shear strain due to the steric stabilization and became solution at a high shear rate, confirming the advantages of shear–thinning ability of support baths for the printing of cell–only bioinks [105]. Compaan et al., showed a decrease in the viscosity of the hydrogel with the increased shear rate and positive influence on the materials deposition inside gellan gum support gels [103].

3.1.3. Support bath stability & self–healing

Time sweep analysis at specific shear stress helps to assess printing time and stability of support bath systems. Support bath systems need to be compatible for prolonged printing durations, which helps to print complex 3D structures such as organ models. The support baths should recover to their initial mechanical properties after depositing the bioink, which helps to hold the deposited materials in the same position before depositing the next layer of bioinks. Shapira et al., used a support medium formulated with alginate and xanthan gum for printing collagen bioinks, which maintained the print shape for up to 18 h, demonstrating the importance of support bath stability and self–healing abilities [101]. Similarly, Mirdamadi et al., printed alginate ink for 92 h in FRESH support medium for printing a full–size human heart using the FRESH method to evaluate the stability and self–healing properties of the support medium [62].

3.2. Support bath transparency

A transparent support bath is required to visualize materials deposition, print patterns and structural integrity between layers during printing [106,107]. Coloured bioinks may enhance visibility when printing inside a support bath compared to colorless inks [36,49]. However, the coloring agent should not alter the biocompatibility and inherent properties of the bioink. Transparent support bath systems are necessary for crosslinking photoreactive bioinks through easy penetration [106]. Ning et al., evaluated the significance of transparency in the Carbopol support bath systems by comparing the mechanical properties of constructs printed in conventional print bed based (printing in air) and support bath systems. Constructs printed in 0.4 % Carbopol support bath with 10 % GelMA exhibited decreased stiffness compared to constructs printed in air at constant UV light exposure (5 min). The difference in mechanical properties is due to the hindrance of UV light inside the Carbopol support bath that signifies the role of support bath concentration, UV light intensity and exposure duration which have great impact on mechanical properties of printed constructs [73]. Similarly,

transparency of support bath is required when the sacrificial inks are printed into support baths to form channel-like structures or vasculature and for assessing the functionality of the fabricated tissues through cell attachment, dye diffusion, and perfusion. Moreover, when the support bath is transparent, it is easier to track the printing location and monitor the progress of printing process.

3.3. Support bath toxicity

The supportive medium should facilitate a biocompatible environment during printing and should not cause any damage during post–processing or removal of support structures [108]. The balance between the printing and curing time inside the support bath is crucial in determining the cell viability of the constructs. The effect of supportive bath residential time on cell viability was evaluated by Bessler et al., using HEK293 cells, where decreased viability was observed with the increased incubation time in the support bath (60 min–80 % viability; 90 min–70 % viability; 120 min–50 % viability) [82].

3.4. Swelling and shrinkage

The swelling and shrinkage of printed constructs inside the support bath should be minimal to reduce shape deformation. For example, a low concentrated Carbopol (<0.8 % w/v) support bath has higher water content, which causes additional swelling of the printed structures. In contrast, a high concentrated Carbopol support bath (1 % w/v) with less water content causes the shrinkage of printed structures. Support baths prepared using 0.8 % (w/v) Carbopol minimized both swelling and shrinkage of alginate/gelatin bioink [74]. However, the optimal concentration of support bath also depends on the concentration and crosslinking mechanism (ionic, thermal & photocrosslinking) of the bioink used for fabrication of tissue constructs [109]. The addition of low concentrated crosslinkers or pre–crosslinked hydrogels may help to overcome the swelling and shrinkage problems.

3.5. Extraction of post printed constructs from support bath

During post–processing, the method to remove printed constructs from the support bath may vary and depends mainly on the polymer used in the support bath. Depending on the type of support bath, it is preferable to use biocompatible solutions like PBS or 0.9 % NaCl using physiological conditions such as solution temperature and pH [67,74,106]. However, the estimation of residual support materials present in the printed constructs and their effects on the properties of the printed constructs need to be assessed. Additionally, when sacrificial inks, such as gelatin, Pluronics, etc., are used to integrate the vasculature within embedded printed constructs, temperature is used as trigger to remove them from printed constructs [49,59]. Enzymatic degradation of the support bath has an essential role in obtaining printable constructs. Noor et al., used alginate lyase to degrade the alginate present in the support bath [49]. Enzymes like cellulase & hyaluronidase can also be used to remove printed structures from the support bath based on the composition of the support bath.

4. Printing parameters

Optimizing printing conditions is necessary to print the objects similar to 3D designs by tuning printing parameters such as printing

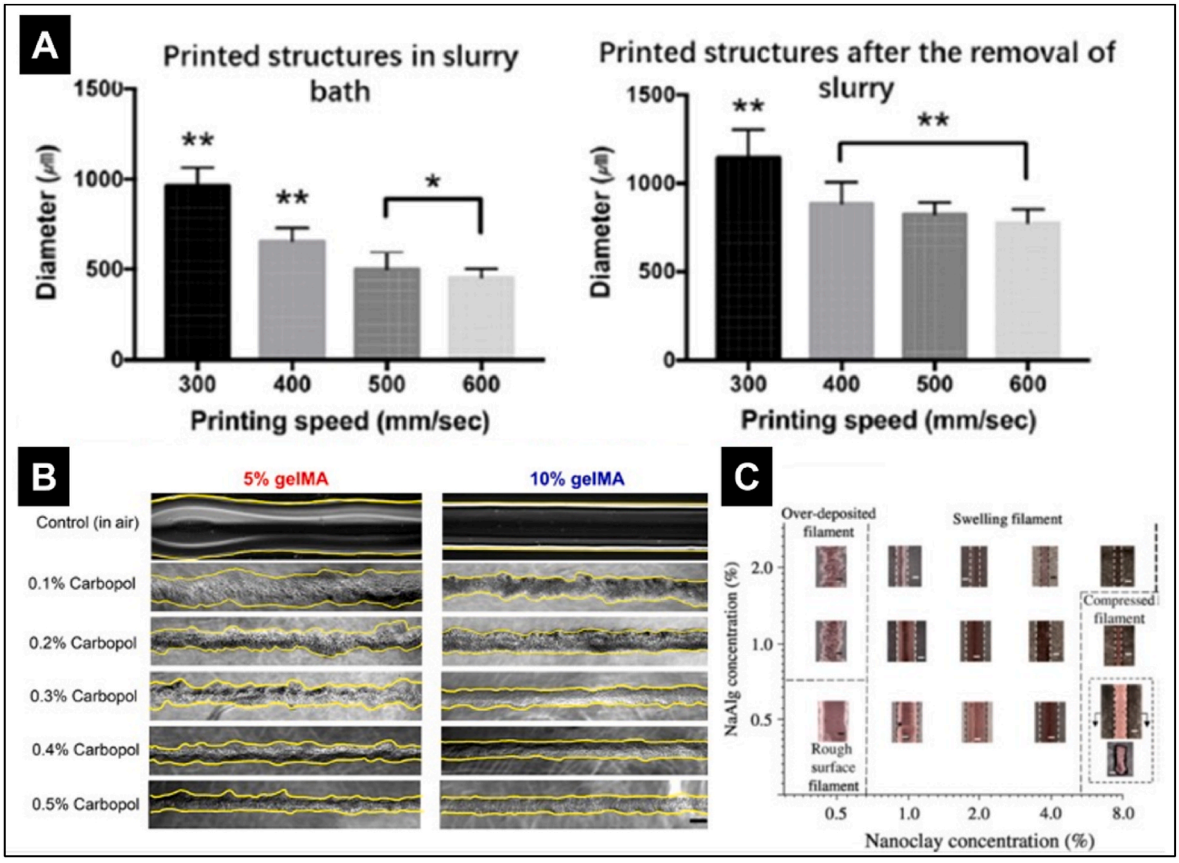

Fig. 9. Optimization of print strand width for biofabrication of tissues/organs. [A] Effect of printing speed on strand diameter of oxidized alginate/gelatin bioink inside the gelatin–based slurry bath (Reproduced with permission from Ref. [116]); [B] Bright–field images of 5 and 10 % gelMA strands are printed in different concentrations of carbopol gels and air (Reproduced with permission from Ref. [73]) and [C] Effects of nanoclay concentration on the filament diameter (Reproduced with permission from Ref. [54]).

pressure, printing speed, nozzle diameter, printing temperature, concentration of functional bioink and concentration of support bath material [110–115]. Usually, the flow rate of bioink is adjusted by fine–tuning the pressure and speed to get the precise strand length and width as designed. This helps to maintain the cell viability during the printing process. Heo et al., observed a decrease in strand width with increase in printing speed. Initially when the constructs were printed at 300 mm/min print speed, merging of the printed strands (diameter 1 mm) with adjacent strands were observed. Further, when the printing speed was increased to 600 mm/min, decrease in the strand width of printed constructs were observed (diameter – 500 μm) (Fig. 9A) [116]. Similarly, Shapira et al., varied the feed rate from 5 to 40 mm/s to get the printed strand resolution in the range of 20–60 μm [101]. The diameter of the printed strands can be further reduced by decreasing the printing pressure or flow rate. Jin et al., explained the relation between the filament width, nozzle diameters and printing pressures using 2 % alginate & 10 % gelatin (w/v) blend bioink in a 4 % (w/v) nanoclay support bath with different nozzle diameters and printing pressures. Bioinks dispensed with 400 μm nozzles showed high filament width (~950 μm), and a further decrease in the filament width was observed while using smaller diameter nozzles (<100 μm). Similarly, filament width was low (175 μm) when the structures were printed at low pressure (5 psi), and it was increased to 450 μm while printing at the pressure of 30 psi [54].

A few procedures were developed to identify the similarities or changes in the 3D designs and printed constructs, such as strand diameter ratio (D_p), strand uniformity ratio (L_p), strand angle ratio (α_p) and inter strand area ratio (A_p). Ning et al., used different concentrations (0.1 %, 0.2 %, 0.3 %, 0.4 %, 0.5 %) of Carbopol support bath for the fabrication of complex structures. Based on the printability analysis results, strands extruded in 0.4 % Carbopol support medium showed good printability and shape fidelity compared to other concentrations [73]. Inter strand area ratio (A_p) of 5 % and 10 % GelMA bioinks printed in different concentrations of Carbopol support showed that 10 % GelMA has fewer variations compared to 5 % GelMA (Fig. 9B) [73]. Navara et al., printed different concentrations of poly (N–isopropylacrylamide (PNIPAAm) based bioinks in different concentrations (17.5 %, 26.25 % and 35 %) of poloxamer support baths (25 %, 30 % and 35 %) with different needle gauge sizes (25G, 27G, 30G, 32G) and shape deformation was observed in lower concentrated inks and support baths [117].

Storage modulus, shear–thinning, and recovery of bioinks are the important parameters that significantly affect the shape fidelity and print resolution of constructs. A higher concentration (8 %) of laponite support bath led to compressed filaments, and a lower concentration (0.5 %) resulted in irregular filaments with a rough surface (Fig. 9C) [54]. Afghah et al., used 7.5 %, 10 %, 12.5 % Pluronic F127 (PF), 3 % laponite and 1 % $CaCl_2$ for support bath preparation. Viscoelastic properties of these support baths showed increased modulus in 10 % PF based support bath compared to 7.5 % and 12.5 % due to the electrostatic interactions and hydrogen bonds formed between the components used for support bath preparation. Usually, in composite gel systems, an increase in the viscoelastic properties such as viscosity and moduli are observed until a saturation level. After saturation, a further increase in the polymer concentration will not necessarily increase the elastic interactions but may decrease the modulus [118]. Jin et al., reported a significant increase in the storage modulus of laponite support baths with an increase in the concentrations where the low concentration bath showed 0.1 Pa for 0.5 % (w/v) nanoclay suspension and 1000 Pa for 8 % (w/v) nanoclay suspension [54].

5. Stabilization strategies for embedded printing

Bioprinted constructs need to be stabilized by crosslinking with covalent or non–covalent interactions to maintain shape fidelity and mechanical stability [119]. Due to the surface tension of weak hydrogels, printed constructs lose shape after printing, and it is necessary to add crosslinkers simultaneously to maintain shape. There should be two distinct or different crosslinking approaches for the support bath and functional bioinks to ensure collecting the printed constructs from the support bath without damage. Modifying the native polymers with photoactive groups [120] or thermoresponsive groups [121] is often required to produce easily crosslinkable bioinks with self–support and cytocompatibility. Thermosensitive polymers form hydrogels by non–covalent interactions by increasing or decreasing the temperatures without the requirement of additional crosslinking [122]. Polymers such as agarose [123], methylcellulose [124], gelatin [125], decellularized ECM [32], collagen [126], Matrigel® [127] and Pluronic F–127 [33] were used for the fabrication of complex structures by maintaining the printing bed temperature.

Ionic crosslinking is the formation of non–covalent bonds between the ions and oppositely charged polymers that create stable, branched polymer networks [128]. Polymers, through ionic crosslinking, can easily and instantly crosslink by diffusion of ions [75]. The addition of ion concentrations can vary mechanical properties of the hydrogels. Several polymers such as alginate [129], gellan gum [130], pectin [131] and chitosan [132] could be crosslinked by the addition of calcium chloride, sodium tetraborate (borax) and tripolyphosphate (TPP). Alginate is a common anionic polymer composed of mannuronic (M) and guluronic (G) subunits with negatively charged COO^- groups forming hydrogels in contact with divalent cations [128]. Ionic crosslinking of chitosan depends on the pH of the solution and the charge density of chitosan & tripolyphosphate (TPP) [132]. However, it is challenging to penetrate ions to the core of impenetrable constructs, and ion leaching can lead to unstable gel formations.

Enzymatic crosslinking is more specific due to the covalent crosslinking of bioink moieties by supplementing the enzymes in the support bath [133,134]. Enzymes such as transglutaminase are used to crosslink gelatin or collagen by forming an isopeptide bond between glutamine and lysine [135]. Fibrinogen is a blood–clotting protein that can crosslink by thrombin in the presence of calcium, factor XIII and forms a covalent crosslinking between the adjacent fibrin fibres [136]. The stability of the printed structures entirely depends on the type, concentration of substances or enzymes and the time required for enzyme activity.

Photo crosslinking is the formation of covalent bonds between polymers containing photoactive groups and photoinitiators [137]. It is a contact–free rapid gelation method with tunable mechanical properties [137]. Modifying polymers with unsaturated groups such as acrylate or diacrylate is necessary to crosslink the polymers through free–radical chain–growth polymerization upon exposure to light of a specific wavelength [138]. Several photoinitiators such as Irgacure 2959 [139], Lithium phenyl–2,4,6–trimethylbenzoylphosphinate (LAP) [139], riboflavin [140], Eosin Y and camphorquinone [141] are commercially available to induce gel formation in UV and visible light wavelengths. Photopolymerization occurs through the generation of free radicals by decomposing or abstracting the hydrogen atoms from the donor along with co–initiators. In photocrosslinking, gelation process, cytocompatibility and feasibility generally depends on the light wavelength, light intensity, and exposure time. Most photopolymerization mechanisms will occur in the range of 365 (UV) – 405 nm (visible – blue) wavelength. Due to covalent bonding, these photopolymerized gels are stable compared to the other gelation methods [138]. To use photocrosslinking in support bath systems, either the support bath material or the functional bioink should be photoactive [55]. Since it has selective polymerization by exposing light to a specific area, it can precisely control the gelation of printed constructs.

6. Materials used for support bath preparation

Support bath materials are very helpful in preventing the collapse of printed three–dimensional complex structures. Several studies have

reported the use of various synthetic materials such as Laponite, Carbopol, Pluronic F127 and natural materials like agarose, alginate, silk fibroin and gelatin in support bath systems to fabricate complex organs using extrusion–based bioprinting [36,49,54,57,59,142].

6.1. Laponite

Laponite ($Na_{0.7}Si_8Mg_{5.5}Li_{0.3}O_{20}(OH)_4$) is a synthetic clay that contains a low polydispersity index with disc–shaped nanoparticles of 1 nm thick and 25 nm in diameter, which produces clear, colorless thixotropic gel upon dispersion in water [143]. Laponite has been used in drug delivery, tissue engineering and to increase the viscosity of cosmetic products [143]. By dispersing nanoclay in water, nanoparticles obtain a slight negative charge due to the dissociation of sodium ions and a slight positive charge through the dissociation of hydroxide ions [118]. The positive and negative charge–based interactions make laponite an exciting material to use as supporting material for printing complex structures. Jin et al., named a method as a house–of–cards approach where the nanoclay forms colloidal suspensions with the sol–gel transition upon experiencing stress. When printing in a nanoclay support bath, shear stress around the printer nozzle is higher than the yield stress of the supportive bath. This makes the nanoclay near nozzle behave like a solution and allows the free flow of materials from the extruder to the supportive bath [74]. After the printing process, local yield stress will be higher than the applied shear stress and nanoclay returns from the liquid state to the solid–state by holding the printed constructs and shapes inside the support bath. Laponite forms viscous hydrogels under physiological conditions with different concentrations. Jin et al., used different concentrations of nanoclay dissolved in deionized water to estimate the filament formation in the support bath [54]. Well–defined extruded filaments in a laponite nanoclay bath of 2.0 % (w/v) were observed compared to 0.5 % and 8 % with different speed ratios. However, the support bath materials can separate or inactivate macromolecules such as enzymes and ions employed in the printing process.

6.2. Carbopol

Carbopol is used as a support bath in a granular gels–based approach. Carbopol is commonly used in cosmetics, oral care applications for toothpaste, mouth wash and oral pharmaceutical products [74]. Carbopol is also an excellent biocompatible polymer with transparency and tunable strength, which contains a mesh size of 100 nm that can form easily flowable solutions at low concentrations, and forms soft gels at higher concentrations [144]. Carbopol comprises high molecular weight poly (acrylic acid) with different crosslinking mechanisms, either with allyl sucrose or pentaerythritol [145]. The water absorption capacity of Carbopol is greater than 1000 times to its dry weight due to electrostatic interactions [146]. The complete dissolution of the Carbopol microparticles in water is prevented by the internal crosslinking of polymer with polyalkenyl polyether bonds. Jin et al., evaluated the role of pH and concentration of polymer to use Carbopol in supportive bath fabrication. Low concentration (0.2–0.6 % w/v) gels behave as a solution due to less polymer availability. This free water may cause swelling of the printed structures, whereas, at higher concentrations (>1.2 % w/v), it will absorb the water from the printed constructs to reach equilibrium (maximum swelling ability). At concentrations from 0.8 %–1.2 %, it showed better structural stability with the designed conditions [74,97]. The pH of the solution also affects the thickness of printed constructs, where the printed constructs showed swelling at low pH and shrinkage at higher pH [74]. At neutral pH between 7.0 and 8.0, there was no drastic change in swelling or shrinkage of printed constructs because of limited gelatin release from constructs and minute differences in ionic strength of the Carbopol. Carbopol also has unique rheological properties where it behaves like a fluid at high shear force and forms a gel upon removal of forces [147]. Unfortunately, Carbopol is sensitive to ionic strength and incompatible with multivalent cations commonly used in bioprinting systems [148].

6.3. Pluronics F–127

Pluronics F–127 are a synthetic tri–block copolymer comprised of poly (ethylene oxide)–poly (propylene oxide)–poly (ethylene oxide) (PEO–PPO–PEO) [59]. Pluronics has thermoresponsiveness (sol–gel), which depends on the concentration and molecular weight of the polymer [149]. It forms micelles in aqueous solutions due to its amphiphilic nature. Below critical micelle temperature, pluronics remains a solution in water, and above the critical micelle temperature, it self–assembles to form micelles [150]. This temperature–based reversible sol–gel transition and thixotropic behavior at physiological conditions make pluronics an exciting material for support bath. Kolesky et al., used pluronics as fugitive ink in bioprinting, and Rocca et al., used it as a supportive medium for the fabrication of complex structures [34,151]. After crosslinking of printed constructs, pluronics were removed from the printed structures by incubating at 4 °C, where pluronics became liquid.

6.4. Agarose

Agarose is a natural polysaccharide composed of alternate β–1,3–linked D–galactose and α–1,4–linked 3,6–anhydro–α–L–galactose residues [152]. The gelation temperature of melted agarose is between 30 and 35 °C, and it majorly depends on the source, molecular weight, and concentration of the polymer [153]. Low agarose concentrations (0.5–5 % (w/v)) are preferred for tissue engineering and bioprinting applications due to thermoresponsiveness, ease of gelation and mechanical strength [154–156]. Agarose is also used to encapsulate drugs and as a sacrificial layer when printing hollow and complex structures with low viscous non–thermoresponsive materials such as alginate and fibrinogen [57]. Agarose is used in the bioprinting of biomimetic tissues such as bone, cartilage, nerve, and blood vessels due to the easy diffusion of nutrients through the pores of agarose [127,157,158]. Agarose was used as support slurry by Mirdamadi et al., called a CLASS using cell–laden alginate and gelatin methacrylate (GelMA)–based bioinks. Agarose (1 %) supportive bath with 60 & 90 s blending time has given the best prints compared to 30 and 120 s. Furthermore, agarose support slurry was more suitable for printing complex defect–free structures compared to gelatin [57]. In another study, Cidonioi used 0.5 % agarose as a support bath matrix for skeletal muscle regeneration using laponite & gellan gum bioink. Myoblasts cells (C2C12) in printed structures retained their functionality within day 1 and maintained stability & proliferation over 21 days [88].

6.5. Gelatin

Gelatin is a natural polymer derived from collagen by treating with strong acids (type A) or bases (type B) [159]. Usually, gelatin behaves as a solution at physiological temperatures and forms into stable hydrogels at lower temperatures [160]. Gelatin is most commonly used as hydrogels, films, nanofibers and bioinks for the regeneration of various biomimetic tissues by crosslinking with enzymes like transglutaminase or by treating with chemicals such as glutaraldehyde [161], genipin [162], and dialdehydes [163]. Gelatin methacrylate (GelMA) is commonly used as a bioink for printing cells in predetermined shapes with the help of photo and thermal crosslinking [164]. Gelatin is also used as a support material by blending hydrogels to generate microparticles as a support matrix [165]. In FRESH printing, the gelatin

microgels were maintained at very low temperatures (4 °C), where it behaves as Bingham plastic used as a support bath (at 22 °C) to hold the constructs during printing [70]. After crosslinking, the printed constructs can be removed from the support bath by maintaining at 37 °C, where it becomes a solution. Heo et al., used gelatin crosslinked with transglutaminase (TG) and blended with a laboratory blender to form crosslinked gelatin microparticles. Further, this suspension was washed with deionized water to remove uncrosslinked gelatin and TG to stop crosslinking reactions. The resultant solution was dispersed in oxidized alginate in different proportions and maintained at 23 °C to use as a support bath. Furthermore, 6 % Gel–CDH (carbohydrazide–modified gelatin) was printed inside the support bath comprised of 70 % gelatin microparticles and 30 % oxidized alginate solution to print meshed tube, meshed sphere, humerus model and ball–in–cage structures [116].

6.6. Gellan gum

Gellan is a linear anionic, water–soluble bacterial polysaccharide and is commonly used as a gelling agent due to the easy formation of hydrogels with the addition of divalent cations [166]. It comprises a repeated tetrasaccharide sequence of two β–D–glucose residues, one β–D–glucuronate residue, and one α–L–rhamnose residue. Gellan polymers maintain as random coils in aqueous solutions at high temperatures, and upon cooling, they will aggregate and form junction zones by forming double helices for the formation of hydrogels [167]. Hydrogel formation was majorly dependent on gellan concentration, salts and pH of the medium [168]. Low acyl gellan hydrogels are transparent and brittle. Gellan microgels are used as support bath systems due to the yield stress dependent deformation and smooth flow of materials [51,169].

6.7. Xanthan gum

Xanthan gum is an anionic polysaccharide derived from Xanthomonas bacteria. Xanthan gum is structurally similar to cellulose, composed of linear (1–4) linked D–glucose with side chains of alternating residues of D–mannose and D–glucuronic acid in a ratio of 2:1. Xanthan gum solutions show pseudoplastic and shear thinning behavior with changes in time or shear rate [148,170]. Due to non–toxicity, biocompatibility, biodegradability, and cost–effectiveness, xanthan gum is widely used as a viscosity enhancer in cosmetics, drug delivery, water–based paints, tissue engineering, and regenerative medicine applications [171,172]. Shapira et al., used xanthan gum and alginate to fabricate a hybrid support bath that enables continuous printing for up to 18 h with the smallest print widths (10 μm) using custom nozzles. The addition of xanthan gum in support medium fabrication provides a lubrication–like effect and prevents the aggregation of alginate particles. It helps print complex structures such as heart models with parenchymal tissue and major blood vessels [101]. Patrício et al., prepared photocrosslinkable xanthan gum methacrylate using a permanent support matrix and pristine xanthan gum as a removable support matrix. Xanthan gum support matrix (1.5 %) with 50 mM $CaCl_2$ allowed printing centimetre–sized branched structures at 30 mm/s speed without compromising printing resolution. Xanthan gum methacrylate support bath helps to print perfusable constructs by depositing alginate into the photocrosslinkable matrix. Furthermore, removing alginate by adding EDTA leaves the channels inside the support bath matrix similar to vasculature in native tissue [148].

6.8. Methylcellulose and carboxymethylcellulose

In methylcellulose and carboxymethylcellulose, hydroxyl groups of cellulose are replaced with methyl or carboxymethyl groups in the main β–glucose chain thereby reducing the intermolecular hydrogen bonding [173]. Reversible and thermoresponsive hydrogels can be prepared using these polymers by altering polymer concentrations or by adding salts. Addition of salts may increase the hydrophobic interactions between polymer chains, which eventually decrease water availability and promote hydrogel formation [174]. These are widely used as thickening agents and viscosity modifiers in various food, medicinal products, beauty creams, ointments, and eye drops [154]. Due to shear–thinning and thixotropic properties, these cellulose derivatives alone or in combination with other polymers have been used as bioinks for printing multi–layered complex shapes in recent years [175,176]. Li et al., prepared a support bath comprised of 9 % alginate and 6 % methylcellulose to print constructs using 10 % GelMA bioink, which were further crosslinked by UV light exposure for 10 s. The crosslinked constructs were incubated in DPBS with gentle mechanical agitation to remove alginate and methylcellulose. Further, the printed constructs were stable for 15 days and broken into pieces on day 20. C2C12 mouse myoblasts cell–laden constructs showed more than 95 % viability and cell spreading at day 5, demonstrating the advantages of methylcellulose as a support bath [106].

6.9. Fluorocarbons

Fluorocarbons are non–aqueous, cytocompatible, and highly oxygenated fluids with high buoyant density. Among the fluorocarbons, fluorobutyltetrahydrofuran (FX–80) and perfluorotributylamine are widely explored for biological applications [177,178]. Perfluorotributylamine ($C_{12}F_{27}N$) is an inert, hydrophobic, cytocompatible and viscous fluorocarbon rarely used in support bath systems. Due to high density (1.9 g cm^{-3}) and the non–miscibility, perfluorotributylamine is used as support bath to print large tubular constructs. Further, the hydrophobicity of the fluorocarbons enable precise shape control over the deposited droplets and help to form large Y–shaped constructs [100].

7. Applications of embedded bioprinting

Fabrication of organs or tissues with appropriate vascularization is the major challenge in tissue engineering and regenerative medicine. Traditional tissue fabrication techniques allowed users to fabricate constructs similar to native tissues and organs [179]. However, it lacks several essential features like vascularity, mechanical strength, morphology, cellular heterogeneity, uniformity and customizable designs with desired shape and size. Three–dimensional bioprinting shows outstanding features that enables printing precise heterocellular tissue constructs with tunable mechanical properties at high speed [180]. However, due to the complexity and heterogeneity of the native tissues, it is difficult to print large, hollow tubular constructs and complete organs. The support bath based method facilitates the printing of several complex structures, including spiral, Y–shaped tubular constructs, bone, kidneys and heart with enhanced shape fidelity [49,69,88,105,181]. In the future, embedded bioprinted models hold the potential to accurately replicate intricate tissue structures and functions, thus aiding research in the fields of regenerative medicine, disease modeling, and drug development.

7.1. Skin

Skin has a complex structure made up of three layers (epidermis, dermis, and hypodermis). Severe injuries can eventually lead to the destruction of these structures, and inadequate healing can lead to scarring of the tissue and limits its function [182,183]. Using an embedded printing strategy, Moakes et al. printed tri–layered human skin equivalent tissues using cell–laden (ADCSs – adipose–derived mesenchymal stem cells; HDFs – dermal fibroblasts) collagen and pectin bioink in agarose support bath. Different layers of skin tissue were fabricated by mixing different ratios of collagen and pectin with different cell types (hypodermis layer – 1:1 blend containing ADCSs 5×10^5 cells/mL; reticular layer – 2:1 blend containing HDFs 1.5×10^6 cells/mL and papillary layer 2:1 blend containing HDFs 3.0×10^6

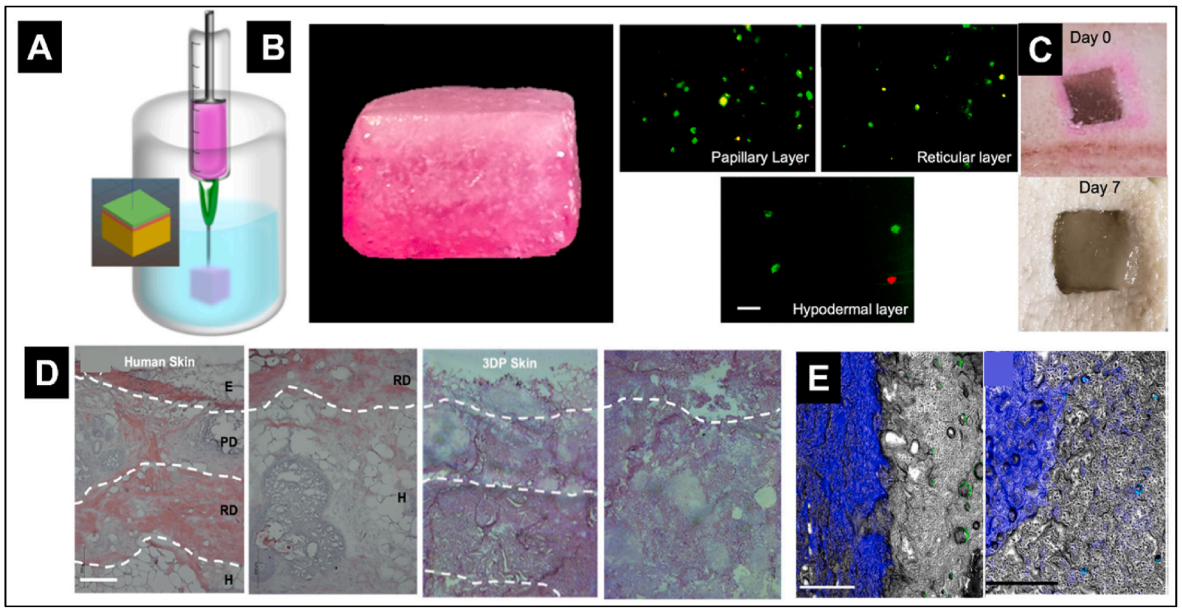

Fig. 10. Fabrication of skin tissue model through embedded bioprinting strategies. [A] Process of tri–layered skin fabrication; [B] Macroscopic image of the skin construct (15 × 15 × 9 mm^3) & live–dead staining (scale bar - 200 μm); [C] Images of the skin constructs after implantation within the defect and after 7 days of culture; [D] Histological characterization of different layers of human skin and 3D printed skin after 21 days of culture (scale bar - 200 μm) and [E] Fluorescence staining of hypodermal layer for infiltration of the surrounding porcine tissue (scale bar - 500 μm) (Reproduced with permission from Ref. [184]).

cells/mL). Printed constructs were implanted in an *ex vivo* skin wound model, which showed excellent integration, microstructures, and cellular environments close to the native structures (Fig. 10). Therefore, these implants have the potential to replicate skin by providing an implant that is much equivalent to that of human skin, which may be utilized to enhance wound healing [184]. Although this model exhibited distinct layers within the fabricated skin construct, further investigations utilizing *in vivo* models and clinical trials are necessary to comprehensively assess the effectiveness of the developed model for regenerative medicine applications.

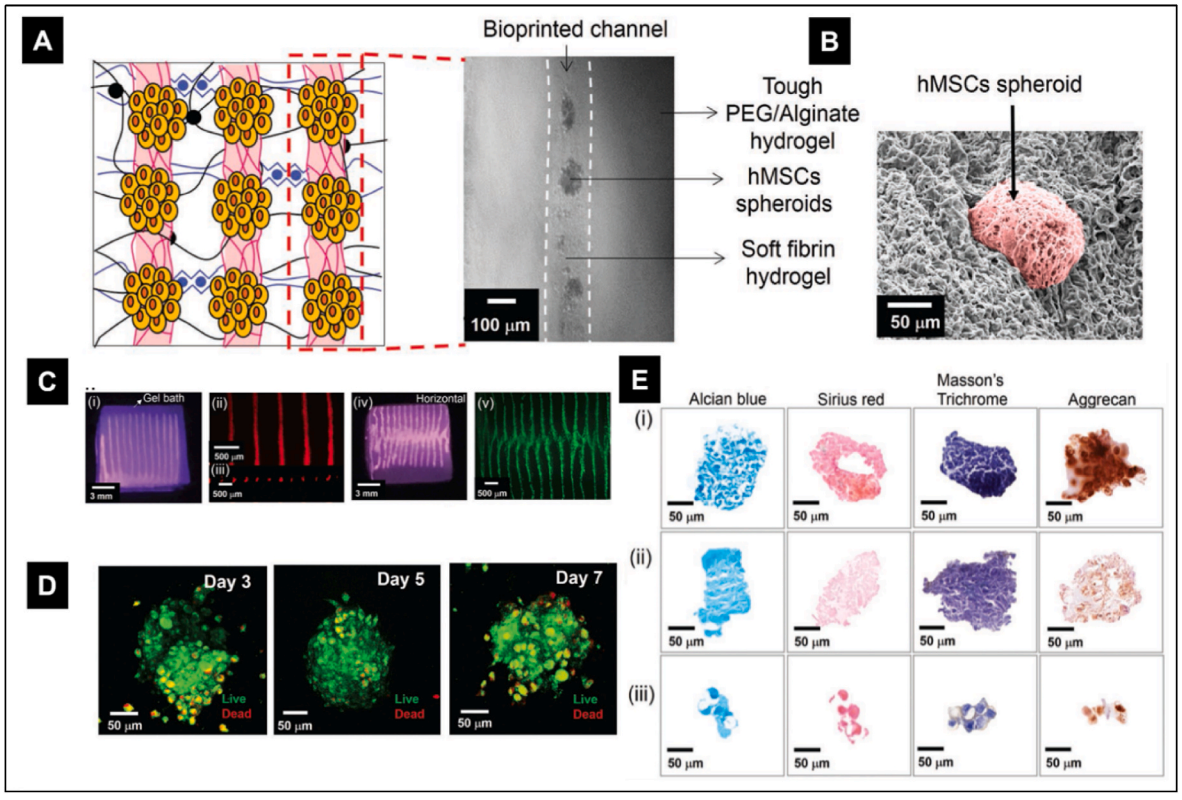

Fig. 11. Bioprinting of hMSC spheroids inside alginate–PEG support bath. [A] 3D printed line inside the support bath; [B] SEM image of hMSCs spheroid; [C] Images of bioprinted fibrin in 20 % PEG–2.5 % alginate; [D] Live/dead images of bioprinted spheroids at different time points; [E] Histological images of (i) bioprinted spheroids cultured in a chondrogenic medium, (ii) regular medium (control) and (iii) bioprinted single cells cultured in a chondrogenic medium after 21 days of culture (Reproduced with permission from Ref. [189]).

7.2. Cartilage

Cartilage is a semi–transparent, tough, and flexible connective tissue comprised of chondrocytes, which are usually found in joints, ears, ribs, nose, etc. It provides sliding of one bone over the other smoothly and reduces the friction thereby preventing damage by acting as a shock absorber [185]. Cartilage has limited ability to regenerate since it is avascular, resulting in untreatable degenerative joint diseases that impact millions of people worldwide [186]. Several treatment strategies are available to treat cartilage defects, such as cell therapies to restore joint motion and relieve pain. Also, various tissue–engineered cartilage scaffolds have been developed to create cartilage–like tissue models by engineering the matrix stiffness with a polysaccharide or protein–based materials. However, these scaffolds do not match cartilage's native features, which include mechanical properties for the pericellular matrix to surround chondrocytes and a stiff extracellular matrix for maintaining macromechanical tissue properties [187,188]. To fabricate cartilage tissue with two different mechanical stiffness, de Melo et al., used an embedded printing system with alginate/polyethylene glycol (PEG) as a support bath for high stiffness matrix and fibrin as a soft material for the maintenance of chondrocytes. Support bath was developed through semi–interpenetrating networks (IPN) formed by 15 %, 20 % PEG and 2.5 % alginate for covalent and ionic crosslinking of the hydrogels. Further, human mesenchymal stem cells were used to develop spheroids and mixed with fibrinogen solution to extrude vertically into the support bath. hMSC spheroids–laden fibrinogen filaments extruded into the support bath showed higher viability (91.2 ± 1.0 %) on day 5 compared to cells encapsulated in PEG–alginate IPN hydrogel (79.3 ± 1.8 %). Also, after three weeks of culture, hMSC spheroids showed GAG and collagen deposition, indicating that this environment promoted

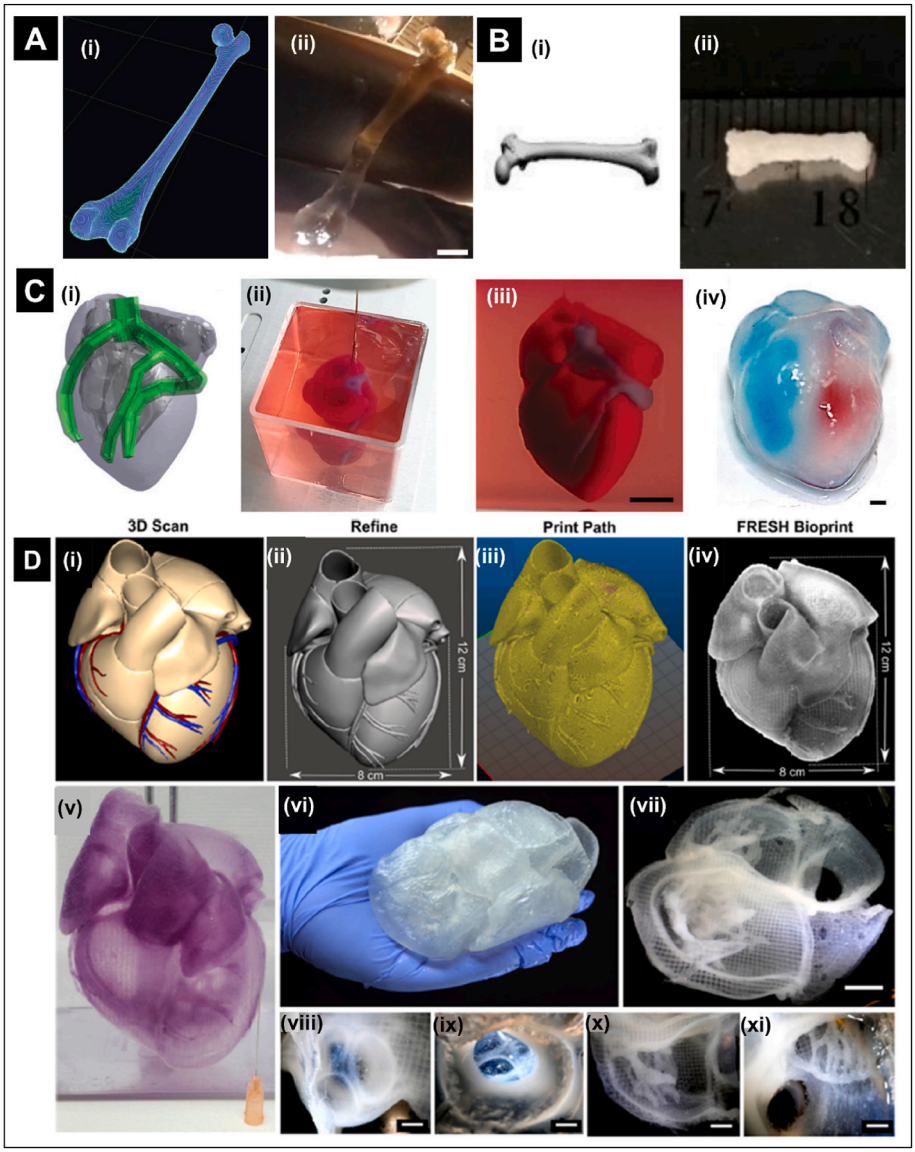

Fig. 12. Bone & heart models fabricated through embedded bioprinting methods. [A] Human femur bone fabricated using FRESH method. (i) 3D model of human femur bone. (ii) Femur bone after extracting from support bath (scale bar – 10 mm). (Reproduced with permission from Ref. [50]); [B] (i) 3D model and (ii) Bone model printed using cell-only bioink. (Reproduced with permission from Ref. [105]); [C] A printed small–scaled cellularized human heart. (i-ii) The human heart CAD model was printed in an alginate–based support bath system, and (iv) A hollow chambered heart was injected with red and blue dyes (scale bar – 0.5 cm and 1 mm) (Reproduced with permission from Ref. [49]); [D] Printing of full–size human heart models using the FRESH technique – (i) 3D model. (ii) Refining of 3D model to a printable file. (iii) G–code pathing. (iv) Full–size human heart printed in the FRESH bath.; (v & vi) Alginate heart model stained with alizarin red & handled in air. Internal structures of heart models printed using FRESH (vii) Printed half heart (scale bar = 1.5 cm). (vii) pulmonary. (ix) Aortic valves. (x) Papillary muscle and (xi) Trabeculae carnae (scale bar = 1 cm) (Reproduced with permission from Ref. [62]).

chondrogenic–like differentiation (Fig. 11). According to these findings, the cartilage–like tissue fabrication approach employed here offers a lot of potential for future cartilage regeneration research using embedded printing approaches [189].

7.3. Bone

Various embedded bioprinting approaches have been used for fabricating bone constructs [190]. Recently, Cidonio et al., combined laponite and gellan gum to print 3D sleeve and lattice structures inside an agarose support bath for repairing long bone defects [88]. Thomas et al., printed acellular bone constructs with 50 % infill density using a 4 % alginate bioink into the support bath comprised of gelatin particles and 11 mM $CaCl_2$ (FRESH method) (Fig. 12A). Mechanical properties were compared between the printed constructs and casted alginate hydrogels. Remarkably, the mechanical properties of FRESH bioprinted constructs showed lower (nine times) elastic modulus and higher (two times) strain to failure ratio due to anisotropy in printed constructs. The observed differences may be due to the anisotropy and porosity of the bioprinted constructs due to 50 % infill density and internal cracks. Printing bone structures through 3D bioprinting showed the effectiveness of the FRESH method in organ fabrication [50]. Similarly, Jeon et al., developed a photoactive alginate–based microgel supporting medium for printing different shaped constructs, including a letter C, a cube, and a femur bone using cell–only bioinks containing hMSC. The cell-laden bone model printed in support bath closely resembled the intricately designed 3D models (Fig. 12B). The alginate microgels exhibited shear–thinning behavior around the nozzle and were stabilized by exposure to UV light, creating a stable support gel construct. The hydrogel layer of support gel–covered the printed cell–only bioinks and the support bath hydrogel provided nutrients and improved cell–cell communication, tissue formation and maturation [105]. Although these printed models mimic the macroscopic structure of bones, they are mechanically weak compared to the native bones (6.9 GPa–25 GPa) or currently used materials such as titanium (113.8 GPa). Research on utilizing hydroxyapatite-based inks for the osseous matrix and soft gel-like materials for the inner bone marrow are critical to develop bone constructs that mimic the anatomical and mechanical characteristics of natural bones.

7.4. Heart

The cardiovascular system (CVD) is one of the most complex organ systems in the human body. Researchers around the globe have developed several approaches to fabricate complete organs, including the heart, kidney, brain, etc. [27,191]. Hinton et al., developed a strategy to print a complete heart model using FRESH printing using a 3D digital heart model (2.5 mm) by scanning 5–day old embryonic chick heart using confocal microscopy. This 3D model was scaled up to 2.5 cm, and the printed whole heart model was similar to the 3D model (10 % variability) and the internal trabeculation showed efficacy of the FRESH method in printing of submillimeter length scale structures. However, the developed model had several limitations such as inability to integrate with the host system due to the lack of major blood vessels and the coronary artery [50]. Lee et al., fabricated the human cardiac ventricle model using collagen bioink in the FRESH v2.0 support bath with better printing resolution (20 μm) with small–sized gelatin microparticles. A left ventricle model with an early–stage fetal heart size was designed as an open ellipsoidal shell with a 6.6 mm outer diameter and 8 mm length from base to apex. This model was made of two different cell types (ESC–CM and human ventricular cardiac fibroblasts) and two different bioinks (20 mg/mL fibrinogen; 24 mg/mL collagen type 1). Electrophysiological analysis of the printed constructs was assessed under spontaneous and stimulated conditions. Paced contractions (80 V, 20 m s, square wave pulse at 1, 2, and 4 Hz) were performed with two parallel platinum electrodes and point stimulation was driven by using a concentric bipolar microelectrode composed of an inner platinum–iridium pole and outer stainless–steel pole (20 V, 20 m s square wave pulse at 1 and 2 Hz). The synchronous beating was observed after seven days of culture and the printed constructs were expanded inward and outward, similar to the native heart in systole and diastole [70].

Noor et al., fabricated personalized patient–specific vascularized cardiac patches and whole heart models in an alginate–based support bath using decellularized omentum hydrogel as bioinks. Patient–derived omental stromal cells were reprogrammed into iPSC cells and differentiated into cardiomyocytes (CMs) and endothelial cells (ECs). Vascularized cardiac patches were printed using omentum bioinks with 30 G needles in a pattern with two layers of cardiomyocytes and one layer of omentum bioink with spaces to deposit endothelial cells contained in gelatin bioink. The support gelatin structures in the patch were removed by maintaining the construct at 37 °C. Further, the whole heart structure was printed using two different omentum bioinks composed of cardiomyocytes and endothelial cells with blue or red polystyrene microparticles. Small scale human whole heart construct with wall septation (four chambers) was printed in a support medium with the specific dimensions (height: 20 mm; diameter: 14 mm) and incubated at 37 °C for 45 min for crosslinking of bioink (Fig. 12C). The printed constructs showed spatial interactions between CMs and ECs similar to the 3D model and staining against sarcomeric α-actinin revealed the homogenous distribution of the cardiomyocytes throughout the construct. However, the printed construct still served as a prototype, and the functionality of the printed constructs needs to be evaluated for implantation in patients [49]. Similarly, the full–sized adult human heart ($8 \times 10 \times 12$ cm^3) and the coronary artery were bioprinted by Mirdamadi et al., using a 4 % alginate and FRESH method with complete structural and anatomical similarity by altering a customized 3D printer to print for extended durations. The total time for printing the whole heart model with 100 μm resolution was 92 h. The mechanical properties of the bioprinted heart using 4 % alginate with low infill (10 %) were similar to the native heart (Fig. 12D) [62]. Although this work establishes the proof of concept, it is challenging to understand the cell–material interactions and biocompatibility of the printing method with acellular models [50].

7.5. Vascular constructs

There is an increasing necessity for the vascularization of bioprinted constructs to transport nutrient–containing fluids, both *in vitro* and *in vivo* [192]. A major limitation in tissue engineering is to recapitulate native vasculature in the engineered constructs which is imperative for nutrient diffusion, gaseous exchange and transportation of body fluids in *vivo* conditions. Several researchers are working on the fabrication of anatomically equivalent vascular grafts by using template-based and template-free approaches [193–196]. By using template based 3D bioprinting technologies, well assembled tubular vascular grafts are widely prepared using different types of bioinks and characterized for *in vitro & in vivo* applications [47,197,198]. Also, template-free processes such as 3D wet writing have the capability to produce perfusable, customizable, biomimetic bi-layered tubular constructs (BLT) with native mechanical properties [196]. However, fabrication of microvascular structures with conventional methods is difficult due to size and resolution limitations [64]. FRESH printing supported the printing of less than 1 mm wall thickness constructs with lumen diameters of 1–3 mm and showed good print fidelity with 15 % print variation. Perfusion of constructs with black food colour dye showed little diffusion and better integrity of the 3D printed layers [50]. Using the FRESH printing method, Mirdamadi et al., printed a superimposed coronary artery segment on the left ventricle with slight modifications from the initial design using Meshmixer. Further, the potential of the developed model to allow free flow of liquids inside the bifurcated structure was evaluated by perfusing with blood–like glycerol solution. Interestingly, the developed model demonstrated the structural and anatomical features of coronary artery

similar to native conditions [62].

In the direct bioprinting approach, free–standing of printed filaments in air is difficult since gravitational force significantly affects the structure of the final construct. In a recent study, Jin et al., printed vascular constructs inside 2 % (w/v) laponite support bath using 2.0 % (w/v) alginate and 10.0 % (w/v) gelatin bioink containing 5×10^6 cells/mL 3T3 fibroblasts (NID – 25G; pressure – 15 psi; print speed – 2.0 mm/s). Y–shaped tubular constructs were printed with dimensions of 4.0 mm in diameter, 1.0 mm in wall thickness and 2.2 cm in height, with an inclination angle of 45° at branches. Compared to general bioprinting method, the developed localized layer–by–layer printing reduces printing time by 30 min with minor increments in the printed construct diameter. The cell–laden constructs were cultured for three days with cell viability more than 80 %, showing cytocompatibility of the developed constructs and printing method [54]. Through the freeform reversible embedding (FRE) method, large tubular constructs (length 2 cm & diameter 1.2 cm) were fabricated in a Carbopol support bath system with PDMS ink at the printing speed of 20 mm/s. After completing the printing process, the constructs were removed from the container by immersing in 10*X* PBS. Perfusion of printed constructs with black food dye showed the leak–proof printing ability of the FRE printing method [67].

Lee et al., printed perfusable collagen tubes resembling the left anterior descending artery (LAD) of human heart with dimensions of 1.4 mm inner diameter lumen, 0.3 mm wall thickness and 9 mm length using C2C12 cells. Further, the patency of printed blood vessels was confirmed by perfusing the multiscale vasculature through the root of the LAD. C2C12 cell–laden tubes were perfused using fluorescently labelled dextran and cultured for five days in static and dynamic conditions using a peristaltic pump at a 0.4 mL/min flow rate. Furthermore, constructs cultured in static showed minimal compaction and cell death at the middle portion of the constructs, whereas perfused constructs showed good compaction, cell viability and active remodeling. Likewise, the developed models have great potential in regenerating the heart and associated vascular networks with 3D bioprinting using the FRESH model. However, several additional elements are also required for the development of implantable models, such as billions of cells, the recapitulation of native architecture, and structural flexibility [70].

7.6. Other shapes

Human brain 3D models were also developed using higher resolution MRI imaging and printed with 100 % infill using alginate bioink. Construct size was scaled down to 3 cm, and the exterior surface of the

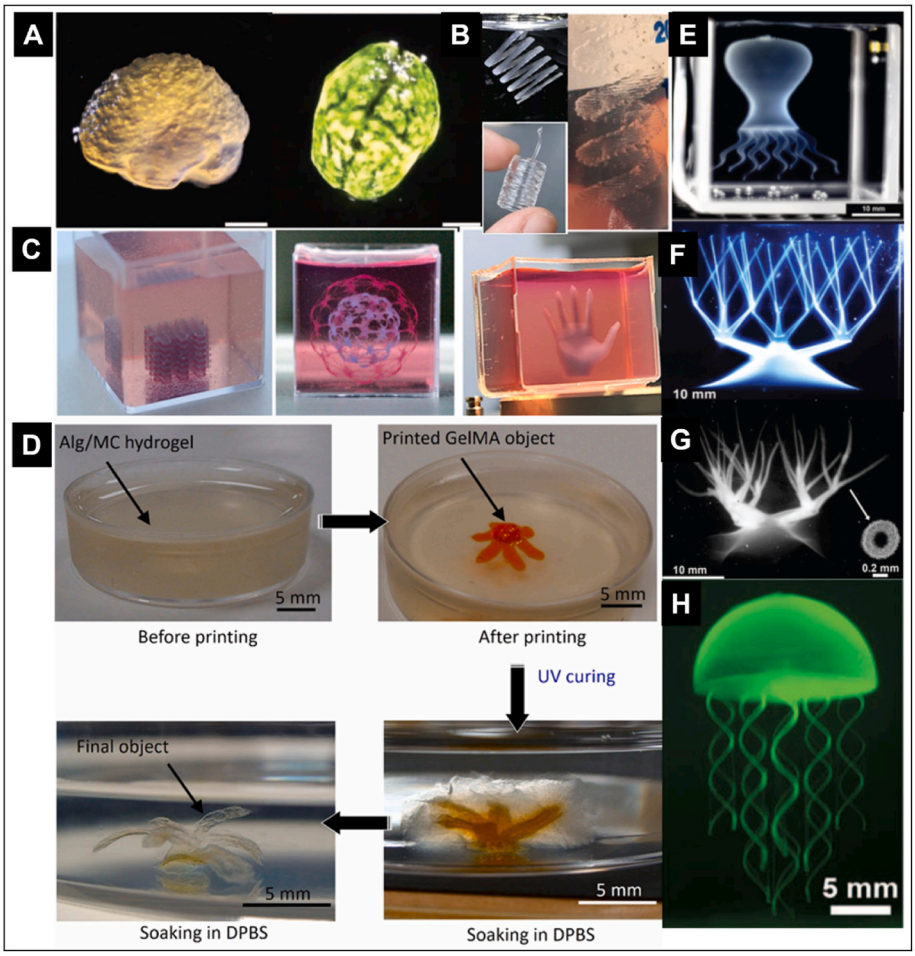

Fig. 13. Different shapes printed in an embedded bioprinting system. [A] 3D brain model was printed with alginate bioink in gelatin support bath (FRESH) and top–down view of the 3D printed brain with high print fidelity and visible white matter (Reproduced with permission from Ref. [50]); [B] PDMS structures printed in Carbopol support (helix print, printed tubes with fused layers, helical tube) (Reproduced with permission from Ref. [67]); [C] Printing different shapes in alginate support medium (A multi–layered crisscross construct, hollow ball–like structures, and a hand (Reproduced with permission from Ref. [49]); [D] Hierarchical branched tubular networks. A continuous network of hollow vessels and crosslinked construct after removal from the granular support gel (Reproduced with permission from Ref. [106]); [E] A thin–shell octopus model is made from multiple connected hydrogel parts; A continuous network of hollow vessels [F] Inside support bath and [G] After removing from support bath; [H] A model jelly fish incorporates flexible high aspect ratio tentacles attached to a closed–shell body (Reproduced with permission from Ref. [56]).

brain model was printed using alginate with clearly defined frontal and temporal lobes of the cortex and the cerebellum in a gelatin support bath (Fig. 13A) [50]. Carbopol based printing bath was supported to print different shaped constructs such as helix and spiral tubes with PDMS inks (Fig. 13B) [67]. Thomas et al., printed helix shapes and coaxial cylinders with red and green fluorescently labelled alginate inside the support bath. Noor et al., printed different shaped acellular constructs such as a multi–layered crisscross construct, a double–layered construct, single–layered hollow ball–like structures, and a hand in alginate–based transparent support medium with omentum bioink (Fig. 13C) [49]. Li et al., developed non–submerged (direct printing) and submerged (printing in support bath) printing approaches to fabricate complex models using methylcellulose (MC), alginate and GelMA. Complex structures such as line (3 mm), triangle (6 mm), and 3D grid structure (12 mm) were fabricated using a non–submerged method, and the 3D flower was printed in a support bath containing MC/Alg using 10 % GelMA. Printed structures were easily removed from the support bath by placing the constructs in DPBS with slight mechanical agitation (Fig. 13D) [106]. Bhattacharjee et al., fabricated several complex shapes like an octopus, jellyfish and Russian doll models in granular support gel (Fig. 13E–H). The octopus model was printed with 100 μm vertical pitch dimensions and 100 μm line widths and allowed to crosslink under UV light for 6 h. Further, the post–crosslinked constructs were extracted from the support bath and found to have high mechanical strength and layer integrity. Similarly, the developed jelly fish model with solid tentacles also showed life–like motion and the printing of Russian doll models with closed shells showed the efficacy of the granular gel model in the development of complex structures [56]. Rocca et al., fabricated concept models of the heart and kidney–like structures and three different coloured alginate bioinks in Pluronics F–127 support bath system [34]. A photocurable alginate–based support bath was used to print ears and bone structures using cell–only bioink [105]. Centimeter–sized gut tubes were prepared with collagen I bioinks to observe cellular infiltration in a granular support medium for creating heterogeneously populated engineered tissue structures [199].

7.7. Tumor organoids

In vitro drug screening for various clinical challenges, including cancer, significantly helps in translating drugs from pre–clinical to clinical studies. Although most of the drugs showed efficacy *in vitro,* could not be translated because of poor resemblances of *in vitro* models with *in vivo* conditions, resulting in a loss of time and money [200]. Advancements in biomaterials and 3D bioprinting have enabled the fabrication of biomimetic tissues, providing an alternative to traditional animal experiments for testing pharmaceutical substances tailored to individual patients [201]. Developing tumor models for drug testing using bioprinting is challenging since bioinks are vital in defining cancer cell responses. In recent years, embedded bioprinting has gained interest in reproducing tumor microenvironments due to its ability to print low-viscosity ECM components (like collagen, elastin, hyaluronic acid, etc.) residing at tumor sites and affecting adhesion, proliferation, migration, and vascularization [202]. Although Matrigel® is commonly used to develop tumor models, it is not ideal for maintaining native cellular morphology and responses, such as epithelial to mesenchymal transitions in many cancer cells [203].

To overcome the drawbacks of tumor matrix based bioinks, Shi et al., developed a novel bioink to create a breast cancer model using low-concentration collagen, hyaluronic acid (HA), and poly (*N*-isopropylacrylamide) (pNIPAM) by depositing into a support bath made up of silk fibroin. To evaluate the efficacy of the developed bioinks, three different breast cancer cells such as 76NTERT cells (non-tumorigenic), 21 P T cells (non-invasive tumorigenic), and MDA-MB-231 cells (invasive & mesenchymal), were used. Interestingly all three cell types retained their morphology and features in the developed collagen-HA-pNIPAM (CH) bioink compared to only collagen (C) and Matrigel (M) models. Moreover, tumor organoids were developed by printing breast cancer cells in the core region and fibroblast cells in the peripheral region. Among the three bioinks (C, CH, M), CH bioink uniquely preserved the phenotypic characteristics of both epithelial tumor cells and fibroblasts due to their ability to replicate the *in vivo* breast cancer tumor microenvironment demonstrating the importance of extracellular matrix (ECM) components in the fidelity of tumor models [142]. In another study, Maloney et al., used embedded bioprinting technology to screen chemotherapeutic drugs for HepG2, Caco2, and patient–derived glioblastoma and sarcoma. Patient tumor organoid models (PTO) are created by mixing and printing tumor cells, methacrylated collagen, and thiolated hyaluronic acid into a gelatin support bath and exposed to UV light for crosslinking. The PTO models are further exposed to different drugs, such as dacomitinib for glioblastoma and imatinib and doxorubicin for sarcoma in different dosages. Dose–dependent decrease in ATP activity was observed in immersed PTO models suggesting a new drug screening method to overcome the limitations of existing screening methods [204]. In future, tumor-specific bioinks could be developed for assessing drug effectiveness across diverse cancer models before clinical trials, which would potentially save substantial amount of time and money [205,206].

8. Challenges in clinical translation of embedded bioprinted constructs

3D bioprinting is an efficient method to create geometrically complex models with biomimetic microenvironments for drug screening and tissue regeneration [207]. Implantation and functional evaluation of bioprinted constructs using pre–clinical models have increased in the last decade [201]. However, immediate clinical translation of bioprinted products is difficult due to the limitations in fabricating large–sized complex organs such as the heart and kidney. This is because the existing bioprinters may not replicate the native microvasculature but also cause larger constructs to collapse due to gravitational forces [208]. Moreover, suturing of 3D bioprinted vascular models with native microvasculature is challenging and could lead to leaky blood vessels [209]. As a potential alternative, embedded bioprinting has been currently researched to augment the clinical translation of bioprinted constructs. This method helps to overcome print size limitations by providing a removable and stable support medium to fabricate full–sized organs. However, the requirement of high cell densities, prolonged printing durations (few hours to days) and removal of support medium from printed large & complex organs are the major difficulties in the biofabrication of organs [62,97]. Although the printed structures were removed from the supportive medium, during printing with cell–laden bioinks, for extensive printing durations and post-processing steps may cause a reduction in cell viability, leading to decreased functionality of the final constructs. Further, storage of bioprinted tissues and organs without affecting the viability of the cells inside the constructs remains a great challenge [210,211].

Regulatory and ethical considerations are crucial in implementing embedded bioprinting for human applications to ensure safety, efficacy, and adherence to established guidelines and moral principles. In recent years, utilization of iPSCs for tissue engineering and regenerative medicine has increased due to the remarkable potential for personalized therapies, disease modeling, and reduced ethical concerns compared with ESC. Using iPSCs for cell therapies and fabricating tissue-engineered constructs may reduce challenges like immune responses and tissue rejection since they are derived from a patient's own cells, thus reducing the risk of immune-related complications. For organ fabrication, integrating iPSCs into functional bioinks, subsequently printed using embedded printing techniques, has enabled the possibility of establishing a viable path toward the clinical translation of bioprinted constructs for organ fabrication [83,212,213]. However, to meet the prerequisites for clinical implementation, it is crucial to systematically establish the safety and effectiveness of bioprinted organs and tissues

containing cells (including stem cells and primary cells) through comprehensive *in vitro* and *in vivo* assessments, adhering to regulatory authority guidelines. This approach is essential to address typical challenges such as teratoma formation, insufficient maturation, and proper host tissue integration before embarking on clinical trials [214–216]. The FDA Modernization Act 2.0 revised mandatory drug efficacy evaluations in animal models with tests involving *in vitro*, *in silico*, and non-human *in vivo* assessments, utilizing three-dimensional models containing human cells before clinical trials highlight the potential of bioprinted tissues/organs for drug testing and tissue engineering evaluations, offering promising alternatives for the approaches currently in practice [217]. In many countries, 3D-printed or bioprinted products are categorized as pharmaceutical or cellular products and do not have specific clinical translation and commercialization regulations. However, bioprinted products require special regulations and standards for easy clinical translation and commercialization [26].

9. Future directions & conclusions

Bioprinting has a wide range of applications in regenerative medicine, including biomimetic and complex tissue fabrication for implantation [218]. However, the major limitations of nozzle–based bioprinting technologies for organ fabrication are the less availability of printable bioinks, poor printing resolution, less vascularization, and challenges in printing of large–scale structures [219]. Though embedded bioprinting is at its infancy, it can be used as an alternative to conventional bioprinting. The utilization of embedded bioprinting has increased remarkably in the last five years owing to its ability to fabricate long tubular structures, complex tissues, and organs with micro vascularization [220]. For organ fabrication, embedded bioprinting has several drawbacks due to the incompatibility of bioprinters for embedded bioprinting, limited materials availability for support bath preparation, similar crosslinking mechanisms for support bath and functional bioinks, sterilization of support baths, regulations and commercialization of the bioprinted organs [221]. Bioprinter based limitations include the cost of bioprinters, build volume, hardware and software integration that is compatible with embedded bioprinting. As a consequence of technical breakthroughs in bioprinter hardware, the cost of bioprinters has reduced dramatically in recent years compared to the early 2000s [222]. For example, bioprinters are commercially available at costs ranging from $10,000 to $300,000 depending on features such as the number of print heads, heating & cooling features of print heads & print bed, and types of print heads equipped with bioprinters, etc. [223]. However, customization of bioprinters has gained more interest for using embedded bioprinting since it requires a large build volume to house the support bath containers [50,82]. Long needles are another crucial need for embedded bioprinting to minimize contamination concerns caused by contact with the support bath. Also, the development and integration of user–friendly software for easy operation of support bath–based printing provides additional advantages.

Identifying low–cost, easily removable next–generation biomaterials for support bath preparation that are compatible with a broad range of bioinks, and crosslinking methods is also required to build complex tissues and organs. Current strategies used for removing printed structures from the support baths, such as adjusting pH or ion concentrations, agitations or manual removal of constructs from the support bath, are not biocompatible [221]. Hence, removing the printed constructs from the support bath should be easy and gentle to prevent cellular damage and maintain the structural integrity of printed constructs. Creating microvascularized tissues with existing support bath methods is very difficult due to the diameter of capillaries (<10 μm) in the native systems, where the lowest resolution achievable with the currently using embedded printing strategies is about 10 μm [101,224]. In addition, removal of the micron–sized vascular structures from support baths are critical. Also, it is difficult to adopt existing procedures such as filtration, autoclaving, UV, and ethylene oxide (EtO) for sterilizing of support baths and to maintain sterile printing environments [225,226]. Since support baths have high viscosity, the filtration process is difficult and as a result, requires a greater volume of liquid and more time. Autoclaving the support bath at high temperatures and pressures may damage its components. UV sterilization is often used to disinfect printing environment, apparatus, and ingredients used for bioprinting. However, it has significant drawbacks, such as limited penetration into the turbid support baths and chemical cleavage of incompatible support bath components. To print large–scale structures, bioprinters must be accommodated in advanced facilities such as clean rooms to ensure sterility and avoid contamination.

Bioprinting is a promising platform for delivering biological molecules such as growth factors and drugs that are essential for cell adhesion, proliferation, migration, differentiation, and maturation in the bioprinted tissues and organs [227]. Embedded bioprinting can integrate drug delivery systems to enable the controlled release of therapeutic agents to specific regions of the bioprinted tissues by directly mixing biomolecules with bioinks, incorporating drug/growth factor loaded micro/nanoparticles into bioinks, and microvascular-based delivery [70,88]. In the first approach, growth factors are incorporated into bioinks (by directly mixing or covalently linking them with biomaterials) prior to printing promote maturation of printed tissues by slowly releasing the growth factors [228]. Alternatively, drug-loaded particles or microspheres might also be loaded within the hydrogel matrix used for bioprinting to release the drug/growth factors in a controlled manner for sustained and localized delivery to the surrounding cells [229–231]. Finally, microvasculature can also be incorporated into the bioprinted tissues to enable the controlled delivery to specific regions for promoting cell proliferation and tissue maturation [232]. Stimuli-responsive materials are an important class of materials for on-demand drug or growth factor delivery in tissue engineering through bioprinting [233,234]. These bioinks/biomaterials are designed to respond to specific stimuli, such as changes in temperature, pH, light, and electricity, which can trigger the release of growth factors [171]. More research on developing 3D printed scaffolds that can release growth factors in response to specific mechanical stimuli (compression or tension) for precise control over the release kinetics of growth factors may help in functional tissue maturation.

As an alternative to traditional biofabrication methods, embedded bioprinting can produce tissues/organs based on patient anatomical data with higher resolution and better vasculature, utilizing ECM-based bioinks [235]. However, ECM bioinks like collagen often exhibit batch–to–batch differences, and the risk of disease transmission from xenogeneic sources make it difficult to use ECM bioinks for the fabrication of implantable tissue constructs [236]. Alternatively, synthetic peptides might be used as bioink for embedded bioprinting because of their controlled manufacturing, chemical composition, biocompatibility, and functionality. Finally, millions to billions of cells must be mixed with bioinks to print large tissues/organ models, with uniform cell distribution and long–term cell viability is very critical. Replicating the structural organization of native tissues remains a significant challenge when printing heterogeneous materials for embedded bioprinting. Table 3 shows the requirements to fabricate tissues/organs using embedded printing along with challenges and future outlook.

In conclusion, the process of fabricating biomimetic tissues and organs using 3D bioprinting has improved significantly over the last two decades. From scale–up to ultimate implantation, 3D bioprinting needs optimization, validation and commercialization. In the normal bioprinting (printing in air support) approach, tissues and organs are fabricated through a layer–by–layer process without additional support structures. Embedding bioprinting systems use a support medium to print large–scale tissues and organs without collapsing their shape. Printing large size and tubular–shaped constructs with the desired diameter requires self–standing and cell–supportive bioinks with high stability for long–term cultures and tissue maturation. Further, significant progress in the creation of support bioinks is required to produce

Table 3
Challenges and future outlook in embedded bioprinting for tissue/organ fabrication.

Requirements to fabricate biomimetic tissues/organs via embedded bioprinting	Challenges	Future Outlook
Selection and development of suitable bioinks	• Poor stability •Higher swelling •Similar crosslinking mechanisms for bioink & support bath	•Bioinks with novel crosslinking strategies should be developed to control swelling & improve the stability for long-term *in vitro* culture •Usage of synthetic peptides as bioinks
Support bath stability for long-term printing	•Drying of support bath during printing for long hours •Changes in viscoelastic properties of support bath	•Development of support baths which maintains their viscoelastic properties •Bioprinting facilities required to maintain in controlled environment to prevent drying & adverse environmental factors
Support bath stability for long-term *in vitro* culture	•Disintegration of embedded printed constructs due to poor mechanical properties of support bath	•Support baths which allows easy nutrient penetration, sustained cell growth and tissue maturation over prolonged periods required to achieve tissue maturation & functionality
Vascularization	•Constructs with microvasculature •Integration of vascularized bioprinted constructs with host vasculature	•Developing strategies to anastomose microvasculature of printed constructs with host vasculature to provide nutrients and oxygen
Printing duration/time	•Strategies used now are time consuming depending on the resolution & size of tissue/organ	•The advancement of embedded printing methods is necessary to achieve the fabrication of tissues and organs within a short timeframe with high-resolution
Scalability & maturation	•Translation from laboratory-scale organs to clinically viable larger tissues or organs •Single-time usage of support baths	•Printing parameters optimization to match the scalability without affecting cell viability •Advancements in automation and standardization to increase the productivity •Maintenance of bioprinted tissues & organs in bioreactors to develop fully matured tissues & organs to match the organ demands
Regulatory issues	•Clinical trial approvals and marketing approvals for bioprinted constructs are yet to be achieved •Revisions on regulations required for translating bioprinted constructs	•Developing common international regulations/guidelines is essential to overcome the existing challenges
Storage	•Preservation of printed organs •Quality assessment	•Implementation of cryopreservation strategies to the embedded printed tissues/organs for prolonged storage & minimize the risk of damage •Quality assessment for evaluating the bioprinted tissues/organs functionality & efficacy
Commercialization	•Cost •Batch-to-batch variations •Demand vs supply	•Developing cost-effective & reusable support baths •Development of bioprinters with multiple printing stations for accommodating & simultaneously printing different tissues & organs •Usage of standard materials and printing conditions to minimize batch-to-batch variations

transparent and non–toxic support baths for the fabrication of organ models that are close to native. Longer–term culture of the printed constructs in support baths is required to assess stability, since cells make their own ECM under *in vitro* conditions, which may improve the functionalities of the final product. Furthermore, the support–based printing technique still needs to produce more robust, clog–free, and cost–effective printing methods to construct implantable biomimetic organs.

Ethics approval and consents to participant

Not applicable.

Declaration of competing interest

Swaminathan Sethuraman *is an editorial board member for Bioactive Materials and was not involved in the editorial review or the decision to publish this article. All authors declare that there are no competing interests.*

Acknowledgements

The authors wish to acknowledge Nano Mission, Department of Science & Technology (DST) (SR/NM/TP–83/2016 (G)), and Prof. T. R. Rajagopalan R & D Cell of SASTRA Deemed University for financial and infrastructural support. We also wish to acknowledge ATGC grant, Department of Biotechnology (DBT) (BT/ATGC/127/SP41147/2021), Adhoc funding, Indian Council of Medical Research (ICMR) (17x3/Adhoc/23/2022–ITR) and DST SERB CRG (Exponential Technologies) grant (CRG/2021/007847) for financial support. First author is thankful to Indian Council of Medical Research (ICMR) for the senior research fellowship (3/1/1(4)/CVD/2020–NCD–1).

References

[1] D.F. Williams, Challenges with the development of biomaterials for sustainable tissue engineering, Front. Bioeng. Biotechnol. (2019), https://doi.org/10.3389/fbioe.2019.00127.
[2] A. Khademhosseini, R. Langer, A decade of progress in tissue engineering, Nat. Protoc. 11 (2016) 1775–1781, https://doi.org/10.1038/nprot.2016.123.
[3] P. Kuppan, S. Sethuraman, U.M. Krishnan, Fabrication and investigation of nanofibrous matrices as esophageal tissue scaffolds using human non-keratinized, stratified, squamous epithelial cells, RSC Adv. (2016), https://doi.org/10.1039/c5ra24303c.
[4] J. Radhakrishnan, A. Manigandan, P. Chinnaswamy, A. Subramanian, S. Sethuraman, Gradient nano-engineered in situ forming composite hydrogel for osteochondral regeneration, Biomaterials 162 (2018) 82–98, https://doi.org/10.1016/j.biomaterials.2018.01.056.
[5] A. Sola, J. Bertacchini, D. D'Avella, L. Anselmi, T. Maraldi, S. Marmiroli, M. Messori, Development of solvent-casting particulate leaching (SCPL) polymer scaffolds as improved three-dimensional supports to mimic the bone marrow niche, Mater. Sci. Eng. C 96 (2019) 153–165, https://doi.org/10.1016/j.msec.2018.10.086.
[6] S. Bersini, I.K. Yazdi, G. Talò, S.R. Shin, M. Moretti, A. Khademhosseini, Cell-microenvironment interactions and architectures in microvascular systems, Biotechnol. Adv. (2016), https://doi.org/10.1016/j.biotechadv.2016.07.002.
[7] Y. Kim, H. Ko, I.K. Kwon, K. Shin, Extracellular matrix revisited: roles in tissue engineering, Int. Neurourol. J. (2016), https://doi.org/10.5213/inj.1632600.318.
[8] M.D. Grounds, Obstacles and Challenges for Tissue Engineering and Regenerative Medicine: Australian Nuances, Clinical and Experimental Pharmacology and Physiology, 2018, https://doi.org/10.1111/1440-1681.12899.
[9] D.S. Muthu Parkkavi Sekar, Harshavardhan Budharaju, Zennifer Allen, Sethuraman Swaminathan, Four dimension printing in healthcare, in: 3D Printing in Medicine, second ed., 2022, https://doi.org/10.1016/B978-0-323-89831-7.00010-9.
[10] J.J. Ballyns, L.J. Bonassar, Image-guided tissue engineering, J. Cell Mol. Med. (2009), https://doi.org/10.1111/j.1582-4934.2009.00836.x.
[11] H. Budharaju, S. Suresh, M.P. Sekar, B. De Vega, S. Sethuraman, D. Sundaramurthi, D.M. Kalaskar, Ceramic materials for 3D printing of biomimetic bone scaffolds – current state-of-the-art & future perspectives, Mater. Des. 231 (2023), 112064, https://doi.org/10.1016/j.matdes.2023.112064.

[12] J. Li, M. Chen, X. Fan, H. Zhou, Recent advances in bioprinting techniques: approaches, applications and future prospects, J. Transl. Med. 14 (2016) 271, https://doi.org/10.1186/s12967-016-1028-0.

[13] P.S.S. Gungor-Ozkerim, I. Inci, Y.S.S. Zhang, A. Khademhosseini, M.R. R. Dokmeci, Bioinks for 3D bioprinting: an overview, Biomater. Sci. 6 (2018) 915–946, https://doi.org/10.1039/c7bm00765e.

[14] P. Rider, Ž.P. Kačarević, S. Alkildani, S. Retnasingh, M. Barbeck, Bioprinting of tissue engineering scaffolds, J. Tissue Eng. (2018), https://doi.org/10.1177/2041731418802090.

[15] I. Angelopoulos, M.C. Allenby, M. Lim, M. Zamorano, Engineering inkjet bioprinting processes toward translational therapies, Biotechnol. Bioeng. (2020), https://doi.org/10.1002/bit.27176.

[16] L. Koch, M. Gruene, C. Unger, B. Chichkov, Laser assisted cell printing, Curr. Pharmaceut. Biotechnol. 14 (2013) 91–97, https://doi.org/10.2174/138920113804805368.

[17] A. Zennifer, A. Subramanian, S. Sethuraman, Design considerations of bioinks for laser bioprinting technique towards tissue regenerative applications, Bioprinting 27 (2022), e00205, https://doi.org/10.1016/j.bprint.2022.e00205.

[18] I.T. Ozbolat, M. Hospodiuk, Current advances and future perspectives in extrusion-based bioprinting, Biomaterials 76 (2016) 321–343, https://doi.org/10.1016/j.biomaterials.2015.10.076.

[19] H. Budharaju, A. Subramanian, S. Sethuraman, Recent advancements in cardiovascular bioprinting and bioprinted cardiac constructs, Biomater. Sci. 9 (2021) 1974–1994, https://doi.org/10.1039/d0bm01428a.

[20] P. Datta, A. Barui, Y. Wu, V. Ozbolat, K.K. Moncal, I.T. Ozbolat, Essential steps in bioprinting: from pre- to post-bioprinting, Biotechnol. Adv. 36 (2018) 1481–1504, https://doi.org/10.1016/j.biotechadv.2018.06.003.

[21] M. Thangadurai, A. Ajith, H. Budharaju, S. Sethuraman, D. Sundaramurthi, Advances in electrospinning and 3D bioprinting strategies to enhance functional regeneration of skeletal muscle tissue, Biomater. Adv. 142 (2022), 213135, https://doi.org/10.1016/j.bioadv.2022.213135.

[22] A.K. Miri, I. Mirzaee, S. Hassan, S. Mesbah Oskui, D. Nieto, A. Khademhosseini, Y. S. Zhang, Effective bioprinting resolution in tissue model fabrication, Lab Chip 19 (2019) 2019–2037, https://doi.org/10.1039/c8lc01037d.

[23] X. Li, B. Liu, B. Pei, J. Chen, D. Zhou, J. Peng, X. Zhang, W. Jia, T. Xu, Inkjet bioprinting of biomaterials, Chem. Rev. 120 (2020) 10793–10833, https://doi.org/10.1021/acs.chemrev.0c00008.

[24] J.F. Gomes Gama, E.A. Dias, R.M.G. Aguiar Coelho, A.M. Chagas, J. Aguiar Coelho Nt, L.A. Alves, Development and implementation of a significantly low-cost 3D bioprinter using recycled scrap material, Front. Bioeng. Biotechnol. 11 (2023) 1–16, https://doi.org/10.3389/fbioe.2023.1108396.

[25] S. Derakhshanfar, R. Mbeleck, K. Xu, X. Zhang, W. Zhong, M. Xing, 3D bioprinting for biomedical devices and tissue engineering: a review of recent trends and advances, Bioact. Mater. 3 (2018) 144–156, https://doi.org/10.1016/j.bioactmat.2017.11.008.

[26] M.P. Sekar, H. Budharaju, A. Zennifer, S. Sethuraman, N. Vermeulen, D. Sundaramurthi, D.M. Kalaskar, Current standards and ethical landscape of engineered tissues-3D bioprinting perspective, J. Tissue Eng. 12 (2021), 20417314211027676, https://doi.org/10.1177/20417314211027677.

[27] H. Budharaju, D. Sundaramurthi, S. Sethuraman, Efficient dual crosslinking of protein–in–polysaccharide bioink for biofabrication of cardiac tissue constructs, Biomater. Adv. 152 (2023), 213486, https://doi.org/10.1016/j.bioadv.2023.213486.

[28] M.P. Mani, M. Sadia, S.K. Jaganathan, A.Z. Khudzari, E. Supriyanto, S. Saidin, S. Ramakrishna, A.F. Ismail, A.A.M. Faudzi, A review on 3D printing in tissue engineering applications, J. Polym. Eng. 42 (2022) 243–265, https://doi.org/10.1515/polyeng-2021-0059.

[29] S. Ramesh, O.L.A. Harrysson, P.K. Rao, A. Tamayol, D.R. Cormier, Y. Zhang, I. V Rivero, Extrusion bioprinting: recent progress, challenges, and future opportunities, Bioprinting 21 (2021), e00116, https://doi.org/10.1016/j.bprint.2020.e00116.

[30] S. Vanaei, M.S. Parizi, S. Vanaei, F. Salemizadehparizi, H.R. Vanaei, An overview on materials and techniques in 3D bioprinting toward biomedical application, Eng. Regeneration 2 (2021) 1–18, https://doi.org/10.1016/j.engreg.2020.12.001.

[31] S. Das, S.W. Kim, Y.J. Choi, S. Lee, S.H. Lee, J.S. Kong, H.J. Park, D.W. Cho, J. Jang, Decellularized extracellular matrix bioinks and the external stimuli to enhance cardiac tissue development in vitro, Acta Biomater. 95 (2019) 188–200, https://doi.org/10.1016/j.actbio.2019.04.026.

[32] J. Jang, H.J. Park, S.W. Kim, H. Kim, J.Y. Park, S.J. Na, H.J. Kim, M.N. Park, S. H. Choi, S.H. Park, S.W. Kim, S.M. Kwon, P.J. Kim, D.W. Cho, 3D printed complex tissue construct using stem cell-laden decellularized extracellular matrix bioinks for cardiac repair, Biomaterials 112 (2017) 264–274, https://doi.org/10.1016/j.biomaterials.2016.10.026.

[33] R. Suntornnond, E.Y.S. Tan, J. An, C.K. Chua, A highly printable and biocompatible hydrogel composite for direct printing of soft and perfusable vasculature-like structures, Sci. Rep. 7 (2017), 16902, https://doi.org/10.1038/s41598-017-17198-0.

[34] M. Rocca, A. Fragasso, W. Liu, M.A. Heinrich, Y.S. Zhang, Embedded Multimaterial Extrusion Bioprinting, SLAS Technology, 2018, https://doi.org/10.1177/2472630317742071.

[35] M. Müller, J. Becher, M. Schnabelrauch, M. Zenobi-Wong, Printing thermoresponsive reverse molds for the creation of patterned two-component hydrogels for 3D cell culture, J. Vis. Exp. (2013), https://doi.org/10.3791/50632.

[36] V. Ozbolat, M. Dey, B. Ayan, I.T. Ozbolat, Extrusion-based Printing of Sacrificial Carbopol Ink for Fabrication of Microfluidic Devices, Biofabrication, 2019, https://doi.org/10.1088/1758-5090/ab10ae.

[37] Z. Wang, S.J. Lee, H.-J.J. Cheng, J.J. Yoo, A. Atala, 3D bioprinted functional and contractile cardiac tissue constructs, Acta Biomater. 70 (2018) 48–56, https://doi.org/10.1016/j.actbio.2018.02.007.

[38] J.Y. Park, J.C. Choi, J.H. Shim, J.S. Lee, H. Park, S.W. Kim, J. Doh, D.W. Cho, A comparative study on collagen type i and hyaluronic acid dependent cell behavior for osteochondral tissue bioprinting, Biofabrication (2014), https://doi.org/10.1088/1758-5082/6/3/035004.

[39] S. Liu, T. Wang, S. Li, X. Wang, Application status of sacrificial biomaterials in 3D bioprinting, Polymers 14 (2022) 2182, https://doi.org/10.3390/polym14112182.

[40] R. Suntornnond, J. An, C.K. Chua, Roles of support materials in 3d bioprinting - present and future, Int. J. Bioprinting (2017), https://doi.org/10.18063/IJB.2017.01.006.

[41] N.V. Arguchinskaya, E.E. Beketov, A.A. Kisel, E.V. Isaeva, E.O. Osidak, S. P. Domogatsky, N.V. Mikhailovsky, F.E. Sevryukov, N.K. Silantyeva, T. A. Agababyan, S.A. Ivanov, P.V. Shegay, A.D. Kaprin, The technique of thyroid cartilage scaffold support formation for extrusion-based bioprinting, Int. J. Bioprinting 7 (2021) 104–113, https://doi.org/10.18063/IJB.V7I2.348.

[42] M. Chen, Z. Feng, W. Guo, D. Yang, S. Gao, Y. Li, S. Shen, Z. Yuan, B. Huang, Y. Zhang, M. Wang, X. Li, L. Hao, J. Peng, S. Liu, Y. Zhou, Q. Guo, PCL-MECM-Based hydrogel hybrid scaffolds and meniscal fibrochondrocytes promote whole meniscus regeneration in a rabbit meniscectomy model, ACS Appl. Mater. Interfaces (2019), https://doi.org/10.1021/acsami.9b13611.

[43] F. Pati, J. Jang, D.H. Ha, S. Won Kim, J.W. Rhie, J.H. Shim, D.H. Kim, D.W. Cho, Printing three-dimensional tissue analogues with decellularized extracellular matrix bioink, Nat. Commun. 5 (2014) 1–11, https://doi.org/10.1038/ncomms4935.

[44] C. Pan, J. Xu, Q. Gao, W. Li, T. Sun, J. Lu, Q. Shi, Y. Han, G. Gao, J. Li, Sequentially suspended 3D bioprinting of multiple-layered vascular models with tunable geometries for in vitro modeling of arterial disorders initiation, Biofabrication 15 (2023), 045017, https://doi.org/10.1088/1758-5090/aceffa.

[45] A. Shapira, N. Noor, M. Asulin, T. Dvir, Stabilization strategies in extrusion-based 3D bioprinting for tissue engineering, Appl. Phys. Rev. 5 (2018), 041112, https://doi.org/10.1063/1.5055659.

[46] B. Grigoryan, S.J. Paulsen, D.C. Corbett, D.W. Sazer, C.L. Fortin, A.J. Zaita, P. T. Greenfield, N.J. Calafat, J.P. Gounley, A.H. Ta, F. Johansson, A. Randles, J. E. Rosenkrantz, J.D. Louis-Rosenberg, P.A. Galie, K.R. Stevens, J.S. Miller, Multivascular networks and functional intravascular topologies within biocompatible hydrogels, Science 364 (2019) 458–464, https://doi.org/10.1126/science.aav9750.

[47] G. Tang, Z. Luo, L. Lian, J. Guo, S. Maharjan, C.E. Garciamendez-Mijares, M. Wang, W. Li, Z. Zhang, D. Wang, M. Xie, H. Ravanbakhsh, C. Zhou, X. Kuang, Y. Hou, X. Yu, Y.S. Zhang, Liquid-embedded (bio)printing of alginate-free, standalone, ultrafine, and ultrathin-walled cannular structures, Proc. Natl. Acad. Sci. USA 120 (2023), https://doi.org/10.1073/pnas.2206762120.

[48] J. Zhao, N. He, A mini-review of embedded 3D printing: supporting media and strategies, J. Mater. Chem. B 8 (2020) 10474–10486, https://doi.org/10.1039/d0tb01819h.

[49] N. Noor, A. Shapira, R. Edri, I. Gal, L. Wertheim, T. Dvir, 3D printing of personalized thick and perfusable cardiac patches and hearts, Adv. Sci. 6 (2019), 119536, https://doi.org/10.1002/advs.201900344.

[50] T.J. Hinton, Q. Jallerat, R.N. Palchesko, J.H. Park, M.S. Grodzicki, H.-J. Shue, M. H. Ramadan, A.R. Hudson, A.W. Feinberg, Three-dimensional printing of complex biological structures by freeform reversible embedding of suspended hydrogels, Sci. Adv. 1 (2015), e150075, https://doi.org/10.1126/sciadv.1500758.

[51] A.M. Compaan, K. Song, W. Chai, Y. Huang, Cross-linkable microgel composite matrix bath for embedded bioprinting of perfusable tissue constructs and sculpting of solid objects, ACS Appl. Mater. Interfaces (2020), https://doi.org/10.1021/acsami.9b15451.

[52] G. Luo, Y. Yu, Y. Yuan, X. Chen, Z. Liu, T. Kong, Freeform, reconfigurable embedded printing of all-aqueous 3D architectures, Adv. Mater. 31 (2019), 1904631, https://doi.org/10.1002/adma.201904631.

[53] M. Rahimnejad, A. Adoungotchodo, N.R. Demarquette, S. Lerouge, FRESH bioprinting of biodegradable chitosan thermosensitive hydrogels, Bioprinting 27 (2022), e00209, https://doi.org/10.1016/j.bprint.2022.e00209e.

[54] Y. Jin, W. Chai, Y. Huang, Printability study of hydrogel solution extrusion in nanoclay yield-stress bath during printing-then-gelation biofabrication, Mater. Sci. Eng. C 80 (2017) 313–325, https://doi.org/10.1016/j.msec.2017.05.144.

[55] X. Zeng, Z. Meng, J. He, M. Mao, X. Li, P. Chen, J. Fan, D. Li, Embedded bioprinting for designer 3D tissue constructs with complex structural organization, Acta Biomater. 140 (2022) 1–22, https://doi.org/10.1016/j.actbio.2021.11.048.

[56] T. Bhattacharjee, S.M. Zehnder, K.G. Rowe, S. Jain, R.M. Nixon, W.G. Sawyer, T. E. Angelini, Writing in the granular gel medium, Sci. Adv. (2015), https://doi.org/10.1126/sciadv.1500655.

[57] E. Mirdamadi, N. Muselimyan, P. Koti, H. Asfour, N. Sarvazyan, Agarose slurry as a support medium for bioprinting and culturing freestanding cell-laden hydrogel constructs, 3D Print. Addit. Manuf. 6 (2019) 158–164, https://doi.org/10.1089/3dp.2018.0175.

[58] C.B. Highley, C.B. Rodell, J.A. Burdick, Direct 3D printing of shear-thinning hydrogels into self-healing hydrogels, Adv. Mater. (2015), https://doi.org/10.1002/adma.201501234.

[59] W. Wu, A. DeConinck, J.A. Lewis, Omnidirectional printing of 3D microvascular networks, Adv. Mater. 23 (2011), https://doi.org/10.1002/adma.201004625. H178–H183.

[60] M.A. Skylar-Scott, S.G.M. Uzel, L.L. Nam, J.H. Ahrens, R.L. Truby, S. Damaraju, J. A. Lewis, Biomanufacturing of organ-specific tissues with high cellular density and embedded vascular channels, Sci. Adv. (2019), https://doi.org/10.1126/sciadv.aaw2459.

[61] E. Mueller, F. Xu, T. Hoare, FRESH bioprinting of dynamic hydrazone-cross-linked synthetic hydrogels, Biomacromolecules (2022), https://doi.org/10.1021/acs.biomac.2c01046.

[62] E. Mirdamadi, J.W. Tashman, D.J. Shiwarski, R.N. Palchesko, A.W. Feinberg, FRESH 3D bioprinting a full-size model of the human heart, ACS Biomater. Sci. Eng. 6 (2020) 6453–6459, https://doi.org/10.1021/acsbiomaterials.0c01133.

[63] J. Zhao, M. Hussain, M. Wang, Z. Li, N. He, Embedded 3D printing of multi-internal surfaces of hydrogels, Addit. Manuf. 32 (2020), 101097, https://doi.org/10.1016/j.addma.2020.101097.

[64] C.W. Beh, D.S. Yew, R.J. Chai, S.Y. Chin, Y. Seow, S.S. Hoon, A fluid-supported 3D hydrogel bioprinting method, Biomaterials 276 (2021), 121034, https://doi.org/10.1016/j.biomaterials.2021.121034.

[65] J. Bliley, J.W. Tashman, M.A. Stang, B.D. Coffin, D.J. Shiwarksi, A. Lee, T. J. Hinton, A.W. Feinberg, FRESH 3D bioprinting a contractile heart tube using human stem cell-derived cardiomyocytes, Biofabrication 51 (2022), 404001, https://doi.org/10.1088/1758-5090/ac58be.

[66] Ç. Bilici, M. Altunbek, F. Afghah, A.G. Tatar, B. Koç, Embedded 3D Printing of Cryogel-Based Scaffolds, ACS Biomaterials Science & Engineering, 2023, https://doi.org/10.1021/acsbiomaterials.3c00751.

[67] T.J. Hinton, A. Hudson, K. Pusch, A. Lee, A.W. Feinberg, 3D printing PDMS elastomer in a hydrophilic support bath via freeform reversible embedding, ACS Biomater. Sci. Eng. (2016), https://doi.org/10.1021/acsbiomaterials.6b00170.

[68] C.S. O'Bryan, T. Bhattacharjee, S. Hart, C.P. Kabb, K.D. Schulze, I. Chilakala, B. S. Sumerlin, W.G. Sawyer, T.E. Angelini, Self-assembled micro-organogels for 3D printing silicone structures, Sci. Adv. 3 (2017), https://doi.org/10.1126/sciadv.1602800.

[69] S. Abdollahi, A. Davis, J.H. Miller, A.W. Feinberg, Expert-guided optimization for 3D printing of soft and liquid materials, PLoS One 13 (2018) 1–19, https://doi.org/10.1371/journal.pone.0194890.

[70] A. Lee, A.R. Hudson, D.J. Shiwarski, J.W. Tashman, T.J. Hinton, S. Yerneni, J. M. Bliley, P.G. Campbell, A.W. Feinberg, 3D bioprinting of collagen to rebuild components of the human heart, Science (2019), https://doi.org/10.1126/science.aav9051.

[71] A.C. Daly, M.D. Davidson, J.A. Burdick, 3D bioprinting of high cell-density heterogeneous tissue models through spheroid fusion within self-healing hydrogels, Nat. Commun. 12 (2021) 753, https://doi.org/10.1038/s41467-021-21029-2.

[72] Z.-T. Xie, D.-H. Kang, M. Matsusaki, Resolution of 3D bioprinting inside bulk gel and granular gel baths, Soft Matter 17 (2021) 8769–8785, https://doi.org/10.1039/D1SM00926E.

[73] L. Ning, R. Mehta, C. Cao, A. Theus, M. Tomov, N. Zhu, E.R. Weeks, H. Bauser-Heaton, V. Serpooshan, Embedded 3D bioprinting of gelatin methacryloyl-based constructs with highly tunable structural fidelity, ACS Appl. Mater. Interfaces (2020), https://doi.org/10.1021/acsami.0c15078.

[74] Y. Jin, A. Compaan, T. Bhattacharjee, Y. Huang, Granular gel support-enabled extrusion of three-dimensional alginate and cellular structures, Biofabrication 8 (2016), 025016, https://doi.org/10.1088/1758-5090/8/2/025016.

[75] K. Zhu, S.R. Shin, T. van Kempen, Y.C. Li, V. Ponraj, A. Nasajpour, S. Mandla, N. Hu, X. Liu, J. Leijten, Y.D. Lin, M.A. Hussain, Y.S. Zhang, A. Tamayol, A. Khademhosseini, Gold nanocomposite bioink for printing 3D cardiac constructs, Adv. Funct. Mater. 27 (2017) 1–12, https://doi.org/10.1002/adfm.201605352.

[76] D.C. Corbett, E. Olszewski, K. Stevens, A FRESH take on resolution in 3D bioprinting, Trends Biotechnol. 37 (2019) 1153–1155, https://doi.org/10.1016/j.tibtech.2019.09.003.

[77] M. Bordoni, E. Karabulut, V. Kuzmenko, V. Fantini, O. Pansarasa, C. Cereda, P. Gatenholm, 3D printed conductive nanocellulose scaffolds for the differentiation of human neuroblastoma cells, Cells 9 (2020), https://doi.org/10.3390/cells9030682.

[78] F. Kreimendahl, C. Kniebs, A.M. Tavares Sobreiro, T. Schmitz-Rode, S. Jockenhoevel, A.L. Thiebes, FRESH bioprinting technology for tissue engineering – the influence of printing process and bioink composition on cell behavior and vascularization, J. Appl. Biomater. Funct. Mater. 19 (2021), https://doi.org/10.1177/22808000211028808.

[79] A.I. Cernencu, M. Ioniță, The current state of the art in gellan-based printing inks in tissue engineering, Carbohydr. Polym. 309 (2023), 120676, https://doi.org/10.1016/j.carbpol.2023.120676.

[80] D.J. Shiwarski, A.R. Hudson, J.W. Tashman, A.W. Feinberg, Emergence of FRESH 3D printing as a platform for advanced tissue biofabrication, APL Bioeng. 5 (2021), https://doi.org/10.1063/5.0032777.

[81] K. Flegeau, A. Puiggali, M. Zenobi-Wong, Cartilage tissue engineering by extrusion bioprinting utilizing porous hyaluronic acid microgel bioinks, Biofabrication (2022), https://doi.org/10.1088/1758-5090/ac6b58.

[82] N. Bessler, D. Ogiermann, M.B. Buchholz, A. Santel, J. Heidenreich, R. Ahmmed, H. Zaehres, B. Brand-Saberi, Nydus One Syringe Extruder (NOSE): a Prusa i3 3D printer conversion for bioprinting applications utilizing the FRESH-method, HardwareX (2019), https://doi.org/10.1016/j.ohx.2019.e00069.

[83] E.M. Shen, K.E. McCloskey, Affordable, high-resolution bioprinting with embedded concentration gradients, Bioprinting (2020), https://doi.org/10.1016/j.bprint.2020.e00113.

[84] D. Ribezzi, M. Gueye, S. Florczak, F. Dusi, D. de Vos, F. Manente, A. Hierholzer, M. Fussenegger, M. Caiazzo, T. Blunk, J. Malda, R. Levato, Shaping synthetic multicellular and complex multimaterial tissues via embedded extrusion-volumetric printing of microgels, Adv. Mater. (2023), https://doi.org/10.1002/adma.202301673.

[85] W. Liu, Y.S. Zhang, M.A. Heinrich, F. De Ferrari, H.L. Jang, S.M. Bakht, M. M. Alvarez, J. Yang, Y.-C. Li, G. Trujillo-de Santiago, A.K. Miri, K. Zhu, P. Khoshakhlagh, G. Prakash, H. Cheng, X. Guan, Z. Zhong, J. Ju, G.H. Zhu, X. Jin, S.R. Shin, M.R. Dokmeci, A. Khademhosseini, Rapid continuous multimaterial extrusion bioprinting, Adv. Mater. 29 (2017), 1604630, https://doi.org/10.1002/adma.201604630.

[86] S. Hassan, E. Gomez-Reyes, E. Enciso-Martinez, K. Shi, J.G. Campos, O.Y.P. Soria, E. Luna-Cerón, M.C. Lee, I. Garcia-Reyes, J. Steakelum, H. Jeelani, L.E. García-Rivera, M. Cho, S.S. Cortes, T. Kamperman, H. Wang, J. Leijten, L. Fiondella, S. R. Shin, Tunable and compartmentalized multimaterial bioprinting for complex living tissue constructs, ACS Appl. Mater. Interfaces 14 (2022) 51602–51618, https://doi.org/10.1021/acsami.2c12585.

[87] B. Yang, T. Liu, G. Gao, X. Zhang, B. Wu, Fabrication of 3D GelMA scaffolds using agarose microgel embedded printing, Micromachines 13 (2022) 469, https://doi.org/10.3390/mi13030469.

[88] G. Cidonio, M. Cooke, M. Glinka, J.I. Dawson, L. Grover, R.O.C. Oreffo, Printing bone in a gel: using nanocomposite bioink to print functionalised bone scaffolds, Mater. Today Bio (2019), https://doi.org/10.1016/j.mtbio.2019.100028.

[89] C. Mandrycky, Z. Wang, K. Kim, D.H. Kim, 3D bioprinting for engineering complex tissues, Biotechnol. Adv. (2016), https://doi.org/10.1016/j.biotechadv.2015.12.011.

[90] J. Lee, H. Lee, E.-J. Jin, D. Ryu, G.H. Kim, 3D bioprinting using a new photo-crosslinking method for muscle tissue restoration, Npj Regenerative Med. 8 (2023) 18, https://doi.org/10.1038/s41536-023-00292-5.

[91] A. Faulkner-Jones, C. Fyfe, D.J. Cornelissen, J. Gardner, J. King, A. Courtney, W. Shu, Bioprinting of human pluripotent stem cells and their directed differentiation into hepatocyte-like cells for the generation of mini-livers in 3D, Biofabrication (2015), https://doi.org/10.1088/1758-5090/7/4/044102.

[92] P.N. Bernal, M. Bouwmeester, J. Madrid-Wolff, M. Falandt, S. Florczak, N. G. Rodriguez, Y. Li, G. Größbacher, R. Samsom, M. van Wolferen, L.J.W. van der Laan, P. Delrot, D. Loterie, J. Malda, C. Moser, B. Spee, R. Levato, Volumetric bioprinting of organoids and optically tuned hydrogels to build liver-like metabolic biofactories, Adv. Mater. 34 (2022), 2110054, https://doi.org/10.1002/adma.202110054.

[93] P.N. Bernal, P. Delrot, D. Loterie, Y. Li, J. Malda, C. Moser, R. Levato, Volumetric bioprinting of complex living-tissue constructs within seconds, Adv. Mater. 31 (2019), 1904209, https://doi.org/10.1002/adma.201904209.

[94] M. Dey, M.H. Kim, M. Nagamine, E. Karhan, L. Kozhaya, M. Dogan, D. Unutmaz, I.T. Ozbolat, Biofabrication of 3D breast cancer models for dissecting the cytotoxic response of human T cells expressing engineered MAIT cell receptors, Biofabrication 14 (2022), 044105, https://doi.org/10.1088/1758-5090/ac925a.

[95] M. Dey, M.H. Kim, M. Dogan, M. Nagamine, L. Kozhaya, N. Celik, D. Unutmaz, I. T. Ozbolat, Chemotherapeutics and CAR-T cell-based immunotherapeutics screening on a 3D bioprinted vascularized breast tumor model, Adv. Funct. Mater. 32 (2022), https://doi.org/10.1002/adfm.202203966.

[96] D.N. Heo, B. Ayan, M. Dey, D. Banerjee, H. Wee, G.S. Lewis, I.T. Ozbolat, Aspiration-assisted bioprinting of co-cultured osteogenic spheroids for bone tissue engineering, Biofabrication 13 (2021), 015013, https://doi.org/10.1088/1758-5090/abc1bf.

[97] B. Ayan, N. Celik, Z. Zhang, K. Zhou, M.H. Kim, D. Banerjee, Y. Wu, F. Costanzo, I. T. Ozbolat, Aspiration-assisted freeform bioprinting of pre-fabricated tissue spheroids in a yield-stress gel, Commun. Phys. 3 (2020) 1–14, https://doi.org/10.1038/s42005-020-00449-4.

[98] M.H. Kim, D. Banerjee, N. Celik, I.T. Ozbolat, Aspiration-assisted freeform bioprinting of mesenchymal stem cell spheroids within alginate microgels, Biofabrication 14 (2022), 024103, https://doi.org/10.1088/1758-5090/ac4dd8.

[99] H. Savoji, L. Davenport Huyer, M.H. Mohammadi, B.F. Lun Lai, N. Rafatian, D. Bannerman, M. Shoaib, E.R. Bobicki, A. Ramachandran, M. Radisic, 3D printing of vascular tubes using bioelastomer prepolymers by freeform reversible embedding, ACS Biomater. Sci. Eng. 6 (2020) 1333–1343, https://doi.org/10.1021/acsbiomaterials.9b00676.

[100] D.F. Duarte Campos, A. Blaeser, M. Weber, J. Jäkel, S. Neuss, W. Jahnen-Dechent, H. Fischer, Three-dimensional printing of stem cell-laden hydrogels submerged in a hydrophobic high-density fluid, Biofabrication 5 (2012), 015003, https://doi.org/10.1088/1758-5082/5/1/015003.

[101] A. Shapira, N. Noor, H. Oved, T. Dvir, Transparent Support Media for High Resolution 3D Printing of Volumetric Cell-Containing ECM Structures, Biomedical Materials, 2020, https://doi.org/10.1088/1748-605X/ab809f. Bristol).

[102] V. Mair, I. Paulus, J. Groll, M. Ryma, Freeform printing of thermoresponsive poly (2-cyclopropyl-oxazoline) as cytocompatible and on-demand dissolving template of hollow channel networks in cell-laden hydrogels, Biofabrication 14 (2022), 025019, https://doi.org/10.1088/1758-5090/ac57a7.

[103] A.M. Compaan, K. Song, Y. Huang, Gellan fluid gel as a versatile support bath material for fluid extrusion bioprinting, ACS Appl. Mater. Interfaces (2019), https://doi.org/10.1021/acsami.8b13792.

[104] N. Paxton, W. Smolan, T. Böck, F. Melchels, J. Groll, T. Jungst, Proposal to assess printability of bioinks for extrusion-based bioprinting and evaluation of

rheological properties governing bioprintability, Biofabrication (2017), https://doi.org/10.1088/1758-5090/aa8dd8.
[105] O. Jeon, Y. Bin Lee, H. Jeong, S.J. Lee, D. Wells, E. Alsberg, Individual cell-only bioink and photocurable supporting medium for 3D printing and generation of engineered tissues with complex geometries, Mater. Horiz. (2019), https://doi.org/10.1039/c9mh00375d.
[106] H. Li, Y.J. Tan, R. Kiran, S.B. Tor, K. Zhou, Submerged and non-submerged 3D bioprinting approaches for the fabrication of complex structures with the hydrogel pair GelMA and alginate/methylcellulose, Addit. Manuf. (2021), https://doi.org/10.1016/j.addma.2020.101640.
[107] M. Sreepadmanabh, M. Ganesh, R. Bhat, T. Bhattacharjee, Jammed microgel growth medium prepared by flash-solidification of agarose for 3D cell culture and 3D bioprinting, Biomed. Mater. 18 (2023), 045011, https://doi.org/10.1088/1748-605X/acd315.
[108] F. Koosha, D. Silverman, S. Taboada, J. Li, M. Rafailovich, Evaluation of rheological properties and cytotoxicity of bioinks, MRS Adv. (2019), https://doi.org/10.1557/adv.2019.40.
[109] I.M. Lei, D. Zhang, W. Gu, J. Liu, Y. Zi, Y.Y.S. Huang, Soft Hydrogel Shapeability via Supportive Bath Matching in Embedded 3D Printing, Advanced Materials Technologies, 2023, https://doi.org/10.1002/admt.202300001.
[110] Y.J. Shin, R.T. Shafranek, J.H. Tsui, J. Walcott, A. Nelson, D.H. Kim, 3D bioprinting of mechanically tuned bioinks derived from cardiac decellularized extracellular matrix, Acta Biomater. 119 (2021) 75–88, https://doi.org/10.1016/j.actbio.2020.11.006.
[111] P. Fisch, M. Holub, M. Zenobi-Wong, Improved accuracy and precision of bioprinting through progressive cavity pump-controlled extrusion, Biofabrication (2021), https://doi.org/10.1088/1758-5090/abc39b.
[112] L. Li, S. Qin, J. Peng, A. Chen, Y. Nie, T. Liu, K. Song, Engineering gelatin-based alginate/carbon nanotubes blend bioink for direct 3D printing of vessel constructs, Int. J. Biol. Macromol. (2020), https://doi.org/10.1016/j.ijbiomac.2019.12.174.
[113] T. Distler, A.A. Solisito, D. Schneidereit, O. Friedrich, R. Detsch, A.R. Boccaccini, 3D printed oxidized alginate-gelatin bioink provides guidance for C2C12 muscle precursor cell orientation and differentiation via shear stress during bioprinting, Biofabrication 12 (2020), 045005, https://doi.org/10.1088/1758-5090/ab98e4.
[114] R.F. Pereira, B.N. Lourenço, P.J. Bártolo, P.L. Granja, Bioprinting a multifunctional bioink to engineer clickable 3D cellular niches with tunable matrix microenvironmental cues, Adv. Healthcare Mater. 10 (2021) 1–10, https://doi.org/10.1002/adhm.202001176.
[115] X. Zhang, Y. Liu, C. Luo, C. Zhai, Z. Li, Y. Zhang, T. Yuan, S. Dong, J. Zhang, W. Fan, Crosslinker-free silk/decellularized extracellular matrix porous bioink for 3D bioprinting-based cartilage tissue engineering, Mater. Sci. Eng. C (2021), https://doi.org/10.1016/j.msec.2020.111388.
[116] D.N. Heo, M.A. Alioglu, Y. Wu, V. Ozbolat, B. Ayan, M. Dey, Y. Kang, I.T. Ozbolat, 3D bioprinting of carbohydrazide-modified gelatin into microparticle-suspended oxidized alginate for the fabrication of complex-shaped tissue constructs, ACS Appl. Mater. Interfaces (2020), https://doi.org/10.1021/acsami.0c05096.
[117] A.M. Navara, Y.S. Kim, Y. Xu, C.L. Crafton, M. Diba, J.L. Guo, A.G. Mikos, A dual-gelling poly(N-isopropylacrylamide)-based ink and thermoreversible poloxamer support bath for high-resolution bioprinting, Bioact. Mater. 14 (2022) 302–312, https://doi.org/10.1016/j.bioactmat.2021.11.016.
[118] F. Afghah, M. Altunbek, C. Dikyol, B. Koc, Preparation and characterization of nanoclay-hydrogel composite support-bath for bioprinting of complex structures, Sci. Rep. 10 (2020) 5257, https://doi.org/10.1038/s41598-020-61606-x.
[119] W.E. Hennink, C.F. van Nostrum, Novel crosslinking methods to design hydrogels, Adv. Drug Deliv. Rev. 64 (2012) 223–236, https://doi.org/10.1016/j.addr.2012.09.009.
[120] J.H. Galarraga, M.Y. Kwon, J.A. Burdick, 3D bioprinting via an in situ crosslinking technique towards engineering cartilage tissue, Sci. Rep. 9 (2019) 1–12, https://doi.org/10.1038/s41598-019-56117-3.
[121] V. Tina, B. Kristel, B. Maarten, V. Jetze, L. J Elder, M. Jos, H. Wim, Thermogelling and chemoselectively cross-linked hydrogels for 3D bioprinting, Front. Bioeng. Biotechnol. (2016), https://doi.org/10.3389/conf.fbioe.2016.01.00909.
[122] Y. Liu, S.H. Hsu, Synthesis and biomedical applications of self-healing hydrogels, Front. Chem. (2018), https://doi.org/10.3389/fchem.2018.00449.
[123] M. Köpf, D.F.D. Campos, A. Blaeser, K.S. Sen, H. Fischer, A tailored three-dimensionally printable agarose-collagen blend allows encapsulation, spreading, and attachment of human umbilical artery smooth muscle cells, Biofabrication (2016), https://doi.org/10.1088/1758-5090/8/2/025011.
[124] H. Rastin, R.T. Ormsby, G.J. Atkins, D. Losic, 3D bioprinting of methylcellulose/gelatin-methacryloyl (MC/GelMA) bioink with high shape integrity, ACS Appl. Bio Mater. 3 (2020) 1815–1826, https://doi.org/10.1021/acsabm.0c00169.
[125] A. Leucht, A.-C.C. Volz, J. Rogal, K. Borchers, P.J. Kluger, Advanced gelatin-based vascularization bioinks for extrusion-based bioprinting of vascularized bone equivalents, Sci. Rep. 10 (2020) 5330, https://doi.org/10.1038/s41598-020-62166-w.
[126] B.A. Nerger, P.T. Brun, C.M. Nelson, Microextrusion printing cell-laden networks of type i collagen with patterned fiber alignment and geometry, Soft Matter 15 (2019) 5728–5738, https://doi.org/10.1039/c8sm02605j.
[127] R. Fan, M. Piou, E. Darling, D. Cormier, J. Sun, J. Wan, Bio-printing cell-laden Matrigel–agarose constructs, J. Biomater. Appl. 31 (2016) 684–692, https://doi.org/10.1177/0885328216669238.
[128] R. Gaetani, P.A. Doevendans, C.H.G. Metz, J. Alblas, E. Messina, A. Giacomello, J. P.G. Sluijter, Cardiac tissue engineering using tissue printing technology and human cardiac progenitor cells, Biomaterials 33 (2012) 1782–1790, https://doi.org/10.1016/j.biomaterials.2011.11.003.
[129] F.E. Freeman, D.J. Kelly, Tuning alginate bioink stiffness and composition for controlled growth factor delivery and to spatially direct MSC Fate within bioprinted tissues, Sci. Rep. 7 (2017), 17042, https://doi.org/10.1038/s41598-017-17286-1.
[130] D. Wu, Y. Yu, J. Tan, L. Huang, B. Luo, L. Lu, C. Zhou, 3D bioprinting of gellan gum and poly (ethylene glycol) diacrylate based hydrogels to produce human-scale constructs with high-fidelity, Mater. Des. 160 (2018) 486–495, https://doi.org/10.1016/j.matdes.2018.09.040.
[131] R.F. Pereira, A. Sousa, C.C. Barrias, P.J. Bártolo, P.L. Granja, A single-component hydrogel bioink for bioprinting of bioengineered 3D constructs for dermal tissue engineering, Mater. Horiz. (2018), https://doi.org/10.1039/c8mh00525g.
[132] T. Fischetti, N. Celikkin, N. Contessi Negrini, S. Farè, W. Swieszkowski, Tripolyphosphate-crosslinked chitosan/gelatin biocomposite ink for 3D printing of uniaxial scaffolds, Front. Bioeng. Biotechnol. (2020), https://doi.org/10.3389/fbioe.2020.00400.
[133] S. Sakai, T. Morita, One-step FRESH bioprinting of low-viscosity silk fibroin inks, ACS Biomater. Sci. Eng. 8 (2022) 2589–2597, https://doi.org/10.1021/acsbiomaterials.2c00269.
[134] D. Petta, A.R. Armiento, D. Grijpma, M. Alini, D. Eglin, M. D'Este, 3D bioprinting of a hyaluronan bioink through enzymatic-and visible light-crosslinking, Biofabrication (2018), https://doi.org/10.1088/1758-5090/aadf58.
[135] V. Baisane, A. Tijore, S. Venkatraman, P. Mhaisalkar, S.A. Irvine, U. Sarig, P. Mhaisalkar, V. Baisane, S. Venkatraman, Contact guidance for cardiac tissue engineering using 3D bioprinted gelatin patterned hydrogel, Biofabrication 10 (2018), 025003, https://doi.org/10.1088/1758-5090/aaa15d.
[136] C.E. Vorwald, T. Gonzalez-Fernandez, S. Joshee, P. Sikorski, J.K. Leach, Tunable fibrin-alginate interpenetrating network hydrogels to support cell spreading and network formation, Acta Biomater. 108 (2020) 142–152, https://doi.org/10.1016/j.actbio.2020.03.014.
[137] L. Li, J.M. Scheiger, P.A. Levkin, Design and applications of photoresponsive hydrogels, Adv. Mater. (2019), https://doi.org/10.1002/adma.201807333.
[138] M. Lee, R. Rizzo, F. Surman, M. Zenobi-Wong, Guiding lights: tissue bioprinting using photoactivated materials, Chem. Rev. (2020), https://doi.org/10.1021/acs.chemrev.0c00077.
[139] H. Xu, J. Casillas, S. Krishnamoorthy, C. Xu, Effect of Irgacure 2959 and lithium phenyl-2,4,6-trimethylbenzoylphosphinate on cell viability, physical properties, and microstructure in 3D bioprinting of vascular-like constructs, Biomed. Mater. (2020), https://doi.org/10.1088/1748-605x/ab954e.
[140] J. Jang, T.G. Kim, B.S. Kim, S.W. Kim, S.M. Kwon, D.W. Cho, Tailoring mechanical properties of decellularized extracellular matrix bioink by vitamin B2-induced photo-crosslinking, Acta Biomater. 33 (2016) 88–95, https://doi.org/10.1016/j.actbio.2016.01.013.
[141] E.A. Kamoun, A. Winkel, M. Eisenburger, H. Menzel, Carboxylated camphorquinone as visible-light photoinitiator for biomedical application: synthesis, characterization, and application Carboxylated camphorquinone as visible-light photoinitiator, Arab. J. Chem. (2016), https://doi.org/10.1016/j.arabjc.2014.03.008.
[142] W. Shi, S. Mirza, M. Kuss, B. Liu, A. Hartin, S. Wan, Y. Kong, B. Mohapatra, M. Krishnan, H. Band, V. Band, B. Duan, Embedded bioprinting of breast tumor cells and organoids using low-concentration collagen-based bioinks, Adv. Healthcare Mater. (2023), https://doi.org/10.1002/adhm.202300905.
[143] H. Tomás, C.S. Alves, J. Rodrigues, Laponite®, A key nanoplatform for biomedical applications? Nanomed. Nanotechnol. Biol. Med. (2018) https://doi.org/10.1016/j.nano.2017.04.016.
[144] T. Bhattacharjee, C.J. Gil, S.L. Marshall, J.M. Urueña, C.S. O'Bryan, M. Carstens, B. Keselowsky, G.D. Palmer, S. Ghivizzani, C.P. Gibbs, W.G. Sawyer, T. E. Angelini, Liquid-like solids support cells in 3D, ACS Biomater. Sci. Eng. 2 (2016) 1787–1795, https://doi.org/10.1021/acsbiomaterials.6b00218.
[145] J. Brady, T. Drig, P.I. Lee, J.X. Li, Polymer properties and characterization, in: Developing Solid Oral Dosage Forms: Pharmaceutical Theory and Practice, second ed., 2017, https://doi.org/10.1016/B978-0-12-802447-8.00007-8.
[146] G. Rathnam, N. Narayanan, R. Ilavarasan, Carbopol-based Gels for Nasal Delivery of Progesterone, AAPS PharmSciTech, 2008, https://doi.org/10.1208/s12249-008-9144-7.
[147] C.X. Srikumar Krishnamoorthy, Mengyun Zhang, Hongtao Song, Bingham fluid-assisted fabrication of 3D vascular-like constructs of interpenetrating network hydrogel, in: International Manufacturing Science and Engineering Conference MSEC2017, Proceedings of the ASME, 2017, pp. 1–6, 2017 12th.
[148] S.G. Patrício, L.R. Sousa, T.R. Correia, V.M. Gaspar, L.S. Pires, J.L. Luís, J. M. Oliveira, J.F. Mano, Freeform 3D printing using a continuous viscoelastic supporting matrix, Biofabrication (2020), https://doi.org/10.1088/1758-5090/ab8bc3.
[149] H. Budharaju, A. Zennifer, S. Sethuraman, A. Paul, D. Sundaramurthi, Designer DNA biomolecules as a defined biomaterial for 3D bioprinting applications, Mater. Horiz. 9 (2022) 1141–1166, https://doi.org/10.1039/D1MH01632F.
[150] E. Gioffredi, M. Boffito, S. Calzone, S.M. Giannitelli, A. Rainer, M. Trombetta, P. Mozetic, V. Chiono, Pluronic F127 hydrogel characterization and biofabrication in cellularized constructs for tissue engineering applications, Proc. CIRP 49 (2016) 125–132, https://doi.org/10.1016/j.procir.2015.11.001.
[151] D.B. Kolesky, K.A. Homan, M.A. Skylar-Scott, J.A. Lewis, Three-dimensional bioprinting of thick vascularized tissues, Proc. Natl. Acad. Sci. USA 113 (2016) 3179–3184, https://doi.org/10.1073/pnas.1521342113.
[152] Q. Zou, X. Tian, S. Luo, D. Yuan, S. Xu, L. Yang, M. Ma, C. Ye, Agarose composite hydrogel and PVA sacrificial materials for bioprinting large-scale, personalized face-like with nutrient networks, Carbohydr. Polym. 269 (2021), 118222, https://doi.org/10.1016/j.carbpol.2021.118222.

[153] Y. Zhang, W. Yu, G. Lv, J. Zhu, W. Wang, X. Ma, X. Liu, The artificial organ, in: Second E. Moo-Young M (Ed.), Comprehensive Biotechnology, Elsevier, Burlington, 2011, pp. 99–114, doi:10.1016/B978-0-08-088504-9.00219-1.
[154] M.P. Sekar, H. Budharaju, S. Sethuraman, D. Sundaramurthi, Carboxymethyl Cellulose-Agarose-Gelatin: A Thermoresponsive Triad Bioink Composition to Fabricate Volumetric Soft Tissue Constructs, SLAS Technology, 2023, https://doi.org/10.1016/j.slast.2023.04.005.
[155] E. Cambria, S. Brunner, S. Heusser, P. Fisch, W. Hitzl, S.J. Ferguson, K. Wuertz-Kozak, Cell-laden agarose-collagen composite hydrogels for mechanotransduction studies, Front. Bioeng. Biotechnol. 8 (2020), https://doi.org/10.3389/fbioe.2020.00346.
[156] G.R. López-Marcial, A.Y. Zeng, C. Osuna, J. Dennis, J.M. García, G.D. O'Connell, G.D. O'Connell, Agarose-based hydrogels as suitable bioprinting materials for tissue engineering, ACS Biomater. Sci. Eng. 4 (2018) 3610–3616, https://doi.org/10.1021/acsbiomaterials.8b00903.
[157] Y.P. Singh, N. Bhardwaj, B.B. Mandal, Potential of agarose/silk fibroin blended hydrogel for in vitro cartilage tissue engineering, ACS Appl. Mater. Interfaces 8 (2016) 21236–21249, https://doi.org/10.1021/acsami.6b08285.
[158] M.E. Prendergast, S.-J. Heo, R.L. Mauck, J.A. Burdick, Suspension bath bioprinting and maturation of anisotropic meniscal constructs, Biofabrication (2023), https://doi.org/10.1088/1758-5090/acc3c3.
[159] A.B. Bello, D. Kim, D. Kim, H. Park, S.-H. Lee, Engineering and functionalization of gelatin biomaterials: from cell culture to medical applications, Tissue Eng. B Rev. 26 (2020) 164–180, https://doi.org/10.1089/ten.teb.2019.0256.
[160] Y. Liu, L.M. Geever, J.E. Kennedy, C.L. Higginbotham, P.A. Cahill, G. B. McGuinness, Thermal behavior and mechanical properties of physically crosslinked PVA/Gelatin hydrogels, J. Mech. Behav. Biomed. Mater. 3 (2010) 203–209, https://doi.org/10.1016/j.jmbbm.2009.07.001.
[161] O.S. Yin, I. Ahmada, M.C.I. Mohd Aminb, Synthesis of chemical cross-linked gelatin hydrogel reinforced with cellulose nanocrystals (CNC), in: AIP Conference Proceedings, 2014, https://doi.org/10.1063/1.4895226.
[162] D.M. Kirchmajer, C.A. Watson, M. Ranson, M. In Het Panhuis, Gelapin, a degradable genipin cross-linked gelatin hydrogel, RSC Adv. (2013), https://doi.org/10.1039/c2ra22859a.
[163] D. Dranseikiene, S. Schrüfer, D.W. Schubert, S. Reakasame, A.R. Boccaccini, Cell-laden alginate dialdehyde–gelatin hydrogels formed in 3D printed sacrificial gel, J. Mater. Sci. Mater. Med. 31 (2020) 31, https://doi.org/10.1007/s10856-020-06369-7.
[164] B.H. Lee, N. Lum, L.Y. Seow, P.Q. Lim, L.P. Tan, Synthesis and Characterization of Types A and B Gelatin Methacryloyl for Bioink Applications, 2016, https://doi.org/10.3390/ma9100797. Materials.
[165] Y.-J. Choi, Y.-J. Jun, D.Y. Kim, H.-G. Yi, S.-H. Chae, J. Kang, J. Lee, G. Gao, J.-S. Kong, J. Jang, W.K. Chung, J.-W. Rhie, D.-W. Cho, A 3D cell printed muscle construct with tissue-aderived bioink for the treatment of volumetric muscle loss, Biomaterials 206 (2019) 160–169, https://doi.org/10.1016/j.biomaterials.2019.03.036.
[166] J.T. Oliveira, R.L. Reis, Hydrogels from polysaccharide-based materials: fundamentals and applications in regenerative medicine, in: Natural-Based Polymers for Biomedical Applications, 2008, https://doi.org/10.1533/9781845694814.4.485.
[167] J. Tang, R. Mao, M.A. Tung, B.G. Swanson, Gelling temperature, gel clarity and texture of gellan gels containing fructose or sucrose, Carbohydr. Polym. 44 (2001) 197–209, https://doi.org/10.1016/S0144-8617(00)00220-4.
[168] H. Grasdalen, O. Smidsrød, Gelation of Gellan Gum, Carbohydrate Polymers, 1987, https://doi.org/10.1016/0144-8617(87)90004-X.
[169] Z. Xie, J. Zeng, D. Kang, S. Saito, S. Miyagawa, Y. Sawa, M. Matsusaki, 3D printing of collagen scaffold with enhanced resolution in a citrate-modulated gellan gum microgel bath, Adv. Healthcare Mater. (2023), https://doi.org/10.1002/adhm.202301090.
[170] A. Kumar, K.M. Rao, S.S. Han, Application of xanthan gum as polysaccharide in tissue engineering: a review, Carbohydr. Polym. (2018), https://doi.org/10.1016/j.carbpol.2017.10.009.
[171] V.D. Trikalitis, N.J.J. Kroese, M. Kaya, C. Cofiño-Fabres, S. ten Den, I.S.M. Khalil, S. Misra, B.F.J.M. Koopman, R. Passier, V. Schwach, J. Rouwkema, Embedded 3D printing of dilute particle suspensions into dense complex tissue fibers using shear thinning xanthan baths, Biofabrication 15 (2023), 015014, https://doi.org/10.1088/1758-5090/aca124.
[172] R. Mohammadinejad, A. Kumar, M. Ranjbar-Mohammadi, M. Ashrafizadeh, S. S. Han, G. Khang, Z. Roveimiab, Recent Advances in Natural Gum-Based Biomaterials for Tissue Engineering and Regenerative Medicine: A Review, 2020, https://doi.org/10.3390/polym12010176. Polymers.
[173] A. Zennifer, P. Senthilvelan, S. Sethuraman, D. Sundaramurthi, Key advances of carboxymethyl cellulose in tissue engineering & 3D bioprinting applications, Carbohydr. Polym. 256 (2021), 117561, https://doi.org/10.1016/j.carbpol.2020.117561.
[174] C. Payne, E.B. Dolan, J.O. Sullivan, S. Cryan, H.M. Kelly, H.M. Kelly, A methylcellulose and collagen based temperature responsive hydrogel promotes encapsulated stem cell viability and proliferation in vitro, Drug Delivery Transl. Res. (2017) 132–146, https://doi.org/10.1007/s13346-016-0347-2.
[175] T. Ahlfeld, V. Guduric, S. Duin, A.R. Akkineni, K. Schütz, D. Kilian, J. Emmermacher, N. Cubo-Mateo, S. Dani, M.V. Witzleben, J. Spangenberg, R. Abdelgaber, R.F. Richter, A. Lode, M. Gelinsky, Methylcellulose – a versatile printing material that enables biofabrication of tissue equivalents with high shape fidelity, Biomater. Sci. 8 (2020) 2102–2110, https://doi.org/10.1039/D0BM00027B.
[176] T. Ahlfeld, T. Köhler, C. Czichy, A. Lode, M. Gelinsky, A methylcellulose hydrogel as support for 3D plotting of complex shaped calcium phosphate scaffolds, Gels (2018) 4, https://doi.org/10.3390/gels4030068.
[177] K.C. Lowe, M.R. Davey, J.B. Power, Perfluorochemicals: their applications and benefits to cell culture, Trends Biotechnol. 16 (1998) 272–277, https://doi.org/10.1016/S0167-7799(98)01205-0.
[178] C. L, G. Frank, Survival of mammals breathing organic liquids equilibrated with oxygen at atmospheric pressure, Science 152 (1966) 1755–1756, https://doi.org/10.1126/science.152.3730.1755.
[179] T. Lu, Y. Li, T. Chen, Techniques for fabrication and construction of three-dimensional scaffolds for tissue engineering, Int. J. Nanomed. (2013), https://doi.org/10.2147/IJN.S38635.
[180] M.D. Sarker, S. Naghieh, N.K. Sharma, X. Chen, 3D biofabrication of vascular networks for tissue regeneration: a report on recent advances, J. Pharmaceu. Anal. (2018), https://doi.org/10.1016/j.jpha.2018.08.005.
[181] H. Ding, R.C. Chang, Printability Study of Bioprinted Tubular Structures Using Liquid Hydrogel Precursors in a Support Bath, Applied Sciences, Switzerland, 2018, https://doi.org/10.3390/app8030403.
[182] D. Sundaramurthi, U.M. Krishnan, S. Sethuraman, Epidermal Differentiation of Stem Cells on Poly(3-Hydroxybutyrate-Co-3-Hydroxyvalerate) (PHBV) Nanofibers, Annals of Biomedical Engineering, 2014, https://doi.org/10.1007/s10439-014-1124-3.
[183] D. Sundaramurthi, U.M. Krishnan, S. Sethuraman, Electrospun nanofibers as scaffolds for skin tissue engineering, Polym. Rev. 54 (2014) 348–376, https://doi.org/10.1080/15583724.2014.881374.
[184] R.J.A. Moakes, J.J. Senior, T.E. Robinson, M. Chipara, A. Atansov, A. Naylor, A. D. Metcalfe, A.M. Smith, L.M. Grover, A suspended layer additive manufacturing approach to the bioprinting of tri-layered skin equivalents, APL Bioeng. 5 (2021), https://doi.org/10.1063/5.0061361.
[185] J. Parvizi, G.K. Kim, Cartilage, in: J. Parvizi, G.K. Kim (Eds.), High Yield Orthopaedics, Elsevier, Philadelphia, 2010, pp. 80–81. https://doi.org/10.1016/B978-1-4160-0236-9.00050-X.
[186] J. Radhakrishnan, A. Subramanian, S. Sethuraman, Injectable glycosaminoglycan–protein nano-complex in semi-interpenetrating networks: a biphasic hydrogel for hyaline cartilage regeneration, Carbohydr. Polym. 175 (2017) 63–74, https://doi.org/10.1016/j.carbpol.2017.07.063.
[187] O. Bas, E.M. De-Juan-Pardo, C. Meinert, D. D'Angella, J.G. Baldwin, L.J. Bray, R. M. Wellard, S. Kollmannsberger, E. Rank, C. Werner, T.J. Klein, I. Catelas, D. W. Hutmacher, Biofabricated soft network composites for cartilage tissue engineering, Biofabrication 9 (2017), 25014, https://doi.org/10.1088/1758-5090/aa6b15.
[188] Q. Zhang, Y. Yu, H. Zhao, The effect of matrix stiffness on biomechanical properties of chondrocytes, Acta Biochim. Biophys. Sin. 48 (2016) 958–965, https://doi.org/10.1093/abbs/gmw087.
[189] B.A.G. de Melo, Y.A. Jodat, S. Mehrotra, M.A. Calabrese, T. Kamperman, B. B. Mandal, M.H.A. Santana, E. Alsberg, J. Leijten, S.R. Shin, 3D printed cartilage-like tissue constructs with spatially controlled mechanical properties, Adv. Funct. Mater. 29 (2019) 1–13, https://doi.org/10.1002/adfm.201906330.
[190] Z. Wang, S.J. Florczyk, Freeze-FRESH: a 3D printing technique to produce biomaterial scaffolds with hierarchical porosity, Materials 13 (2020), https://doi.org/10.3390/ma13020354.
[191] Y. Fang, Y. Guo, B. Wu, Z. Liu, M. Ye, Y. Xu, M. Ji, L. Chen, B. Lu, K. Nie, Z. Wang, J. Luo, T. Zhang, W. Sun, Z. Xiong, Expanding embedded 3D bioprinting capability for engineering complex organs with freeform vascular networks, Adv. Mater. (2023), 2205082, https://doi.org/10.1002/adma.202205082.
[192] R. Cadle, D. Rogozea, L. Moldovan, P. Parsons-Wingerter, N.I. Moldovan, An image analysis-based workflow for 3D bioprinting of anatomically realistic retinal vascular patterns, Bioprinting 23 (2021), e00152, https://doi.org/10.1016/j.bprint.2021.e00152.
[193] S. Pashneh-Tala, S. MacNeil, F. Claeyssens, The tissue-engineered vascular graft—past, present, and future, Tissue Eng. B Rev. 22 (2016) 68–100, https://doi.org/10.1089/ten.teb.2015.0100.
[194] S.-H. Sohn, T.-H. Kim, T.-S. Kim, T.-J. Min, J.-H. Lee, S.-M. Yoo, J.-W. Kim, J.-E. Lee, C.-H. Kim, S.-H. Park, W.-M. Jo, Evaluation of 3D templated synthetic vascular graft compared with standard graft in a rat model: potential use as an artificial vascular graft in cardiovascular disease, Materials 14 (2021) 1239, https://doi.org/10.3390/ma14051239.
[195] Z. Wang, C. Liu, Y. Xiao, X. Gu, Y. Xu, N. Dong, S. Zhang, Q. Qin, J. Wang, Remodeling of a cell-free vascular graft with nanolamellar intima into a neovessel, ACS Nano 13 (2019) 10576–10586, https://doi.org/10.1021/acsnano.9b04704.
[196] A. Manigandan, R. Dhandapani, S. Bagewadi, P. Sethu, S. Sethuraman, A. Subramanian, Facile fabrication of Bi-layered perfusable hydrogel tubes as biomimetic 3D arterial construct, Biomed. Mater. 17 (2022), 065008, https://doi.org/10.1088/1748-605x/ac91ba.
[197] A. Arslan-Yildiz, R. El Assal, P. Chen, S. Guven, F. Inci, U. Demirci, Towards artificial tissue models: past, present, and future of 3D bioprinting, Biofabrication 8 (2016), 014103, https://doi.org/10.1088/1758-5090/8/1/014103.
[198] C.M. Owens, F. Marga, G. Forgacs, C.M. Heesch, Biofabrication and testing of a fully cellular nerve graft, Biofabrication 5 (2013), 045007, https://doi.org/10.1088/1758-5082/5/4/045007.
[199] Y. Zhang, S.T. Ellison, S. Duraivel, C.D. Morley, C.R. Taylor, T.E. Angelini, 3D printed collagen structures at low concentrations supported by jammed microgels, Bioprinting 21 (2021), e00121, https://doi.org/10.1016/j.bprint.2020.e00121.

[200] Y.C.E. Li, Y.A. Jodat, R. Samanipour, G. Zorzi, K. Zhu, M. Hirano, K. Chang, A. Arnaout, S. Hassan, N. Matharu, A. Khademhosseini, M. Hoorfar, S.R. Shin, Toward a neurospheroid niche model: optimizing embedded 3D bioprinting for fabrication of neurospheroid brain-like co-culture constructs, Biofabrication 13 (2020), https://doi.org/10.1088/1758-5090/abc1be.
[201] P. Jain, H. Kathuria, N. Dubey, Advances in 3D bioprinting of tissues/organs for regenerative medicine and in-vitro models, Biomaterials 287 (2022), 121639, https://doi.org/10.1016/j.biomaterials.2022.121639.
[202] D. Nothdurfter, C. Ploner, D.C. Coraça-Huber, D. Wilflingseder, T. Müller, M. Hermann, J. Hagenbuchner, M.J. Ausserlechner, 3D bioprinted, vascularized neuroblastoma tumor environment in fluidic chip devices for precision medicine drug testing, Biofabrication 14 (2022), 035002, https://doi.org/10.1088/1758-5090/ac5fb7.
[203] O. Habanjar, M. Diab-Assaf, F. Caldefie-Chezet, L. Delort, 3D cell culture systems: tumor application, advantages, and disadvantages, Int. J. Mol. Sci. 22 (2021), 12200, https://doi.org/10.3390/ijms222212200.
[204] E. Maloney, C. Clark, H. Sivakumar, K. Yoo, J. Aleman, S.A.P. Rajan, S. Forsythe, A. Mazzocchi, A.W. Laxton, S.B. Tatter, R.E. Strowd, K.I. Votanopoulos, A. Skardal, Immersion bioprinting of tumor organoids in multi-well plates for increasing chemotherapy screening throughput, Micromachines (2020), https://doi.org/10.3390/mi11020208.
[205] A. Spreafico, A.R. Hansen, A.R. Abdul Razak, P.L. Bedard, L.L. Siu, The future of clinical trial design in oncology, Cancer Discov. 11 (2021) 822–837, https://doi.org/10.1158/2159-8290.CD-20-1301.
[206] A. Satpathy, P. Datta, Y. Wu, B. Ayan, E. Bayram, I.T. Ozbolat, Developments with 3D bioprinting for novel drug discovery, Expet Opin. Drug Discov. 13 (2018) 1115–1129, https://doi.org/10.1080/17460441.2018.1542427.
[207] M. Tang, D. Berry, K. Miller, X. Ma, S. Chen, Chapter 2 - bioprinting of biomimetic tissue models for disease modeling and drug screening, in: L.G. Zhang, J.P. Fisher, K.W. Leong (Eds.), 3D Bioprinting and Nanotechnology in Tissue Engineering and Regenerative Medicine, second ed.), second ed., Academic Press, 2022, pp. 33–70, https://doi.org/10.1016/B978-0-12-824552-1.00002-5.
[208] E.S. Bishop, S. Mostafa, M. Pakvasa, H.H. Luu, M.J. Lee, J.M. Wolf, G.A. Ameer, T.-C. He, R.R. Reid, 3-D bioprinting technologies in tissue engineering and regenerative medicine: current and future trends, Genes & Dis. 4 (2017) 185–195, https://doi.org/10.1016/j.gendis.2017.10.002.
[209] H. Cui, W. Zhu, Y. Huang, C. Liu, Z.-X. Yu, M. Nowicki, S. Miao, Y. Cheng, X. Zhou, S.-J. Lee, Y. Zhou, S. Wang, M. Mohiuddin, K. Horvath, L.G. Zhang, In vitro and in vivo evaluation of 3D bioprinted small-diameter vasculature with smooth muscle and endothelium, Biofabrication 12 (2019), 015004, https://doi.org/10.1088/1758-5090/ab402c.
[210] H. Ravanbakhsh, Z. Luo, X. Zhang, S. Maharjan, H.S. Mirkarimi, G. Tang, C. Chávez-Madero, L. Mongeau, Y.S. Zhang, Freeform cell-laden cryobioprinting for shelf-ready tissue fabrication and storage, Matter 5 (2022) 573–593, https://doi.org/10.1016/j.matt.2021.11.020.
[211] Z. Luo, G. Tang, H. Ravanbakhsh, W. Li, M. Wang, X. Kuang, C.E. Garciamendez-Mijares, L. Lian, S. Yi, J. Liao, M. Xie, J. Guo, Z. Zhou, Y.S. Zhang, Vertical extrusion cryo(bio)printing for anisotropic tissue manufacturing, Adv. Mater. 34 (2022), 2108931, https://doi.org/10.1002/adma.202108931.
[212] J.P. Jung, D.B. Bhuiyan, B.M. Ogle, Solid organ fabrication: comparison of decellularization to 3D bioprinting, Biomater. Res. 20 (2016) 27, https://doi.org/10.1186/s40824-016-0074-2.
[213] S. Mehrotra, B.A.G.G. de Melo, M. Hirano, W. Keung, R.A. Li, B.B. Mandal, S. R. Shin, Nonmulberry silk based ink for fabricating mechanically robust cardiac patches and endothelialized myocardium-on-a-chip application, Adv. Funct. Mater. 30 (2020), 1907436, https://doi.org/10.1002/adfm.201907436.
[214] N. Tasnim, L. De la Vega, S. Anil Kumar, L. Abelseth, M. Alonzo, M. Amereh, B. Joddar, S.M. Willerth, 3D bioprinting stem cell derived tissues, Cell. Mol. Bioeng. 11 (2018) 219–240, https://doi.org/10.1007/s12195-018-0530-2.
[215] A.K. Shukla, G. Gao, B.S. Kim, Applications of 3D bioprinting technology in induced pluripotent stem cells-based tissue engineering, Micromachines 13 (2022) 155, https://doi.org/10.3390/mi13020155.
[216] M.P. Sekar, H. Budharaju, A. Zennifer, S. Sethuraman, N. Vermeulen, D. Sundaramurthi, D.M. Kalaskar, Current standards and ethical landscape of engineered tissues—3D bioprinting perspective, J. Tissue Eng. 12 (2021), 204173142110276, https://doi.org/10.1177/20417314211027677.
[217] E.Y. Adashi, D.P. O'Mahony, I.G. Cohen, The FDA modernization Act 2.0: drug testing in animals is rendered optional, Am. J. Med. (2023), https://doi.org/10.1016/j.amjmed.2023.03.033.
[218] J. Li, C. Wu, P.K. Chu, M. Gelinsky, 3D Printing of Hydrogels: Rational Design Strategies and Emerging Biomedical Applications, Materials Science and Engineering R: Reports, 2020, https://doi.org/10.1016/j.mser.2020.100543.
[219] M. Hospodiuk, K.K. Moncal, M. Dey, I.T. Ozbolat, 3D Printing and Biofabrication, Springer International Publishing, Cham, 2018, https://doi.org/10.1007/978-3-319-45444-3.
[220] K. Min, J.S. Kong, J. Kim, J. Kim, G. Gao, D.-W. Cho, H.H. Han, Three-dimensional microfilament printing of a decellularized extracellular matrix (dECM) bioink using a microgel printing bath for nerve graft fabrication and the effectiveness of dECM graft combined with a polycaprolactone conduit, ACS Appl. Bio Mater. 5 (2022) 1591–1603, https://doi.org/10.1021/acsabm.1c01142.
[221] L.G. Brunel, S.M. Hull, S.C. Heilshorn, Engineered assistive materials for 3D bioprinting: support baths and sacrificial inks, Biofabrication 14 (2022), 032001, https://doi.org/10.1088/1758-5090/ac6bbe.
[222] A. Skardal, Perspective: "Universal" bioink technology for advancing extrusion bioprinting-based biomanufacturing, Bioprinting 10 (2018), e00026, https://doi.org/10.1016/j.bprint.2018.e00026.
[223] Benedict O'Neill, 3D Bioprinting: Comprehensive Guide and Product Selection, Aniwaa, 2022. https://www.aniwaa.com/buyers-guide/3d-printers/3d-bioprinting-3d-bioprinters/.
[224] X. Cao, S. Maharjan, R. Ashfaq, J. Shin, Y.S. Zhang, Bioprinting of small-diameter blood vessels, Engineering 7 (2021) 832–844, https://doi.org/10.1016/j.eng.2020.03.019.
[225] T. Lorson, M. Ruopp, A. Nadernezhad, J. Eiber, U. Vogel, T. Jungst, T. Lühmann, Sterilization methods and their influence on physicochemical properties and bioprinting of alginate as a bioink component, ACS Omega 5 (2020) 6481–6486, https://doi.org/10.1021/acsomega.9b04096.
[226] P. Chansoria, L.K. Narayanan, M. Wood, C. Alvarado, A. Lin, R.A. Shirwaiker, Effects of autoclaving, EtOH, and UV sterilization on the chemical, mechanical, printability, and biocompatibility characteristics of alginate, ACS Biomater. Sci. Eng. 6 (2020) 5191–5201, https://doi.org/10.1021/acsbiomaterials.0c00806.
[227] S. Agarwal, S. Saha, V.K. Balla, A. Pal, A. Barui, S. Bodhak, Current developments in 3D bioprinting for tissue and organ regeneration–A review, Front. Mech. Eng. 6 (2020) 90, https://doi.org/10.3389/fmech.2020.589171.
[228] Z. Yang, P. Yi, Z. Liu, W. Zhang, L. Mei, C. Feng, C. Tu, Z. Li, Stem cell-laden hydrogel-based 3D bioprinting for bone and cartilage tissue engineering, Front. Bioeng. Biotechnol. 10 (2022), https://doi.org/10.3389/fbioe.2022.865770.
[229] L. De la Vega, L. Abelseth, R. Sharma, J. Triviño-Paredes, M. Restan, S. M. Willerth, 3D bioprinting human-induced pluripotent stem cells and drug-releasing microspheres to produce responsive neural tissues, Adv. NanoBiomed. Res. 1 (2021), 2000077, https://doi.org/10.1002/anbr.202000077.
[230] G.L. Koons, A.G. Mikos, Progress in three-dimensional printing with growth factors, J. Contr. Release 295 (2019) 50–59, https://doi.org/10.1016/j.jconrel.2018.12.035.
[231] G. Bouguéon, T. Kauss, B. Dessane, P. Barthélémy, S. Crauste-Manciet, Micro- and nano-formulations for bioprinting and additive manufacturing, Drug Discov. Today 24 (2019) 163–178, https://doi.org/10.1016/j.drudis.2018.10.013.
[232] Q. Gao, Y. He, J. Fu, A. Liu, L. Ma, Coaxial nozzle-assisted 3D bioprinting with built-in microchannels for nutrients delivery, Biomaterials 61 (2015) 203–215, https://doi.org/10.1016/j.biomaterials.2015.05.031.
[233] W. Sun, B. Starly, A.C. Daly, J.A. Burdick, J. Groll, G. Skeldon, W. Shu, Y. Sakai, M. Shinohara, M. Nishikawa, J. Jang, D.-W.W. Cho, M. Nie, S. Takeuchi, S. Ostrovidov, A. Khademhosseini, R.D. Kamm, V. Mironov, L. Moroni, I. T. Ozbolat, The bioprinting roadmap, Biofabrication 12 (2020), 022002, https://doi.org/10.1088/1758-5090/ab5158.
[234] Z. Fu, L. Ouyang, R. Xu, Y. Yang, W. Sun, Responsive biomaterials for 3D bioprinting: a review, Mater. Today 52 (2022) 112–132, https://doi.org/10.1016/j.mattod.2022.01.001.
[235] C. Scognamiglio, A. Soloperto, G. Ruocco, G. Cidonio, Bioprinting stem cells: building physiological tissues one cell at a time, Am. J. Physiol. Cell Physiol. 319 (2020) C465–C480, https://doi.org/10.1152/ajpcell.00124.2020.
[236] W.W. Chan, D.C.L. Yeo, V. Tan, S. Singh, D. Choudhury, M.W. Naing, Additive biomanufacturing with collagen inks, Bioengineering 7 (2020) 66, https://doi.org/10.3390/bioengineering7030066.